AALBORG UNIVERSITY
INSTITUTE OF ELECTRONIC SYSTEMS
DEPARTMENT OF CONTROL ENGINEERING

Fredrik Bajers Vej 7 ▪ DK-9220 Aalborg Øst Phone +45 96 35 80 80

TITLE: Laser Metrology System for SMART-2 with Spherical Mirror as Formation Reference

PROJECT PERIOD: 9th semester, September 4th 2000 - Jan 19th 2001

PROJECT GROUP: IAS-939u

GROUP MEMBERS:
Dan Bhanderi

SUPERVISOR:
Rafal Wisniewski

ESA SUPERVISOR:
Finn Ankersen

Abstract

This project is a feasibility study of using a spherical mirror as a formation reference for the SMART-2 mission. A laser metrology system is used for SMART-2. It is investigated if a simple non-stabilized sphere satellite, can be used as a reference for the SMART-2 formation, which will increase the quality of the demonstrated formation capabilities of SMART-2. In addition the predefined requirements of the sensor and actuator hardware are evaluated.

A mathematical analysis is done in order to describe and analyze the system in the simulation program Xmath. The attitude and position dynamics of the satellites are derived. In addition a Kalman filter with steady state gain is derived as estimator of the measurements. Finally a simple LQG controller has been designed using Xmath.

It is concluded that the spherical mirror amplifies the error angle of the incoming laser beam by a factor that makes mounting practically impossible, due to the requirements of precision. Disregarding the in-feasibility of the laser metrology system when used with a spherical mirror, the estimator and controller have been simulated. It is concluded that the requirements of the attitude hardware should be 5as when used with the designed controller. However this is to be confirmed with other controllers.

NUMBER OF COPIES: 11
NUMBER OF PAGES: 117

Preface

This report is written by Dan Bhanderi (Group 939u) at the European Research and Technology Center, European Space Agency, Noordwijk, The Netherlands from September 23rd 2000 to January 19th 2001.

The project is aimed for the European Space Agency's SMART-2 project, and for the supervisor and censor at Aalborg University.

Figures and tables are numbered successively within each chapter, e.g. Figure 5.4 is the 4th figure in Chapter 5.

Literature references are denoted with the authors surname and the year of publishing in square brackets, [James R. Wertz, 1978].

Symbols and definitions are given in the following pages.

Appendix A on page 111 is a brief description of the DARWIN mission.

Appendix B on page 115 is a description of quaternions and their algebra, which is used in this project.

The writer would like to thank Finn Ankersen and Rafal Wisniewski for their supervision, but especially for making the stage at ESTEC possible.

This project is dedicated to all of my friends at Willem van den Bergh, who made my stay in the Netherlands an unforgettable experience. Dank je wel.

ESTEC, Noordwijk, Jan 19th 2001.

Dan Bhanderi

Symbols and Definitions

The following definitions and symbols are used in the report.

Definitions

Vectors are denoted with lower case bold: $\boldsymbol{v}$
The direction of the vector $\boldsymbol{v}$ is represented by the unit vector in that direction denoted as: $\hat{\boldsymbol{v}}$
The length of vector $\boldsymbol{v}$ is denoted as: $|\boldsymbol{v}|$
The estimate of vector $\boldsymbol{v}$ is denoted as: $\hat{\boldsymbol{v}}$[1]
The working point of vector $\boldsymbol{v}$ is denoted as: $\bar{\boldsymbol{v}}$
The small signal of vector $\boldsymbol{v}$ is denoted as: $\tilde{\boldsymbol{v}}$
Matrices are denoted with uppercase bold: $\boldsymbol{M}$
Cross product matrices are denoted as: $\mathbf{S}(\boldsymbol{v})$
The transposed is denoted with a superscript T: $\boldsymbol{M}^{\mathrm{T}}$
The rotation from frame b to frame s is represented by a rotation matrix as: $\boldsymbol{A}_b^s$
Quaternions are denoted as: $\boldsymbol{q}$
The scalar part of a quaternion $\boldsymbol{q}$ is denoted as: q_1
The vector/complex part of a quaternion $\boldsymbol{q}$ is denoted as: $\boldsymbol{q}_{2-4}$
The complex conjugated of $\boldsymbol{q}$ is denoted with an asterisk: $\boldsymbol{q}^*$
Vector $\boldsymbol{v}$ in frame b is denoted as: $\boldsymbol{x}^b$
The time derivative of a vector $\boldsymbol{v}$ in frame b but given in frame s is denoted as: $\left(\dot{\boldsymbol{v}}^b\right)^s$

[1]The $\hat{}$ operator is used for both unit vector and estimates to maintain notational agreement. The function of the operator should be clear by the context.

Symbols

$\boldsymbol{r}_{\text{in}}$	Laser beam from satellite to sphere
$\boldsymbol{r}_{\text{out}}$	Reflected laser beam from sphere to satellite
$\boldsymbol{r}_{\text{l0}}$	Reference position of laser frame
$\boldsymbol{r}_{\text{r}}$	Position of the reflection point
$\boldsymbol{r}_{\text{s}}$	Relative position of satellite with respect to the spherical mirror
$\boldsymbol{r}_{\text{b}}$	Position of sphere
$\boldsymbol{r}_{\text{c}}$	Position of chaser
$\boldsymbol{r}_{\epsilon}$	Error in satellite position
$\boldsymbol{r}_{\text{l-s}}$	Vector from origin of satellite frame to origin of laser frame
$\boldsymbol{b}$	Baseline
$\hat{\boldsymbol{r}}_{\text{LOS}}$	Signal source line-of-sight
$\boldsymbol{r}_{\text{COP}}$	Vector from center of mass to center of pressure
$\boldsymbol{f}_{\text{Sun}}$	Solar force
$\boldsymbol{f}_{\text{flux}}$	Force of solar flux
$\boldsymbol{f}_{\text{ext}}$	Sum of external forces
$\boldsymbol{f}_{\text{ctrl}}$	Control force
$\boldsymbol{a}_{\text{Sun}}$	Solar acceleration
$\boldsymbol{m}$	Measurement vector
$\boldsymbol{\omega}_{\text{s}}$	Angular velocity of satellite
$\boldsymbol{\omega}_{\text{o}}$	Angular velocity of orbit frame
$\boldsymbol{q}$	Satellite attitude quaternion
$\boldsymbol{x}$	State vector
$\boldsymbol{u}$	Input vector
$\boldsymbol{z}$	Measurement vector
$\boldsymbol{w}$	Process noise
$\boldsymbol{v}$	Measurement noise
$\boldsymbol{n}_{\text{ext}}$	Sum of external torques
$\boldsymbol{n}_{\text{ctrl}}$	Control torque
R_b	Sphere radius
R_s	Sunscreen radius
m_b	Mass of sphere
m_c	Mass of chaser
d	Measured distance of optical path
γ	Laser pitch measured from the CCD plane
α	Rotation of the laser frame

I	Inertial frame
b	Sphere frame
l	Laser frame
s	Satellite frame
B	Satellite body frame
p	CCD plane frame
o	Orbit frame
$\mathbf{0}_{n\times n}$	n by n matrix of zero-elements
$\mathbf{1}_{n\times n}$	n by n identity matrix
$\boldsymbol{F}_{\text{nl}}$	Non-linear system matrix
$\boldsymbol{F}$	Linearized system matrix
$\boldsymbol{G}$	Input system matrix
$\boldsymbol{H}$	Measurement matrix
$\boldsymbol{J}$	Moment of inertia
$\boldsymbol{K}$	Kalman gain matrix
$\boldsymbol{l}$	Angular momentum
$\boldsymbol{P}$	Covariance matrix
$\boldsymbol{Q}$	Process noise covariance matrix
$\boldsymbol{R}$	Measurement noise covariance matrix
$\boldsymbol{V}$	State weighing matrix
$\boldsymbol{W}$	Input weighing matrix
$\boldsymbol{L}$	Feedback gain matrix
$\boldsymbol{M}$	Jacobian Matrix of $\frac{\mathrm{d}\boldsymbol{a}_{\text{Sun}}(\boldsymbol{r})}{\mathrm{d}\boldsymbol{r}}$
$\Delta(n)$	Kronecker's delta function
$\delta(t)$	Dirac's delta function

Contents

List of Figures

Chapter 1

Introduction

This project is a study of using a laser metrology system with a reflecting spherical satellite, for a technical demonstration mission of the European Space Agency (ESA), named SMART-2. The SMART-2 mission precedes the possible cornerstone mission of ESA named DARWIN.

The following is a short description of the concepts of the DARWIN mission and a description of the SMART-2 mission. The project is outlined and a solution strategy is presented.

1.1 DARWIN

The DARWIN mission's main objective is planet detection. The DARWIN formation of satellites searches for planets orbiting other stars than the Sun, and identifies Earth-like planets which could support life as we know it. DARWIN uses interferometry to reject the bright light from a target star, which makes the light from a nearby planet detectable. The interferometer requires free flying telescope satellites in a precisely controlled formation. As many of the technologies needed for the mission have not been used previously, a demonstration mission named SMART-2, must prove the feasibility of the DARWIN mission.

Appendix A on page 111 is a brief presentation of the system elements and terms used for the DARWIN mission.

1.2 SMART-2

Preceding the DARWIN mission, a test of hardware is necessary in order to verify the expected performance of the sensors and actuators intended for use. Some of the new technologies will be used in other missions (i.e. NGST, SIM and FIRST-PLANCK [ES, 5]), and some have to be tested on the ESA demonstration mission SMART-2.

The SMART-2 mission is an ESA demonstration mission, that must prove the feasibility of future missions, including DARWIN. This document is solely concerned with the technology demonstration for DARWIN, and a reference to SMART-2 should be read as a reference to the part of SMART-2 that is intended for the DARWIN mission.

For testing the high precision formation flying used in DARWIN, the SMART-2 mission will launch two satellites. Though three satellites would be required to test planar pointing, only two are available due to economical considerations. In order to test the planar formation, a reflecting sphere will be used as third reference. It is to be shown that the control system of the two satellites, is able to position the satellites with reference to the sphere, pointing the normal to the formation plane within the requirements of the DARWIN mission.

SMART-2 must demonstrate the use of the following systems [CAS, 2000]:

- Formation flying control
  - Metrology for relative translation measurement
  - Actuators of micro Newton thrust level
  - Control laws to the on-board system for formation flying
- Very precise control of the distances between individual telescopes and the central hub[1]
- Perform broad-band interferometry in the near infrared (NIR)
  - Optical components
  - Thermal control
  - High sensitivity detectors
- Achromatic phase-shifting in the NIR

[1] See Appendix A for an explanation of the hub satellite.

1.3 Outlines of This Project

The outlines of this project are based on the study of position and attitude control of the satellites, and will as a consequence not include the challenges of fine optics for the interferometer and thermal aspects of such. The development of the necessary sensors and actuators used for the control systems, will also not be included in the project, however an investigation of the control systems should lead to requirements of necessary hardware.

Formation establishment and collision avoidance is also not in the frame of this project, but the ability to hold a formation within requirements should be demonstrated.

Initial Problems

The primary goal of the SMART-2 mission is to demonstrate formation flying. This is to be accomplished using two or three satellites. Due to economical considerations, a two satellite mission is suggested. This limits the demonstration of formation flying, as two satellites only span a line, and the planar pointing system needed for DARWIN is therefore not shown. An idea is to use a reflecting sphere which the two satellites must use as reference for the formation configuration. The study of this project will be based on this concept, which leads to the problem formulation of this project:

> This project is a study of the SMART-2 demonstration mission by ESA, based on two satellites and a reference sphere. It should analyze the requirements of such a reflecting reference sphere wrt. stabilization, control and geometric precision, upon an analysis of the system and the design of a control system. Based on the results of such requirements, the choice of using a third satellite instead of a reflecting sphere should be clarified. The control system should prove the feasibility of the control requirements or extend the requirements for sensor and actuator hardware.

1.4 Solution Strategy

The feasibility study of the formation flying and high precision control of the formation, based on two satellites and a sphere, will include an investigation in the following areas:

- Identification of sensors and actuators, based on the proposed hardware of the DARWIN and SMART-2 missions.

- An analysis of the laser metrology system, proposed for the relative positioning and attitude control, used with the reflective reference sphere.
- Modeling of satellite dynamics and disturbances.
- Modeling of sensors and actuators.
- Design of controllers and estimators.
- Verification of controllers wrt. system requirements or formulation of new requirements to sensor and/or actuator hardware.

Chapter 2

System Description

This chapter is a description of the SMART-2 system components, and their function. The system consists of two fully equipped satellites, and a single satellite, which is to be kept as simple as possible. In order to control the formation with high precision, a laser metrology system is proposed. This system requires an optical path, in which a laser beam is pointed towards another satellite. A charge coupled device (CCD) is used to measure where the laser beam hits the targeted satellite, in order to estimate the relative translational motion between the two satellites.

In order to acquire the optical an omni-directional metrology system is necessary. An omni-directional system suggests the use of a radio frequency (RF) signals. The attitude of the individual satellites is measured using star trackers.

Based on the choice of an optical laser metrology system, the simple third satellite is chosen to be a reflecting sphere. Choosing a spherical shaped satellite means that there will be no stabilization requirements of the satellite. Hence no thrusters or star trackers, and thus solar panels, are needed. Reflecting the laser beam, moves the sensor equipment from the “receiving” satellite to the transmitting satellite. The equipment needed on the sphere satellite is limited to a transmitting RF source. This equipment must be powered by batteries, because any external devices, like solar panels, would result in stabilization requirements of the sphere satellite.

Based on the above, the overall system elements can be summarized:

- The formation consists of two fully equipped satellites, and a simple spherical satellite. In this project these are referred to as the satellites and the sphere satellite or just sphere, respectively.
- The formation is controlled using laser metrology. Both transmitters and receivers are mounted on the fully equipped satellites. The sphere satellite simply reflects

the laser beams to the sensors on the other two satellites.

- The initial conditions of the laser metrology system, are acquired using an omni-directional RF metrology system. In order to detect the sphere satellite, a transmitter must be mounted inside the sphere. In addition, batteries must be mounted inside the sphere, to power the RF transmitter.

2.1 The Formation

The two baselines shown in Figure 2.1, between the three satellites of SMART-2, span the formation plane. The normal to this plane, is to be pointed towards some given target star. This direction is the target star line of sight (LOS). This will enable the telescope satellites, used in DARWIN, to detect planets orbiting the target star. In order to use interferometry, the length of the baselines in the formation must also be controlled.

The attitudes of the satellites are measured using star trackers. The translation errors of the satellites, causing formation mis-configuration, are estimated using the laser metrology system.

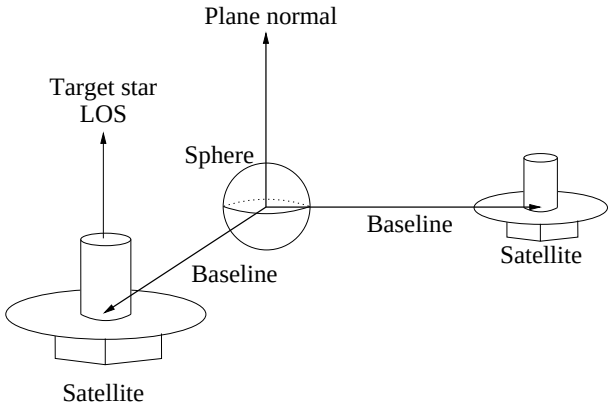

Figure 2.1: *Overview of the satellite formation. The plane spanned by the formation has a normal, that is parallel to the target star LOS.*

2.2 RF Metrology

When the three satellites of SMART-2 are deployed, the optical path of the laser metrology system must be established. In Figure 2.2 the sphere and one satellite is illustrated. The laser leaves the satellite in a known direction. A signal is transmitted from the

sphere, and a receiver in the satellite must estimate a sphere LOS. Knowing the direction of the sphere, the attitude of the satellite must be controlled to point the laser beam towards the sphere. When the laser beam is reflected from the sphere, and the reflected laser beam is directed back to the satellite, the laser metrology system can be activated.

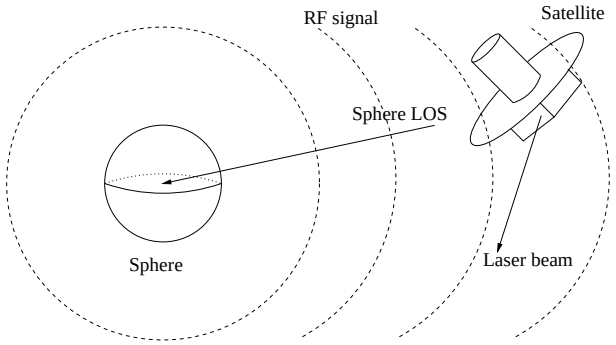

Figure 2.2: *The RF metrology system, uses a transmitter mounted inside the sphere. The receiver at the satellite estimates the sphere LOS and an optical path is acquired for the laser metrology system.*

2.3 Laser Metrology

The laser metrology system, consists of a laser source and a CCD. The CCD measures the return point of the reflected laser beam. In addition the length of the optical path, that is the distance the laser light travels to the sphere and back to the CCD, is measured. The measurements depend on both the attitude and the translation of the satellite, but since the attitude of the satellite is acquired using star trackers, the transition can be decoupled from the measurements.

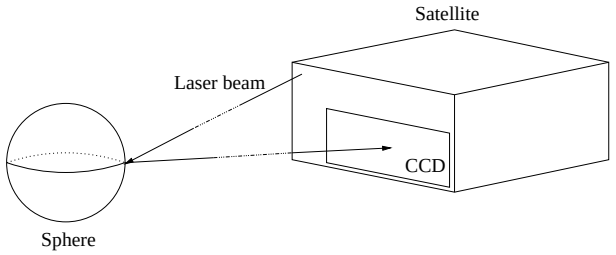

Figure 2.3: *The laser metrology system uses a CCD to measure where the reflected laser beam hits the satellite. In addition the distance of the optical path is measured. Proportions in the figure are exaggerated.*

Chapter 3

Analysis

In this chapter the metrology systems are analyzed mathematically. First the equations needed to obtain the translation error are derived, followed by a the model needed for the simulator, which gives the measurements, based on the simulated translation error. Finally a RF metrology system is analyzed.

3.1 Laser Metrology

This section is a mathematical description of the laser metrology system, used for sensoring formation perturbations. The system is different from that used between three fully equipped satellites, as the laser is reflected by a sphere, instead of being measured directly on the targeted satellite. A spherical geometry is used to minimize the stabilization requirements of the simplified satellite.

Figure 3.1 gives an overview of the system. The satellites reference position is the vector $\boldsymbol{r}_{\mathrm{l}0}$ and the error to the true position is $\boldsymbol{r}_{\epsilon}$. The reflection occurring on the sphere is defined by the tangent plane at the reflection point $\boldsymbol{r}_{\mathrm{r}}$. The laser beam sent from the satellite at an angle γ in the $\boldsymbol{x}_{\mathrm{l}}\boldsymbol{z}_{\mathrm{l}}$ plane is denoted $\boldsymbol{r}_{\mathrm{in}}$ and the reflected beam is denoted $\boldsymbol{r}_{\mathrm{out}}$. The normal to the tangent plane is the vector $\boldsymbol{n}$ and the radius of the sphere is denoted R_{b}.

The frames placed at the center of the sphere and the laser exit point on the satellite respectively, are defined in the following section.

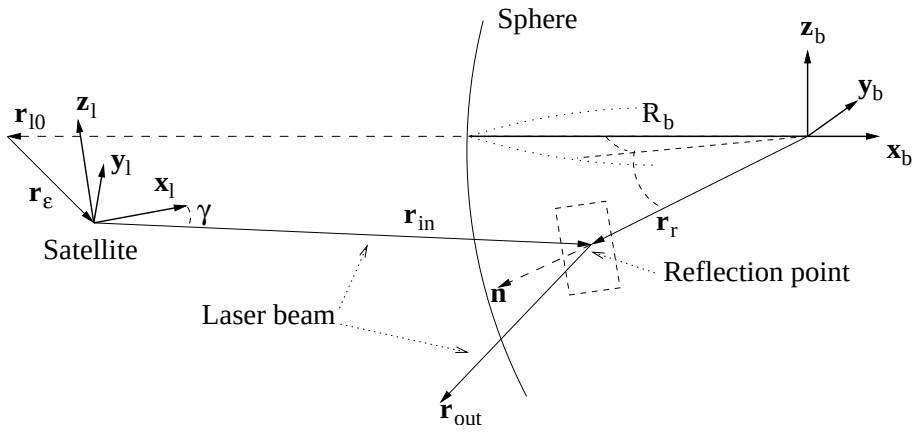

Figure 3.1: *Overview of the laser metrology system, showing the laser beam $\boldsymbol{r}_{in}$, sent towards the sphere from the satellite, and the reflected laser beam $\boldsymbol{r}_{out}$. Both are functions of the satellite's attitude and the position error $\boldsymbol{r}_\epsilon$.*

Frames

Two frames are used to describe the laser metrology system. The laser frame and the sphere frame.

Sphere Frame

The sphere frame is the reference frame of the formation. Its origin is at the center of the sphere. The axes of the system, $\boldsymbol{x}_\mathrm{b}$, $\boldsymbol{y}_\mathrm{b}$ and $\boldsymbol{z}_\mathrm{b}$, are defined by the direction of the star fixed reference system, in which the satellite attitudes are measured using star trackers. Hence the attitude of the satellites are known in this frame. The sphere frame is illustrated in Figure 3.2, together with the star fixed frame spanned by $\boldsymbol{x}_0$, $\boldsymbol{y}_0$ and $\boldsymbol{z}_0$, defining the orientation of $\boldsymbol{x}_\mathrm{b}$, $\boldsymbol{y}_\mathrm{b}$ and $\boldsymbol{z}_\mathrm{b}$.

Laser Frame

The laser frame's origin is at the point where the laser beam exits the plane defined by the surface of the CCD sensor. The $\boldsymbol{x}_\mathrm{l}$ axis is a normal to this plane, and the $\boldsymbol{z}_\mathrm{l}$ axis is in the plane spanned by the $\boldsymbol{x}_\mathrm{l}$ vector and the exiting laser beam $\boldsymbol{r}_\mathrm{in}$, and pointing in the opposite direction as the projection of $\boldsymbol{r}_\mathrm{in}$ onto the plane of the CCD surface. Figure 3.3 illustrates the laser frame. The projection of $\boldsymbol{r}_\mathrm{in}$ onto the CCD plane is denoted $\boldsymbol{p}_\mathrm{in}$ in Figure 3.3. If the projection is the zero vector, that is when γ is zero, $\boldsymbol{z}_\mathrm{l}$ is the negative direction vector to a fixed point on the CCD sensor. The $\boldsymbol{y}_\mathrm{l}$ axis is formed in right handed system.

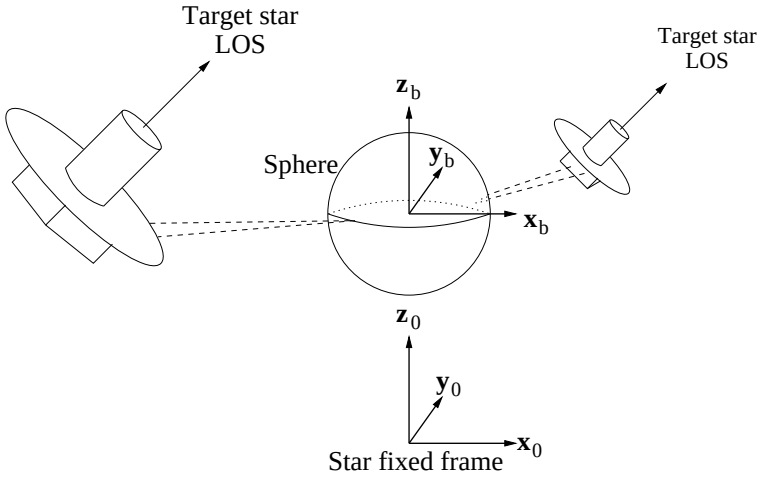

Figure 3.2: *Definition of the sphere frame.*

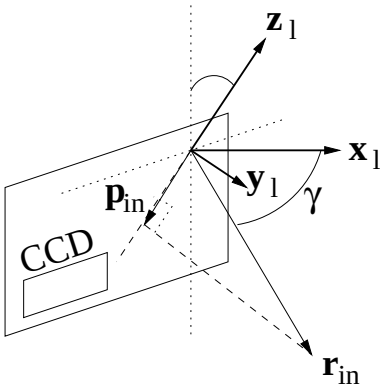

Figure 3.3: *Definition of the laser frame.*

Estimating Satellite Translation

The laser metrology system is based on a known attitude of the satellite, which is measured using star trackers. Since the attitude of the satellite is known, the attitude of the laser frame is also known, because both systems follow the attitude of the satellite, and the fixed attitude between the satellite and the laser frame is known. Figure 3.4 shows the path of the laser beam, $\boldsymbol{r}_{\text{in}}$ and $\boldsymbol{r}_{\text{out}}$, and the vector $\boldsymbol{m}$ measured using a CCD. The vector $\boldsymbol{m}$ is measured in the laser frame. However since the attitude of the satellite is known, it is also given inertially, hence the calculations can be done in either frame.

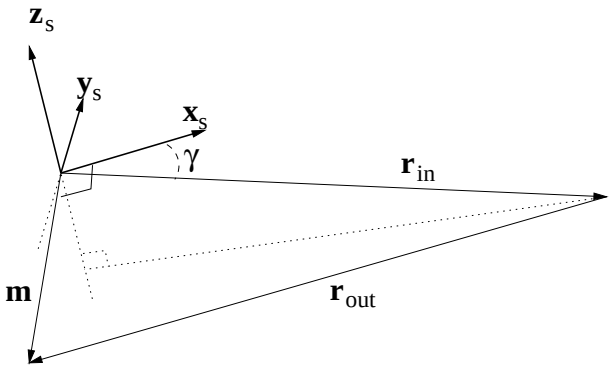

Figure 3.4: *The measurement vector $\boldsymbol{m}$ measured in the laser frame, using a CCD mounted on the satellite.*

The laser metrology system also measures the length of the optical path denoted d, giving

$$d = |\boldsymbol{r}_{\text{in}}| + |\boldsymbol{r}_{\text{out}}| \tag{3.1}$$

Given $\boldsymbol{m}$, d and the attitude of the satellite, the position relative to the sphere is estimated.

The direction of $\boldsymbol{r}_{\text{in}}$ is represented by the unit vector $\hat{\boldsymbol{r}}_{\text{in}}$. Knowing the exit angle γ, $\hat{\boldsymbol{r}}_{\text{in}}$ is given by

$$\hat{\boldsymbol{r}}_{\text{in}} = \begin{bmatrix} \cos(\gamma) \\ 0 \\ -\sin(\gamma) \end{bmatrix} \tag{3.2}$$

Note that the laser frame is defined in a way that makes the second element of $\hat{\boldsymbol{r}}_{\text{in}}$ zero. Using cosine relations on the triangle formed by $\boldsymbol{r}_{\text{in}}$, $\boldsymbol{r}_{\text{out}}$ and $\boldsymbol{m}$, yields

$$|\boldsymbol{r}_{\text{out}}|^2 = |\boldsymbol{r}_{\text{in}}|^2 + |\boldsymbol{m}|^2 - 2\,|\boldsymbol{r}_{\text{in}}|\,|\boldsymbol{m}|\cos\left(\frac{\pi}{2} - \gamma\right) \tag{3.3}$$

From Equation 3.1 it is clear that

$$|\boldsymbol{r}_{\text{out}}| = d - |\boldsymbol{r}_{\text{in}}| \tag{3.4}$$

which combined with Equation 3.3 gives

$$\begin{aligned}
(d - |\boldsymbol{r}_{\text{in}}|)^2 &= |\boldsymbol{r}_{\text{in}}|^2 + |\boldsymbol{m}|^2 - 2\,|\boldsymbol{r}_{\text{in}}|\,|\boldsymbol{m}|\cos\left(\frac{\pi}{2} - \gamma\right) \\
\Updownarrow& \\
d^2 - 2d\,|\boldsymbol{r}_{\text{in}}| &= |\boldsymbol{m}|^2 - 2\,|\boldsymbol{r}_{\text{in}}|\,|\boldsymbol{m}|\cos\left(\frac{\pi}{2} - \gamma\right) \\
\Updownarrow& \\
2\,|\boldsymbol{r}_{\text{in}}|\,|\boldsymbol{m}|\cos\left(\frac{\pi}{2} - \gamma\right) - 2d\,|\boldsymbol{r}_{\text{in}}| &= |\boldsymbol{m}|^2 - d^2 \\
\Updownarrow& \\
2\,|\boldsymbol{r}_{\text{in}}|\left[|\boldsymbol{m}|\cos\left(\frac{\pi}{2} - \gamma\right) - d\right] &= |\boldsymbol{m}|^2 - d^2 \\
\Updownarrow& \\
|\boldsymbol{r}_{\text{in}}| &= \frac{|\boldsymbol{m}|^2 - d^2}{2\left[|\boldsymbol{m}|\cos\left(\frac{\pi}{2} - \gamma\right) - d\right]}
\end{aligned} \tag{3.5}$$

Given the direction and length of $\boldsymbol{r}_{\text{in}}$ from Equations 3.2 and 3.5 respectively, the vector is acquired by

$$\begin{aligned}
\boldsymbol{r}_{\text{in}} &= |\boldsymbol{r}_{\text{in}}|\,\hat{\boldsymbol{r}}_{\text{in}} \\
&= \frac{|\boldsymbol{m}|^2 - d^2}{2\left[|\boldsymbol{m}|\cos\left(\frac{\pi}{2} - \gamma\right) - d\right]} \begin{bmatrix} \cos(\gamma) \\ 0 \\ -\sin(\gamma) \end{bmatrix}
\end{aligned} \tag{3.6}$$

From Figure 3.4 it is clear that

$$\boldsymbol{r}_{\text{out}} = \boldsymbol{m} - \boldsymbol{r}_{\text{in}} \tag{3.7}$$

Since the attitude of the laser frame relative to the sphere frame is known, all vectors are known in both frames. Recall that the attitude of the laser frame is given by the attitude of the satellite and a fixed rotation.

If the attitude matrix $\boldsymbol{A}_b^l$ represents the attitude of the laser frame relative to the sphere frame, the vectors $\boldsymbol{r}_{\text{in}}^b$ and $\boldsymbol{r}_{\text{out}}^b$ in the sphere frame are given by

$$\boldsymbol{r}_{\text{in}}^b = \left(\boldsymbol{A}_b^l\right)^{\text{T}} \boldsymbol{r}_{\text{in}}^l \tag{3.8}$$

$$\boldsymbol{r}_{\text{out}}^b = \left(\boldsymbol{A}_b^l\right)^{\text{T}} \boldsymbol{r}_{\text{out}}^l \tag{3.9}$$

where $\boldsymbol{r}_{\text{in}}^l$ and $\boldsymbol{r}_{\text{out}}^l$ are given in the laser frame, and $\left(\boldsymbol{A}_b^l\right)^{\text{T}}$ is equivalent to $\boldsymbol{A}_l^b$. If the superscript is not given in the following equations, the vectors are given in the sphere frame.

In Figure 3.5 it can be seen that in order to calculate the translation error $\boldsymbol{r}_\epsilon$ from the known reference $\boldsymbol{r}_{\text{l0}}$ the vector $\boldsymbol{r}_{\text{r}}$, which is the vector to the reflection point, must be found. Knowing the vectors $\boldsymbol{r}_{\text{in}}$ and $\boldsymbol{r}_{\text{out}}$, the reflection point on the sphere can be found from the angle between the vectors.

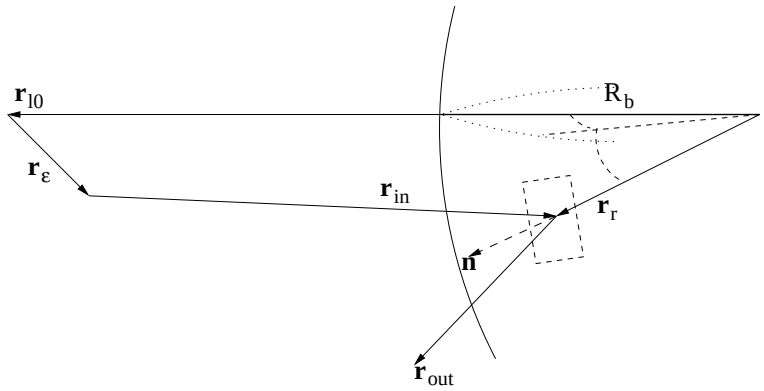

Figure 3.5: *The vectors needed to calculate the translation error* $\boldsymbol{r}_\epsilon$.

The length of $\boldsymbol{r}_{\text{r}}$ is the radius of the sphere, and the direction is the same as the normal to the tangent plane at the reflection point. The unit normal vector $\boldsymbol{n}$ can be calculated by

$$\boldsymbol{n} = \frac{\hat{\boldsymbol{r}}_{\text{out}} - \hat{\boldsymbol{r}}_{\text{in}}}{\left|\hat{\boldsymbol{r}}_{\text{out}} - \hat{\boldsymbol{r}}_{\text{in}}\right|} \tag{3.10}$$

That Equation 3.10 holds can be seen from figures 3.6 and 3.7. The frame in Figure 3.6 has origin at the reflection point, and the $\boldsymbol{x}_{\text{r}}$ axis is a normal to the tangent plane

spanned by the $\boldsymbol{y}_{\mathrm{r}}$ and $\boldsymbol{z}_{\mathrm{r}}$ axes. It is clear that the angle between the projections of the incoming and exiting laser beams onto the $\boldsymbol{y}_{\mathrm{r}}\boldsymbol{z}_{\mathrm{r}}$ plane is π. This means that the $\boldsymbol{x}_{\mathrm{r}}$ axis is always in the subspace, spanned by $\boldsymbol{r}_{\mathrm{in}}$ and $\boldsymbol{r}_{\mathrm{out}}$, unless the two vectors are parallel, in which case no reflection occurs.

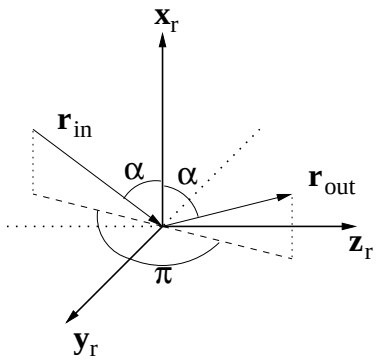

Figure 3.6: *Reflection of a laser beam on the $\boldsymbol{yz}$ tangent plane with normal $\boldsymbol{x}$.*

Figure 3.7 illustrates the sum of to equal length vectors. The angle between the two vectors is 2α which is the case in a reflection, as shown in Figure 3.6. It is clear that the sum of $\boldsymbol{r}_{\mathrm{in}}$ and $\boldsymbol{r}_{\mathrm{out}}$ is a vector angled equally between the two.

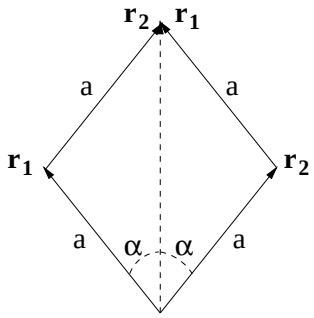

Figure 3.7: *The sum of two equal length vectors.*

Realizing from Figures 3.6 and 3.7, that

$$\boldsymbol{r}_1 = -\boldsymbol{r}_{\mathrm{in}} \tag{3.11}$$

$$\boldsymbol{r}_2 = \boldsymbol{r}_{\mathrm{out}} \tag{3.12}$$

and normalizing all vectors to unit vectors, Equation 3.10 is shown. Since the normalized sum of $\boldsymbol{r}_{\mathrm{in}}$ and $\boldsymbol{r}_{\mathrm{out}}$ is equally angled between the two and in the same subspace, the vector is a normal to the tangent plane of the sphere at the reflection point.

Knowing the plane normal $\boldsymbol{n}$, the vector $\boldsymbol{r}_{\mathrm{r}}$ is given by

$$\begin{aligned} \boldsymbol{r}_{\mathrm{r}} &= R_b \boldsymbol{n} \\ &= R_b \frac{\hat{\boldsymbol{r}}_{\mathrm{out}} - \hat{\boldsymbol{r}}_{\mathrm{in}}}{|\hat{\boldsymbol{r}}_{\mathrm{out}} - \hat{\boldsymbol{r}}_{\mathrm{in}}|} \end{aligned} \tag{3.13}$$

where R_b is the radius of the sphere. From Figure 3.5 it is clear that

$$\boldsymbol{r}_{\mathrm{r}} = \boldsymbol{r}_{\mathrm{l0}} + \boldsymbol{r}_{\epsilon} + \boldsymbol{r}_{\mathrm{in}} \tag{3.14}$$

which solved for $\boldsymbol{r}_{\epsilon}$, yields

$$\boldsymbol{r}_{\epsilon} = \boldsymbol{r}_{\mathrm{r}} - \boldsymbol{r}_{\mathrm{l0}} - \boldsymbol{r}_{\mathrm{in}} \tag{3.15}$$

where $\boldsymbol{r}_{\mathrm{r}}$ is given in Equation 3.13 and $\boldsymbol{r}_{\mathrm{in}}$ in Equation 3.6. Note that $\boldsymbol{r}_{\mathrm{in}}$ and $\boldsymbol{r}_{\mathrm{out}}$ are obtained in the laser frame, and must be rotated to the sphere frame using Equations 3.8 and 3.9, when used in Equation 3.13 and Equation 3.15. Equation 3.15 is the sought translational error of the satellite, to its reference position.

Placing the Laser on the Satellite

A problem arises when placing the laser on the satellite, since the point where the laser beam exits the satellite must be cleared. This means that the reflecting beam cannot be measured at this point, since a CCD in this place would block the laser. The problem is illustrated in Figure 3.8.

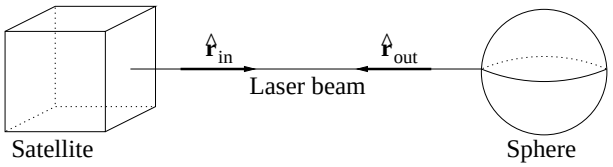

Figure 3.8: *Bad configuration. The reflected laser beam cannot be measured, since a CCD would block the optical path.*

In order to overcome this problem, the laser must be either moved, angled or both, as illustrated in Figure 3.9. The laser beam has been moved to a corner of the satellite, and angled in order to keep then reflected beam on the side of the satellite. The angle γ in the previous section, is introduced for this purpose.

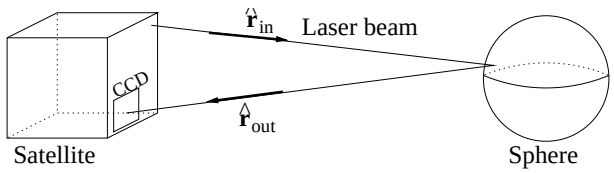

Figure 3.9: *Good configuration. The reflected laser beam is not near the laser exit point of the satellite.*

Calculating Reference Vector and Attitude

The fixed rotation and translation of the laser frame can be calculated when the laser has been placed on the satellite. Usually a satellite is controlled using a satellite frame, e.g. placed conveniently from a dynamics point of view. Hence the reference attitude and position are also given in this frame. Since the laser frame is also placed at a fixed point on the satellite, the rotation and translation between the two frames are constant, hence the references can be given in this frame.

Define an arbitrary frame on the satellite by the vectors $\boldsymbol{x}_s$, $\boldsymbol{y}_s$ and $\boldsymbol{z}_s$, which has the known reference vector $\boldsymbol{r}_{s0}$.

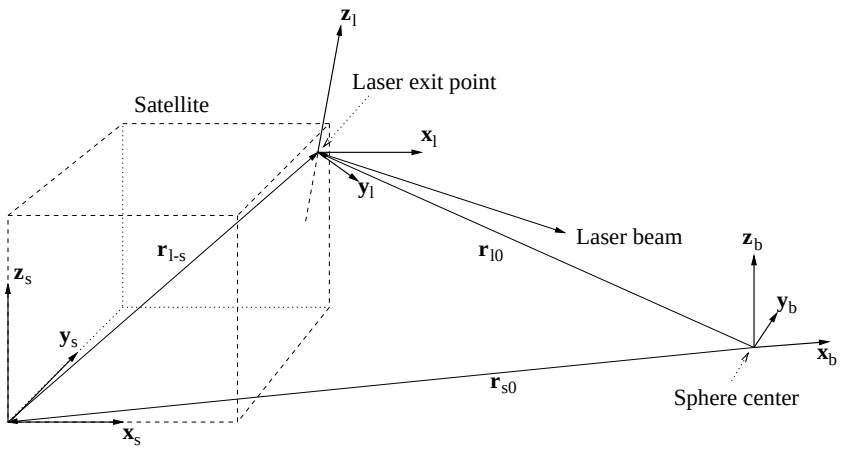

Figure 3.10: *Obtaining the reference vector of the laser frame, given the reference of the satellite frame and the known placement of the laser exit point.*

The frame is illustrated together with the laser frame and sphere frame in Figure 3.10. The satellite frame is to be placed at reference position $\boldsymbol{r}_{s0}$. The estimation of the translation error requires that this reference is modified to a reference for the laser frame.

From Figure 3.10 it is seen that the reference of the laser frame $\boldsymbol{r}_{l0}$ is given by

$$\boldsymbol{r}_{\text{l0}} = \boldsymbol{r}_{\text{s0}} + \boldsymbol{r}_{\text{l-s}} \tag{3.16}$$

Since the position of the laser frame is conveniently given in the satellite frame, Equation 3.16 is written

$$\boldsymbol{r}_{\text{l0}} = \boldsymbol{r}_{\text{s0}} + \left(\boldsymbol{A}_b^{s0}\right)^{\text{T}} \boldsymbol{r}_{\text{l-s}}^{s} \tag{3.17}$$

where $\boldsymbol{A}_b^{s0}$ denotes the attitude of the satellite's reference frame, denoted s0, relative to the sphere frame.

As with the reference position, the reference attitude of the satellite must also be modified into a reference for the laser frame.

From the definition of the laser frame, it is known that the attitude of the laser frame relative to the satellite frame will be a function of the angle γ. It is also a function of the orientation of the CCD plane frame spanned by $\boldsymbol{x}_{\text{p}}$, $\boldsymbol{y}_{\text{p}}$ and $\boldsymbol{z}_{\text{p}}$ illustrated in Figure 3.11.

The plane frame represents the orientation of the satellite surface, on which the CCD is mounted. The attitude of the plane frame relative to the satellite frame is given when the side of the satellite, on which to mount the laser, is chosen, and is denoted $\boldsymbol{A}_s^p$.

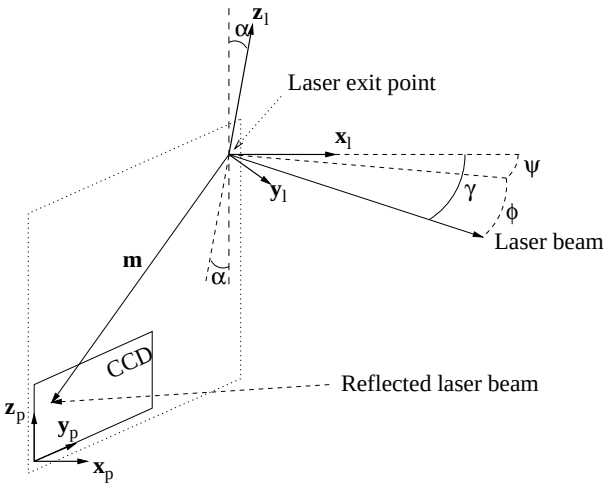

Figure 3.11: *Obtaining the attitude of the laser frame, given the yaw ψ and pitch ϕ in the plane frame of the exiting laser beam.*

The angle γ is a pitch in the laser frame, but can also be expressed as a yaw and pitch in the plane frame, given by the angles ψ and ϕ respectively. The rotation of the laser frame relative to the plane frame is a rotation α about the $\boldsymbol{x}_{\text{p}}$ axis given by the angles ψ and ϕ (Figure 3.11). The angles ψ and ϕ define the direction of $\boldsymbol{r}_{\text{in}}$ in spherical coordinates.

The unit vector pointing in the same direction and converted into Cartesian coordinates, is given by

$$\hat{\boldsymbol{r}}_{\text{in}} = \begin{bmatrix} \sin\left(\frac{\pi}{2}+\phi\right)\cos\left(\psi\right) \\ \sin\left(\frac{\pi}{2}+\phi\right)\sin\left(\psi\right) \\ \cos\left(\frac{\pi}{2}+\phi\right) \end{bmatrix} \tag{3.18}$$

in the plane frame. The angle α is the angle between the projection of $-\hat{\boldsymbol{r}}_{\text{in}}$ onto the $\boldsymbol{y}_{\text{p}}\boldsymbol{z}_{\text{p}}$ plane and the $\boldsymbol{z}_{\text{p}}$ axis. Note that the $\boldsymbol{z}_{\text{l}}$ vector is in fact equal to $-\hat{\boldsymbol{r}}_{\text{in}}$, given by the definition of the laser frame in Section 3.1 unless ψ and ϕ are zero. The projection of $-\hat{\boldsymbol{r}}_{\text{in}}$ onto the $\boldsymbol{y}_{\text{p}}\boldsymbol{z}_{\text{p}}$, denoted $\boldsymbol{z}_{\text{l}}^{p}$, is by definition of Cartesian coordinates

$$\boldsymbol{z}_{\text{l}}^{p} = \begin{bmatrix} 0 \\ -\sin\left(\frac{\pi}{2}+\phi\right)\sin\left(\psi\right) \\ -\cos\left(\frac{\pi}{2}+\phi\right) \end{bmatrix} \tag{3.19}$$

The angle between $\boldsymbol{z}_{\text{l}}^{p}$ and $\boldsymbol{z}_{\text{p}}$ is for two unit vectors

$$\alpha = \cos^{-1}\left(\left(\boldsymbol{z}_{\text{l}}^{p}\right)^{\text{T}}\boldsymbol{z}_{\text{p}}\right) \tag{3.20}$$

The exception is when the projection $\boldsymbol{z}_{\text{l}}^{p}$ is the zero vector, which is the case when ψ and ϕ are zero. Then $\boldsymbol{z}_{\text{l}}^{p}$ is instead defined in Section 3.1 to be in the negative direction of a fixed point on the CCD sensor. Hence α is in this case given by the placement of the CCD sensor.

The attitude matrix $\boldsymbol{A}_{p}^{l}$, describing the rotation α of the laser frame about the $\boldsymbol{x}_{\text{p}}$ axis, is given by

$$\boldsymbol{A}_{p}^{l} = \begin{bmatrix} 1 & 0 & 0 \\ 0 & \cos\left(\alpha\right) & \sin\left(\alpha\right) \\ 0 & -\sin\left(\alpha\right) & \cos\left(\alpha\right) \end{bmatrix} \tag{3.21}$$

The sought attitude of the laser plane relative to the satellite plane can now be calculated, and is given by the matrix

$$\boldsymbol{A}_{s}^{l} = \boldsymbol{A}_{p}^{l}\boldsymbol{A}_{s}^{p} \tag{3.22}$$

3.2 Simulation Model

In Section 3.1 a method for estimating the satellite translation based on the measurements is derived. When simulating the system, a method for calculating the measurements based on the simulated translation is sought.

In Figure 3.1 on page 24 two frames are illustrated. Since the attitude of the laser frame is known, the direction of $\boldsymbol{r}_{\text{in}}$ is known in the sphere frame, represented by the unit vector $\hat{\boldsymbol{r}}_{\text{in}}$. Given the reference position $\boldsymbol{r}_{\text{l0}}$ and the translation $\boldsymbol{r}_{\epsilon}$, the parameter equation of the laser beam exiting the satellite is

$$\begin{bmatrix} x \\ y \\ z \end{bmatrix} = [\boldsymbol{r}_{\text{l0}} + \boldsymbol{r}_{\epsilon}] + \hat{\boldsymbol{r}}_{\text{in}} p \ , \quad p \in \Re \tag{3.23}$$

where p is a free parameter. The equation of the sphere surface centered at the origin of the sphere frame is

$$\begin{bmatrix} x \\ y \\ z \end{bmatrix}^{\text{T}} \begin{bmatrix} x \\ y \\ z \end{bmatrix} = R_{\text{b}}^2 \tag{3.24}$$

where R_{b} is the radius of the sphere. In order to find the reflection point, given by the vector $\boldsymbol{r}_{\text{r}}$, the value of parameter p in Equation 3.23 at the surface of the sphere is sought. Inserting Equation 3.23 in 3.24 yields

$$\begin{aligned}
&[(\boldsymbol{r}_{\text{l0}} + \boldsymbol{r}_{\epsilon}) + \hat{\boldsymbol{r}}_{\text{in}} p]^{\text{T}} [(\boldsymbol{r}_{\text{l0}} + \boldsymbol{r}_{\epsilon}) + \hat{\boldsymbol{r}}_{\text{in}} p] = R_{\text{b}}^2 \\
\Updownarrow \\
&\left[(\boldsymbol{r}_{\text{l0}} + \boldsymbol{r}_{\epsilon})^{\text{T}} + \hat{\boldsymbol{r}}_{\text{in}}^{\text{T}} p\right] [(\boldsymbol{r}_{\text{l0}} + \boldsymbol{r}_{\epsilon}) + \hat{\boldsymbol{r}}_{\text{in}} p] = R_{\text{b}}^2 \\
\Updownarrow \\
&(\boldsymbol{r}_{\text{l0}} + \boldsymbol{r}_{\epsilon})^{\text{T}} (\boldsymbol{r}_{\text{l0}} + \boldsymbol{r}_{\epsilon}) + \left[\hat{\boldsymbol{r}}_{\text{in}}^{\text{T}} (\boldsymbol{r}_{\text{l0}} + \boldsymbol{r}_{\epsilon}) + (\boldsymbol{r}_{\text{l0}} + \boldsymbol{r}_{\epsilon})^{\text{T}} \hat{\boldsymbol{r}}_{\text{in}}\right] p + \hat{\boldsymbol{r}}_{\text{in}}^{\text{T}} \hat{\boldsymbol{r}}_{\text{in}} p^2 = R_{\text{b}}^2
\end{aligned}$$

which gives the second order polynomial equation

$$\hat{\boldsymbol{r}}_{\text{in}}^{\text{T}} \hat{\boldsymbol{r}}_{\text{in}} p^2 + \left[\hat{\boldsymbol{r}}_{\text{in}}^{\text{T}} (\boldsymbol{r}_{\text{l0}} + \boldsymbol{r}_{\epsilon}) + (\boldsymbol{r}_{\text{l0}} + \boldsymbol{r}_{\epsilon})^{\text{T}} \hat{\boldsymbol{r}}_{\text{in}}\right] p + (\boldsymbol{r}_{\text{l0}} + \boldsymbol{r}_{\epsilon})^{\text{T}} (\boldsymbol{r}_{\text{l0}} + \boldsymbol{r}_{\epsilon}) - R_{\text{b}}^2 = 0 \tag{3.25}$$

The roots of this equation corresponds to the two points where the line of Equation 3.23 is on the surface of the sphere. Since the sphere is reflecting, and not transparent, the reflection point will be at the shortest distance from the point $(\boldsymbol{r}_{\text{l0}} + \boldsymbol{r}_{\epsilon})$, where the value of p is denoted p_{r}. Upon calculating the roots p_1 and p_2 of Equation 3.25, p_{r} is chosen by the rule

$$p_{\text{r}} = \begin{cases} p_1 & \text{if } |p_1| \leqslant |p_2| \\ p_2 & \text{if } |p_1| > |p_2| \end{cases} \tag{3.26}$$

The cases of complex or equal roots, corresponding to the laser not hitting the sphere or being a tangent to the sphere surface, are not considered, since no reflections occur.

Given p_{r} the vectors $\boldsymbol{r}_{\text{r}}$ and $\boldsymbol{r}_{\text{in}}$ are given using Equation 3.23 by

$$\boldsymbol{r}_{\text{r}} = [\boldsymbol{r}_{\text{l0}} + \boldsymbol{r}_{\epsilon}] + \hat{\boldsymbol{r}}_{\text{in}} p_{\text{r}} \tag{3.27}$$

$$\boldsymbol{r}_{\text{in}} = \hat{\boldsymbol{r}}_{\text{in}} p_{\text{r}} \tag{3.28}$$

It is seen from Figure 3.6 on page 29, that in a frame where the $\boldsymbol{x}$ axis is normal to the tangent plane, the direction of the reflected laser beam $\hat{\boldsymbol{r}}_{\text{out}}$ is given by

$$\hat{\boldsymbol{r}}_{\text{out}} = \begin{bmatrix} -1 & 0 & 0 \\ 0 & 1 & 0 \\ 0 & 0 & 1 \end{bmatrix} \hat{\boldsymbol{r}}_{\text{in}} \tag{3.29}$$

which is a change of sign in the first element of $\hat{\boldsymbol{r}}_{\text{in}}$.

Equation 3.29 only holds in a frame where the $\boldsymbol{y}$ and $\boldsymbol{z}$ axes span the reflection plane. Hence a reflection frame is defined, in order to calculate $\hat{\boldsymbol{r}}_{\text{out}}$.

Define the reflection frame illustrated in Figure 3.12. The $\boldsymbol{x}_{\text{r}}$ axis is the normal pointing out of the sphere, to the tangent plane spanned by $\boldsymbol{y}_{\text{r}}$ and $\boldsymbol{z}_{\text{r}}$. The $\boldsymbol{y}_{\text{r}}$ and $\boldsymbol{z}_{\text{r}}$ axes are defined such that they are parallel to $\boldsymbol{y}_{\text{b}}$ and $\boldsymbol{z}_{\text{b}}$ axes in the sphere frame, when ψ and ϕ are zero. Note that ψ is larger than π in the figure. Hence the attitude of the plane frame is given by ψ and ϕ which also define the vector $\boldsymbol{r}_{\text{r}}$ in spherical coordinates, knowing the radius of the sphere.

Given $\boldsymbol{r}_{\text{r}}$ from Equation 3.27 the angles ψ and ϕ can be found by

$$\psi = \tan^{-1}\left(\frac{r_{\text{r2}}}{r_{\text{r1}}}\right) \tag{3.30}$$

$$\phi = \cos^{-1}\left(\frac{r_{\text{r3}}}{\sqrt{r_{\text{r1}}^2 + r_{\text{r2}}^2 + r_{\text{r3}}^2}}\right) - \frac{\pi}{2} \tag{3.31}$$

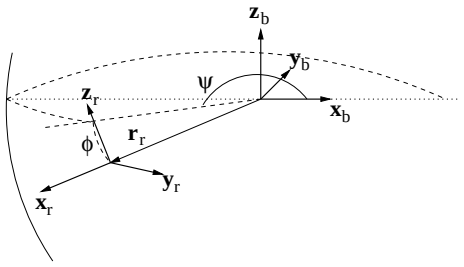

Figure 3.12: *Definition of the reflection frame.*

where r_{r1}, r_{r2} and r_{r3} are the scalar elements of the $\boldsymbol{r}_r$ vector. The attitude matrix $\boldsymbol{A}_b^r$, representing the rotation of the reflection frame with respect to the sphere frame, is obtained using

$$\boldsymbol{A}_b^r = \boldsymbol{A}_2 \boldsymbol{A}_3 \tag{3.32}$$

where $\boldsymbol{A}_2$ and $\boldsymbol{A}_3$ represent the principal rotations about the $\boldsymbol{y}_r$ and $\boldsymbol{z}_r$ axes respectively. This is equivalent to a 3-2-1 Euler sequence, where the rotation around the $\boldsymbol{x}_r$ is zero, consequently the rotation matrix $\boldsymbol{A}_1$ is the identity matrix $\mathbf{1}_{3\times 3}$. The matrices are given by

$$\boldsymbol{A}_2 = \begin{bmatrix} \cos(\phi) & 0 & -\sin(\phi) \\ 0 & 1 & 0 \\ \sin(\phi) & 0 & \cos(\phi) \end{bmatrix} \tag{3.33}$$

$$\boldsymbol{A}_3 = \begin{bmatrix} \cos(\psi) & \sin(\psi) & 0 \\ -\sin(\psi) & \cos(\psi) & 0 \\ 0 & 0 & 1 \end{bmatrix} \tag{3.34}$$

which inserted into Equation 3.32, yields

$$\boldsymbol{A}_b^r = \begin{bmatrix} \cos(\phi)\cos(\psi) & \cos(\phi)\sin(\psi) & -\sin(\phi) \\ -\sin(\psi) & \cos(\psi) & 0 \\ \sin(\phi)\cos(\psi) & \sin(\phi)\sin(\psi) & \cos(\phi) \end{bmatrix} \tag{3.35}$$

The vector $\hat{\boldsymbol{r}}_{\text{in}}$ can now be rotated into the reflection frame, and $\hat{\boldsymbol{r}}_{\text{out}}$ is found in the sphere frame by

$$\hat{\boldsymbol{r}}_{\text{out}} = (\boldsymbol{A}_b^r)^{\text{T}} \begin{bmatrix} -1 & 0 & 0 \\ 0 & 1 & 0 \\ 0 & 0 & 1 \end{bmatrix} \boldsymbol{A}_b^r \hat{\boldsymbol{r}}_{\text{in}} \tag{3.36}$$

using the property of Equation 3.29.

The measurement $\boldsymbol{m}$ can be calculated using the properties of the triangle illustrated in Figure 3.13. The known elements of the triangle is γ, $\boldsymbol{r}_{\text{in}}$ and $\hat{\boldsymbol{r}}_{\text{out}}$.

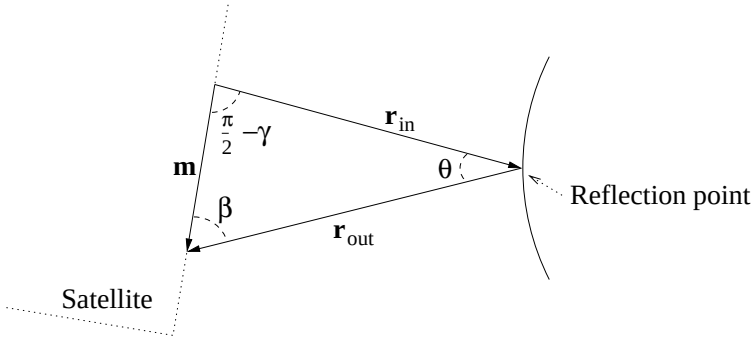

Figure 3.13: *Illustration of the reflected laser beam, and the measurement vector on the satellite.*

The angle θ is given by the angle between $-\hat{\boldsymbol{r}}_{\text{in}}$ and $\hat{\boldsymbol{r}}_{\text{out}}$, which for unit vectors is

$$\theta = \cos^{-1}\left(-\hat{\boldsymbol{r}}_{\text{in}}^{\text{T}}\hat{\boldsymbol{r}}_{\text{out}}\right) \tag{3.37}$$

giving the final angle

$$\begin{aligned}\beta &= \pi - \left(\frac{\pi}{2} - \gamma + \theta\right) \\ &= \frac{\pi}{2} + \gamma - \theta\end{aligned} \tag{3.38}$$

Using sine relations, the length of $\boldsymbol{r}_{\text{out}}$ is given by

$$|\boldsymbol{r}_{\text{out}}| = |\boldsymbol{r}_{\text{in}}| \frac{\sin\left(\frac{\pi}{2} - \gamma\right)}{\sin\left(\beta\right)} \tag{3.39}$$

The vector $\boldsymbol{r}_{\text{out}}$ can now be fully determined by

$$\boldsymbol{r}_{\text{out}} = |\boldsymbol{r}_{\text{out}}|\,\hat{\boldsymbol{r}}_{\text{out}} \tag{3.40}$$

Finally the sought measurement vector $\boldsymbol{m}$ is given from Figure 3.13, as

$$\boldsymbol{m} = \boldsymbol{r}_{\text{in}} + \boldsymbol{r}_{\text{out}} \tag{3.41}$$

In addition the distance of the optical path d of the laser beam, is calculated by

$$d = |\boldsymbol{r}_{\text{in}}| + |\boldsymbol{r}_{\text{out}}| \tag{3.42}$$

3.3 RF Metrology

This section briefly describes the RF system needed before the laser metrology system can be activated. When the satellites of the formation are released, the optical path to the sphere must be established. Since the conditions after release are random, within a given spherical radius, an omni-directional sensor system is needed.

The main problem of using RF metrology is power. To keep the sphere satellite at low cost, the use of solar panels should be avoided, since it would require stabilization of the sphere. Otherwise the laser beam could hit the solar panels instead of the spherical mirror. However the use of batteries mounted inside the sphere solves this problem, but will limit the operational time of the RF metrology system. To minimize power consumption it is chosen to transmit a simple sine signal from the sphere, and fit the two fully equipped satellites with antennas, capable of measuring a LOS vector to the sphere.

Measuring the LOS Vector

The concept of using an array of antennas to measure the LOS vector is equivalent to the one used in GPS based attitude determination, where an array of antennas measure an LOS vector in a body frame. Figure 3.14 shows a baseline $\boldsymbol{b}$ spanned by the master and slave antennas. Given an incoming wave signal, a phase difference p, between the measurements is acquired.

It is seen from Figure 3.14 that the phase difference p, between the signals on the two antennas, is the length of a projection vector, obtained by projecting the baseline onto the LOS vector pointing towards the signal source. The length of this projection is written

$$p = \left| \frac{\boldsymbol{b} \cdot \hat{\boldsymbol{r}}_{\text{LOS}}}{|\hat{\boldsymbol{r}}_{\text{LOS}}|^2} \hat{\boldsymbol{r}}_{\text{LOS}} \right| = \boldsymbol{b} \cdot \hat{\boldsymbol{r}}_{\text{LOS}} \, |\hat{\boldsymbol{r}}_{\text{LOS}}| = \boldsymbol{b} \cdot \hat{\boldsymbol{r}}_{\text{LOS}} \tag{3.43}$$

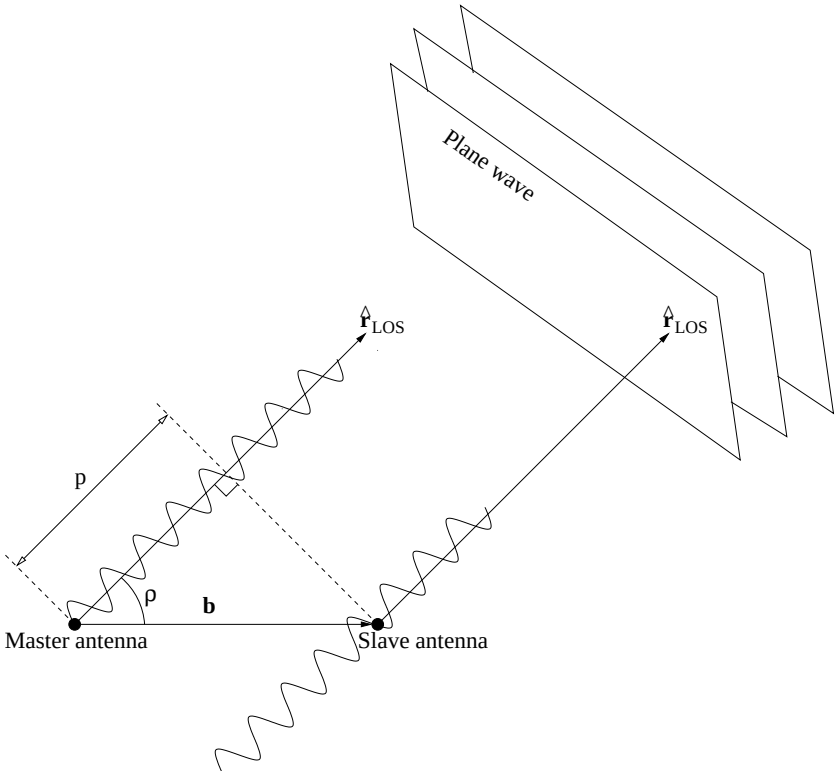

Figure 3.14: *Two antennas measuring the same wave signal but with a phase shift p, depending on the angle ρ. The plane wave is generated by a source in the direction of $\hat{\boldsymbol{r}}_{LOS}$.*

The length of the opposite projection p', that is the projection of the LOS vector onto the baseline, is given by

$$p' = \left| \frac{\hat{\boldsymbol{r}}_{\text{LOS}} \cdot \boldsymbol{b}}{|\boldsymbol{b}|^2} \boldsymbol{b} \right| = \frac{\hat{\boldsymbol{r}}_{\text{LOS}} \cdot \boldsymbol{b}}{|\boldsymbol{b}|^2} |\boldsymbol{b}| = \frac{p}{|\boldsymbol{b}|} \tag{3.44}$$

Knowing that the projection of the LOS vector onto a baseline can be obtained using Equation 3.44, the baselines can be chosen to form a Cartesian coordinate system, as shown in Figure 3.15.

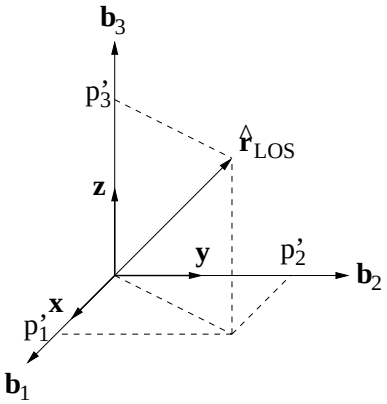

Figure 3.15: *Defining three baselines on the axes of a Cartesian coordinate system.*

By definition of the Cartesian coordinates, the LOS vector to the signal source, is

$$\hat{\boldsymbol{r}}_{\text{LOS}} = \begin{bmatrix} p'_1 \\ p'_2 \\ p'_3 \end{bmatrix} = \begin{bmatrix} \frac{p_1}{|\boldsymbol{b}_1|} \\ \frac{p_2}{|\boldsymbol{b}_2|} \\ \frac{p_3}{|\boldsymbol{b}_3|} \end{bmatrix} \tag{3.45}$$

where p_1, p_2, and p_3 are the phase differences measured by antennas spanning the baselines $\boldsymbol{b}_1$, $\boldsymbol{b}_2$, $\boldsymbol{b}_3$, respectively. Note that the baseline vector is defined pointing from the master antenna to the slave antenna, hence the master antenna will, in the configuration shown in Figure 3.15, be at the origin of the $\boldsymbol{xyz}$ frame and is common for all three baselines.

Required Number of Baselines

That in fact three baselines are necessary, is best shown by illustration. In Figure 3.16 one baseline is illustrated. Given a phase difference between the measurement on the

two antennas of the baseline, an infinite number of unit LOS vectors are found, defining a circle around the baseline. This circle represents the solutions of LOS vectors, that results in the given phase difference p, when projecting them onto the baseline $\boldsymbol{b}_1$. An arbitrary solution is also illustrated in the figure.

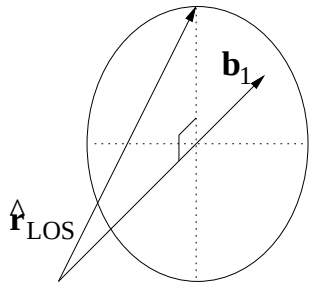

Figure 3.16: *Illustration of the infinite number of unit LOS vectors, which will result in a measured phase difference on baseline $\boldsymbol{b}_1$, represented by the circle around the baseline.*

Using two baselines, as shown in Figure 3.17, will result in an overlap of the two circles. The intersections of the two circles represents the only two solutions, giving a unit LOS vector resulting in two measured phase differences. One of these solutions is illustrated in the figure.

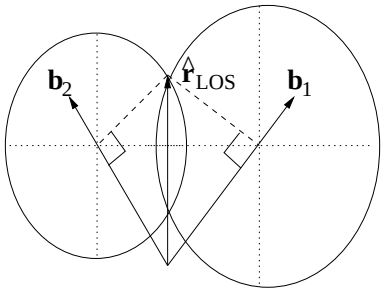

Figure 3.17: *Illustration of the infinite number of solutions giving the phase measurement on either baseline. The intersection of the circles are the two unit LOS vectors, which result in given measurements from both baselines.*

In order to acquire an unique solution, a third baseline must be used, as it is shown in Figure 3.18. Hence using three non-parallel baselines, a unique unit LOS vector can be found. Using three mutual orthogonal baselines, results in the solution given in Equation 3.45.

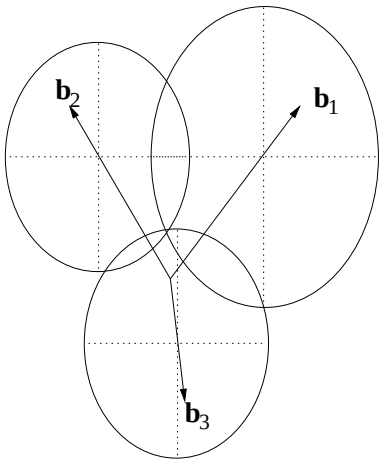

Figure 3.18: *Illustration of three baselines. The intersection of the three circles defines the unit LOS vector resulting in the three measurements obtained on the baselines.*

Establishing The Optical Path

Given the direction of the sphere from Equation 3.45, and a unit vector $\hat{\boldsymbol{r}}_{\mathrm{b}}$, which should be pointed in the same direction, an expression of the attitude error is sought. The vector $\hat{\boldsymbol{r}}_{\mathrm{b}}$ is introduced because the LOS vector of the sphere, measured on the spacecraft, is the direction of the transmitted signal, and not the point to where the laser beam should be pointed. $\hat{\boldsymbol{r}}_{\mathrm{b}}$ is the vector that must be parallel to the sphere LOS, in order to acquire the optical path of the laser metrology system. The vector is given when the direction of the exiting laser beam is chosen. The attitude error is to be interpreted as the rotation of the satellite needed, in order to point the laser towards the sphere.

Due to an attitude error between the satellite frame and the sphere frame, the vectors $\hat{\boldsymbol{r}}_{\mathrm{LOS}}$ and $\hat{\boldsymbol{r}}_{\mathrm{b}}$ are not parallel. From Figure 3.19 it can be seen that the attitude error is a rotation β around a vector, given by the cross-product of the two vectors. Note that the vector $\hat{\boldsymbol{r}}_{\mathrm{LOS}}$ is locked with respect to a reference frame. Hence a rotation of the satellite, will change the angle between the vectors.

The attitude error of the satellite, can be expressed by the quaternion $\boldsymbol{q}_{\epsilon}$, and is given by [Dan Bhanderi et al., 2000]

$$\boldsymbol{q}_{\epsilon} = \begin{bmatrix} \cos\left(\frac{\alpha}{2}\right) \\ \hat{\boldsymbol{r}}\sin\left(\frac{\alpha}{2}\right) \end{bmatrix} \tag{3.46}$$

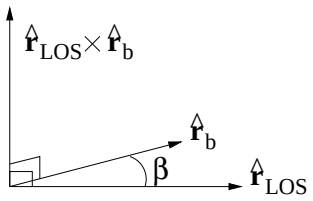

Figure 3.19: *The two vectors are not parallel, because of a rotation error β, around the cross-product of the vectors.*

where α denotes the angle of rotation around the unit vector $\hat{\boldsymbol{r}}$. Substituting the values of Figure 3.19, yields

$$\boldsymbol{q}_{\epsilon} = \begin{bmatrix} \cos\left(\frac{\beta}{2}\right) \\ \left[\frac{\hat{\boldsymbol{r}}_{\mathrm{LOS}} \times \hat{\boldsymbol{r}}_{\mathrm{b}}}{|\hat{\boldsymbol{r}}_{\mathrm{LOS}} \times \hat{\boldsymbol{r}}_{\mathrm{b}}|}\right] \sin\left(\frac{\beta}{2}\right) \end{bmatrix} \tag{3.47}$$

where β is given by

$$\beta = \hat{\boldsymbol{r}}_{\mathrm{LOS}} \cdot \hat{\boldsymbol{r}}_{\mathrm{b}} \tag{3.48}$$

The purpose of the RF control system is to minimize the rotation error $\boldsymbol{q}_{\epsilon}$. This is not included in this project.

Chapter 4

Modeling

This chapter derives the mathematical models needed to describe the position and attitude of the satellites. In addition the disturbance of the solar pressure is investigated, and simplified models of the sensor and actuator hardware are obtained.

4.1 Relative Motion

This section derives the equations of relative motion, describing the position of one spacecraft relative to another. The resulting equations are used to model the motion of the two fully equipped satellites with respect to the sphere satellite. Since the sphere satellite cannot be controlled, it makes sense to use the relative position as reference. The attitude of the spacecrafts are not considered in this section, but are described in Section 4.2 on page 52. This section is based on the work in [Ankersen, 2000].

In an inertial frame, the position of the sphere satellite is denoted $\boldsymbol{r}_{\mathrm{b}}$ and the position of any chasing satellite is denoted $\boldsymbol{r}_{\mathrm{c}}$, used in Rendez-vous and docking terminology. The chasing satellite in the case of SMART-2, is one of the fully equipped satellites. The relative position of the chaser as seen from the sphere is denoted $\boldsymbol{r}_{\mathrm{s}}$, as illustrated in Figure 4.1.

The vector $\boldsymbol{r}_{\mathrm{s}}$ can be expressed as

$$\boldsymbol{r}_{\mathrm{s}} = \boldsymbol{r}_{\mathrm{c}} - \boldsymbol{r}_{\mathrm{b}} \tag{4.1}$$

and the acceleration of $\boldsymbol{r}_{\mathrm{s}}$ is

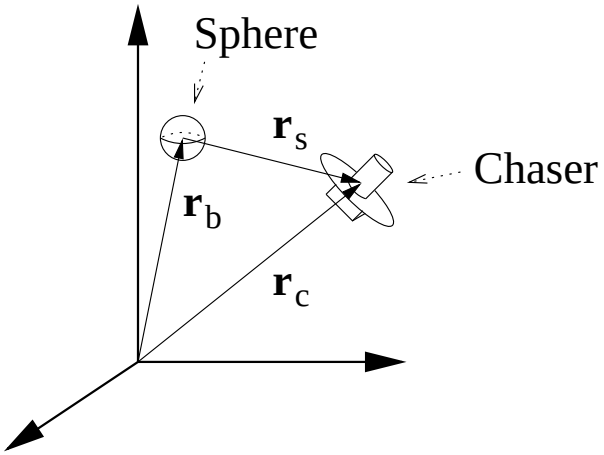

Figure 4.1: *The position of the sphere satellite and a chaser, and the relative position between them.*

$$\ddot{\boldsymbol{r}}_s = \ddot{\boldsymbol{r}}_c - \ddot{\boldsymbol{r}}_b \tag{4.2}$$

The formation of SMART-2 will be orbiting the Sun at the L2 lagrangian point of the Earth-Sun system, in an Earth trailing, helio centric orbit. Hence the gravitational force of the Earth cancels out. The gravity force of the Sun, acting on a spacecraft, is in general described as a function of the spacecraft position $\boldsymbol{r}$ and its mass m, given by

$$\boldsymbol{f}_{\text{Sun}}(\boldsymbol{r}, m) = -GM\frac{m}{|\boldsymbol{r}|^2}\hat{\boldsymbol{r}} \tag{4.3}$$

where G is the universal gravitational constant and M is the mass of the Sun. Equation 4.3 can be written

$$\boldsymbol{f}_{\text{Sun}}(\boldsymbol{r}, m) = -\mu\frac{m}{|\boldsymbol{r}|^3}\boldsymbol{r} \tag{4.4}$$

realizing that

$$\hat{\boldsymbol{r}} = \frac{\boldsymbol{r}}{|\boldsymbol{r}|} \tag{4.5}$$

For the sphere satellite, Newton's second law of motion, yield

$$m_{\mathrm{b}}\ddot{\boldsymbol{r}}_{\mathrm{b}} = \boldsymbol{f}_{\mathrm{Sun}}\left(\boldsymbol{r}_{\mathrm{b}}, m_{\mathrm{b}}\right) \tag{4.6}$$

when assuming that the gravitational force of the Sun is the only force acting on the sphere. The motion of the chaser satellite, is given by

$$m_{\mathrm{c}}\ddot{\boldsymbol{r}}_{\mathrm{c}} = \boldsymbol{f}_{\mathrm{Sun}}\left(\boldsymbol{r}_{\mathrm{c}}, m_{\mathrm{c}}\right) + \boldsymbol{f}_{\mathrm{ext}} \tag{4.7}$$

where the force $\boldsymbol{f}_{\mathrm{ext}}$ is the sum of external forces acting on the system, including the control thrust.

Since disturbances on the sphere are assumed to be zero, any disturbance acting on both spacecrafts, e.g. solar pressure, must be calculated as the relative force acting on the chaser, that is the difference between the force acting on the sphere and the force acting on the chaser.

Solving Equations 4.6 and 4.7 with respect to the accelerations of the sphere and chaser, respectively, and inserting into Equation 4.2, yields

$$\ddot{\boldsymbol{r}}_{\mathrm{s}} = \frac{1}{m_{\mathrm{c}}}\left[\boldsymbol{f}_{\mathrm{Sun}}\left(\boldsymbol{r}_{\mathrm{c}}, m_{\mathrm{c}}\right) + \boldsymbol{f}_{\mathrm{ext}}\right] - \frac{1}{m_{\mathrm{b}}}\boldsymbol{f}_{\mathrm{Sun}}\left(\boldsymbol{r}_{\mathrm{b}}, m_{\mathrm{b}}\right) \tag{4.8}$$

From Equation 4.3 the function describing the gravitational acceleration is found to be

$$\begin{aligned}\boldsymbol{a}_{\mathrm{Sun}}\left(\boldsymbol{r}\right) &= \frac{1}{m}\boldsymbol{f}_{\mathrm{Sun}}\left(\boldsymbol{r}, m\right) \\ &= -\frac{\mu}{\left|\boldsymbol{r}\right|^{3}}\boldsymbol{r}\end{aligned} \tag{4.9}$$

which inserted into Equation 4.8 gives

$$\ddot{\boldsymbol{r}}_{\mathrm{s}} = \boldsymbol{a}_{\mathrm{Sun}}\left(\boldsymbol{r}_{\mathrm{c}}\right) - \boldsymbol{a}_{\mathrm{Sun}}\left(\boldsymbol{r}_{\mathrm{b}}\right) + \frac{1}{m_{\mathrm{c}}}\boldsymbol{f}_{\mathrm{ext}} \tag{4.10}$$

The gravitational acceleration of the chaser $\boldsymbol{a}_{\mathrm{Sun}}\left(\boldsymbol{r}_{\mathrm{c}}\right)$, can be expanded into a first order Taylor series, around the position of the sphere $\boldsymbol{r}_{\mathrm{b}}$, which is given by

$$\boldsymbol{a}_{\mathrm{Sun}}\left(\boldsymbol{r}_{\mathrm{c}}\right) = \boldsymbol{a}_{\mathrm{Sun}}\left(\boldsymbol{r}_{\mathrm{b}}\right) + \left.\frac{\mathrm{d}\boldsymbol{a}_{\mathrm{Sun}}\left(\boldsymbol{r}\right)}{\mathrm{d}\boldsymbol{r}}\right|_{\boldsymbol{r}=\boldsymbol{r}_{\mathrm{b}}}\left[\boldsymbol{r}_{\mathrm{c}} - \boldsymbol{r}_{\mathrm{b}}\right] \tag{4.11}$$

Inserting Equation 4.11 into Equation 4.10 and recalling Equation 4.1, yields

$$\ddot{\boldsymbol{r}}_{\mathrm{s}} = \left.\frac{\mathrm{d}\boldsymbol{a}_{\mathrm{Sun}}(\boldsymbol{r})}{\mathrm{d}\boldsymbol{r}}\right|_{\boldsymbol{r}=\boldsymbol{r}_{\mathrm{b}}} \boldsymbol{r}_{\mathrm{s}} + \frac{1}{m_{\mathrm{c}}}\boldsymbol{f}_{\mathrm{ext}} \tag{4.12}$$

The derivative of $\boldsymbol{a}_{\mathrm{Sun}}(\boldsymbol{r})$ with respect to the vector $\boldsymbol{r}$ is

$$\left.\frac{\mathrm{d}\boldsymbol{a}_{\mathrm{Sun}}(\boldsymbol{r})}{\mathrm{d}\boldsymbol{r}}\right|_{\boldsymbol{r}=\boldsymbol{r}_{\mathrm{b}}} = \begin{bmatrix} \frac{\partial a_{\mathrm{Sun1}}(\boldsymbol{r}_{\mathrm{b}})}{\partial r_{\mathrm{b1}}} & \frac{\partial a_{\mathrm{Sun1}}(\boldsymbol{r}_{\mathrm{b}})}{\partial r_{\mathrm{b2}}} & \frac{\partial a_{\mathrm{Sun1}}(\boldsymbol{r}_{\mathrm{b}})}{\partial r_{\mathrm{b3}}} \\ \frac{\partial a_{\mathrm{Sun2}}(\boldsymbol{r}_{\mathrm{b}})}{\partial r_{\mathrm{b1}}} & \frac{\partial a_{\mathrm{Sun2}}(\boldsymbol{r}_{\mathrm{b}})}{\partial r_{\mathrm{b2}}} & \frac{\partial a_{\mathrm{Sun2}}(\boldsymbol{r}_{\mathrm{b}})}{\partial r_{\mathrm{b3}}} \\ \frac{\partial a_{\mathrm{Sun3}}(\boldsymbol{r}_{\mathrm{b}})}{\partial r_{\mathrm{b1}}} & \frac{\partial a_{\mathrm{Sun3}}(\boldsymbol{r}_{\mathrm{b}})}{\partial r_{\mathrm{b2}}} & \frac{\partial a_{\mathrm{Sun3}}(\boldsymbol{r}_{\mathrm{b}})}{\partial r_{\mathrm{b3}}} \end{bmatrix} \tag{4.13}$$

where $a_{\mathrm{Sun1}}(\boldsymbol{r}_{\mathrm{b}})$, $a_{\mathrm{Sun2}}(\boldsymbol{r}_{\mathrm{b}})$, $a_{\mathrm{Sun3}}(\boldsymbol{r}_{\mathrm{b}})$, r_{b1}, r_{b2} and r_{b3} are the elements of the $\boldsymbol{a}_{\mathrm{Sun}}$ and $\boldsymbol{r}_{\mathrm{b}}$ vectors, respectively. The derivative of the diagonal elements can be expressed as

$$\begin{aligned} \frac{\partial a_{\mathrm{Sun}i}(\boldsymbol{r}_{\mathrm{b}})}{\partial r_{\mathrm{b}i}} &= -\mu\frac{\partial}{\partial r_{\mathrm{b}i}}\left[r_{\mathrm{b1}}^2 + r_{\mathrm{b2}}^2 + r_{\mathrm{b3}}^2\right]^{-\frac{3}{2}} r_{\mathrm{b}i} \\ &= -\mu\left[\left[r_{\mathrm{b1}}^2 + r_{\mathrm{b2}}^2 + r_{\mathrm{b3}}^2\right]^{-\frac{3}{2}} - \frac{3}{2}\left[r_{\mathrm{b1}}^2 + r_{\mathrm{b2}}^2 + r_{\mathrm{b3}}^2\right]^{-\frac{5}{2}} 2r_{\mathrm{b}i}^2\right] \\ &= -\frac{\mu}{|\boldsymbol{r}_{\mathrm{b}}|^3}\left[1 - 3\frac{r_{\mathrm{b}i}^2}{|\boldsymbol{r}_{\mathrm{b}}|^2}\right] \quad , \quad i \in [1,3] \end{aligned} \tag{4.14}$$

The remaining elements of the matrix in Equation 4.13, are given by

$$\begin{aligned} \frac{\partial a_{\mathrm{Sun}i}(\boldsymbol{r}_{\mathrm{b}})}{\partial r_{\mathrm{b}j}} &= -\mu\frac{\partial}{\partial r_{\mathrm{b}j}}\left[r_{\mathrm{b1}}^2 + r_{\mathrm{b2}}^2 + r_{\mathrm{b3}}^2\right]^{-\frac{3}{2}} r_{\mathrm{b}i} \\ &= \mu\frac{3}{2}\left[r_{\mathrm{b1}}^2 + r_{\mathrm{b2}}^2 + r_{\mathrm{b3}}^2\right]^{-\frac{5}{2}} 2r_{\mathrm{b}j}r_{\mathrm{b}i} \\ &= \frac{3\mu}{|\boldsymbol{r}_{\mathrm{b}}|^5} r_{\mathrm{b}j}r_{\mathrm{b}i} \quad , \quad i,j \in [1,3] \ \wedge \ i \neq j \end{aligned} \tag{4.15}$$

The derivative of the gravitational acceleration function can now be inserted into Equation 4.12, giving

$$\ddot{\boldsymbol{r}}_{\mathrm{s}} = \frac{\mu}{|\boldsymbol{r}_{\mathrm{b}}|^3}\begin{bmatrix} 3\frac{r_{\mathrm{b1}}^2}{|\boldsymbol{r}_{\mathrm{b}}|^2} - 1 & \frac{3}{|\boldsymbol{r}_{\mathrm{b}}|^2}r_{\mathrm{b1}}r_{\mathrm{b2}} & \frac{3}{|\boldsymbol{r}_{\mathrm{b}}|^2}r_{\mathrm{b1}}r_{\mathrm{b3}} \\ \frac{3}{|\boldsymbol{r}_{\mathrm{b}}|^2}r_{\mathrm{b1}}r_{\mathrm{b2}} & 3\frac{r_{\mathrm{b2}}^2}{|\boldsymbol{r}_{\mathrm{b}}|^2} - 1 & \frac{3}{|\boldsymbol{r}_{\mathrm{b}}|^2}r_{\mathrm{b2}}r_{\mathrm{b3}} \\ \frac{3}{|\boldsymbol{r}_{\mathrm{b}}|^2}r_{\mathrm{b1}}r_{\mathrm{b3}} & \frac{3}{|\boldsymbol{r}_{\mathrm{b}}|^2}r_{\mathrm{b2}}r_{\mathrm{b3}} & 3\frac{r_{\mathrm{b3}}^2}{|\boldsymbol{r}_{\mathrm{b}}|^2} - 1 \end{bmatrix}\boldsymbol{r}_{\mathrm{s}} + \frac{1}{m_{\mathrm{c}}}\boldsymbol{f}_{\mathrm{ext}} \tag{4.16}$$

which is is written in short hand as

$$\ddot{\boldsymbol{r}}_{\mathrm{s}} = \frac{\mu}{|\boldsymbol{r}_{\mathrm{b}}|^3}\boldsymbol{M}\boldsymbol{r}_{\mathrm{s}} + \frac{1}{m_{\mathrm{c}}}\boldsymbol{f}_{\mathrm{ext}} \tag{4.17}$$

The above equation is for an inertial frame, hence the $\boldsymbol{r}_{\mathrm{s}}$ vector must be given in an inertial frame, denoted $\boldsymbol{r}_{\mathrm{s}}^{I}$. It is the dynamics of the relative position, which are sought. Introducing an orbit frame, which rotates with angular velocity $\boldsymbol{\omega}_{\mathrm{o}}$ and shares origin with the sphere frame, the derivative of $\boldsymbol{r}_{\mathrm{s}}^{I}$ can be expressed in terms of the relative position vector in the orbit frame, denoted $\boldsymbol{r}_{\mathrm{s}}^{o}$. Assuming that the sphere is in a circular orbit with constant angular velocity $\boldsymbol{\omega}_{\mathrm{o}}$, the inertial acceleration can be expressed as

$$\left(\ddot{\boldsymbol{r}}_{\mathrm{s}}^{I}\right)^{o} = \ddot{\boldsymbol{r}}_{\mathrm{s}}^{o} + \boldsymbol{\omega}_{\mathrm{o}} \times [\boldsymbol{\omega}_{\mathrm{o}} \times \boldsymbol{r}_{\mathrm{s}}^{o}] + 2\boldsymbol{\omega}_{\mathrm{o}} \times \dot{\boldsymbol{r}}_{\mathrm{s}}^{o} \tag{4.18}$$

Substituting into Equation 4.17 yields

$$\ddot{\boldsymbol{r}}_{\mathrm{s}}^{o} + \boldsymbol{\omega}_{\mathrm{o}} \times [\boldsymbol{\omega}_{\mathrm{o}} \times \boldsymbol{r}_{\mathrm{s}}^{o}] + 2\boldsymbol{\omega}_{\mathrm{o}} \times \dot{\boldsymbol{r}}_{\mathrm{s}}^{o} - \frac{\mu}{|\boldsymbol{r}_{\mathrm{b}}^{o}|^3}\boldsymbol{M}\boldsymbol{r}_{\mathrm{s}}^{o} = \frac{1}{m_{\mathrm{c}}}\boldsymbol{f}_{\mathrm{ext}}^{o} \tag{4.19}$$

Defining the orbit frame in a convenient way, simplifies $\boldsymbol{\omega}_{\mathrm{o}}$ and $\boldsymbol{r}_{\mathrm{b}}^{o}$ and as a result, Equation 4.19 simplifies as well.

Orbit Frame

The orbit frame is defined as a standard PDP frame [Ankersen, 2000]. It has origin at the center of the sphere. The $\boldsymbol{x}_{\mathrm{o}}$ axis is in the direction of the velocity vector and tangential to the orbit. The $\boldsymbol{z}_{\mathrm{o}}$ axis is in the direction of the Sun. The $\boldsymbol{y}_{\mathrm{o}}$ axis is formed in a right handed system. The orbit frame is illustrated in Figure 4.2.

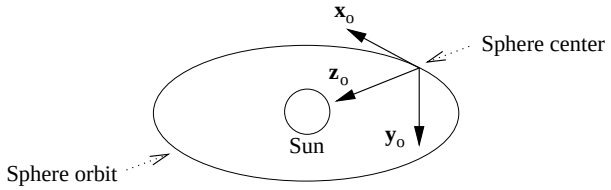

Figure 4.2: *Definition of the orbit frame.*

Position Dynamics in the Orbit Frame

Given the definition of the orbit frame, the position and angular velocity of the sphere frame can be expressed as

$$\boldsymbol{r}_{\mathrm{b}}^{o} = \begin{bmatrix} 0 \\ 0 \\ -r_{\mathrm{b}} \end{bmatrix} \tag{4.20}$$

$$\boldsymbol{\omega}_{\mathrm{o}} = \begin{bmatrix} 0 \\ -\omega_{\mathrm{o}} \\ 0 \end{bmatrix} \tag{4.21}$$

Inserting Equations 4.20 and 4.21 into Equation 4.19, yields

$$\begin{bmatrix} \ddot{r}_{\mathrm{s1}} \\ \ddot{r}_{\mathrm{s2}} \\ \ddot{r}_{\mathrm{s3}} \end{bmatrix} + \begin{bmatrix} 0 \\ -\omega_{\mathrm{o}} \\ 0 \end{bmatrix} \times \omega_{\mathrm{o}} \begin{bmatrix} -r_{\mathrm{s3}} \\ 0 \\ r_{\mathrm{s1}} \end{bmatrix} + 2\omega_{\mathrm{o}} \begin{bmatrix} -\dot{r}_{\mathrm{s3}} \\ 0 \\ \dot{r}_{\mathrm{s1}} \end{bmatrix} - \frac{\mu}{r_{\mathrm{b}}^3} \begin{bmatrix} -1 & 0 & 0 \\ 0 & -1 & 0 \\ 0 & 0 & 2 \end{bmatrix} \begin{bmatrix} r_{\mathrm{s1}} \\ r_{\mathrm{s2}} \\ r_{\mathrm{s3}} \end{bmatrix} =$$
$$\begin{bmatrix} \ddot{r}_{\mathrm{s1}} \\ \ddot{r}_{\mathrm{s2}} \\ \ddot{r}_{\mathrm{s3}} \end{bmatrix} - \omega_{\mathrm{o}}^2 \begin{bmatrix} r_{\mathrm{s1}} \\ 0 \\ r_{\mathrm{s3}} \end{bmatrix} + 2\omega_{\mathrm{o}} \begin{bmatrix} -\dot{r}_{\mathrm{s3}} \\ 0 \\ \dot{r}_{\mathrm{s1}} \end{bmatrix} - \frac{\mu}{r_{\mathrm{b}}^3} \begin{bmatrix} -r_{\mathrm{s1}} \\ -r_{\mathrm{s2}} \\ 2r_{\mathrm{s3}} \end{bmatrix} = \frac{1}{m_{\mathrm{c}}} \begin{bmatrix} f_{\mathrm{ext1}} \\ f_{\mathrm{ext2}} \\ f_{\mathrm{ext3}} \end{bmatrix} \tag{4.22}$$

where all vector elements are given in the orbit frame. The indication of frame is left out in Equation 4.22 and in the remaining equations of this section, since all vectors are given in the orbit frame. Writing Equation 4.22 in terms of the elements, the standard form of the Clohessy-Wiltshire differential equations are obtained, given by

$$\begin{aligned} \ddot{r}_{\mathrm{s1}} - \omega_{\mathrm{o}}^2 r_{\mathrm{s1}} - 2\omega_{\mathrm{o}}\dot{r}_{\mathrm{s3}} + \frac{\mu}{r_{\mathrm{b}}^3} r_{\mathrm{s1}} &= \frac{1}{m_{\mathrm{c}}} f_{\mathrm{ext1}} \\ \ddot{r}_{\mathrm{s2}} + \frac{\mu}{r_{\mathrm{b}}^3} r_{\mathrm{s2}} &= \frac{1}{m_{\mathrm{c}}} f_{\mathrm{ext2}} \\ \ddot{r}_{\mathrm{s3}} - \omega_{\mathrm{o}}^2 r_{\mathrm{s3}} + 2\omega_{\mathrm{o}}\dot{r}_{\mathrm{s1}} - 2\frac{\mu}{r_{\mathrm{b}}^3} r_{\mathrm{s3}} &= \frac{1}{m_{\mathrm{c}}} f_{\mathrm{ext3}} \end{aligned} \tag{4.23}$$

Given the vectors of Equations 4.20 and 4.21, the squared angular velocity of a circular orbit can be expressed as

$$\omega_{\mathrm{o}}^2 = \frac{\mu}{|\boldsymbol{r}_{\mathrm{b}}|^3} \tag{4.24}$$

$$= \frac{\mu}{r_{\mathrm{b}}^3} \tag{4.25}$$

which inserted into Equation 4.23 yields

$$\begin{aligned} \ddot{r}_{\mathrm{s1}} - 2\omega_{\mathrm{o}}\dot{r}_{\mathrm{s3}} &= \frac{1}{m_{\mathrm{c}}} f_{\mathrm{ext1}} \\ \ddot{r}_{\mathrm{s2}} + \omega_{\mathrm{o}}^2 r_{\mathrm{s2}} &= \frac{1}{m_{\mathrm{c}}} f_{\mathrm{ext2}} \\ \ddot{r}_{\mathrm{s3}} + 2\omega_{\mathrm{o}}\dot{r}_{\mathrm{s1}} - 3\omega_{\mathrm{o}}^2 r_{\mathrm{s3}} &= \frac{1}{m_{\mathrm{c}}} f_{\mathrm{ext3}} \end{aligned} \tag{4.26}$$

In order to represent the dynamics of Equation 4.26 in the state space form, the state vector $\boldsymbol{x}$ is defined as

$$\boldsymbol{x} = \begin{bmatrix} r_{\mathrm{s1}} \\ r_{\mathrm{s2}} \\ r_{\mathrm{s3}} \\ \dot{r}_{\mathrm{s1}} \\ \dot{r}_{\mathrm{s2}} \\ \dot{r}_{\mathrm{s3}} \end{bmatrix} \tag{4.27}$$

and the input vector $\boldsymbol{u}$ as

$$\boldsymbol{u} = \begin{bmatrix} f_{\mathrm{ctrl1}} \\ f_{\mathrm{ctrl2}} \\ f_{\mathrm{ctrl3}} \end{bmatrix} \tag{4.28}$$

Equation 4.26 expressed in the state space notation, yields

$$\dot{\boldsymbol{x}} = \begin{bmatrix} \mathbf{0}_{3\times 3} & \mathbf{1}_{3\times 3} \\ \begin{matrix} 0 & 0 & 0 \\ 0 & -\omega_{\mathrm{o}}^2 & 0 \\ 0 & 0 & 3\omega_{\mathrm{o}}^2 \end{matrix} & \begin{matrix} 0 & 0 & 2\omega_{\mathrm{o}} \\ 0 & 0 & 0 \\ -2\omega_{\mathrm{o}} & 0 & 0 \end{matrix} \end{bmatrix} \boldsymbol{x} + \begin{bmatrix} \mathbf{0}_{3\times 3} \\ \begin{matrix} \frac{1}{m_{\mathrm{c}}} & 0 & 0 \\ 0 & \frac{1}{m_{\mathrm{c}}} & 0 \\ 0 & 0 & \frac{1}{m_{\mathrm{c}}} \end{matrix} \end{bmatrix} \boldsymbol{u} \tag{4.29}$$

where $\mathbf{0}_{3\text{x}3}$ is the 3 by 3 zero matrix, and $\mathbf{1}_{3\text{x}3}$ is the 3 by 3 identity matrix. The control force of the thrusters is denoted $\boldsymbol{f}_{\text{ctrl}}$, and is inserted as the external force to the system.

Recalling that the state vector $\boldsymbol{x}$ is given in the orbit frame, the dynamics of the state space system in Equation 4.29, describes the motion of a chaser satellite seen from the orbit frame, which rotates as the sphere moves in its orbit.

4.2 Modeling Satellite Attitude

This section describes the equations used for modeling the kinematics and dynamics of satellite rotations. It is based on the work previously done in [Dan Bhanderi et al., 2000], which should be used as reference, if not otherwise specified.

The direct cosine matrices contain nine parameters with three degrees of freedom. Due to this redundancy, numerous ways of representing the satellite attitude with a minimum set of parameters have been developed. Euler angles describe the rotation around the principal axes and use therefore only three parameters. However some singularities arise for some rotations, which is why Euler angles are commonly used when the attitude of the object involved, is known to be within a certain margin [James R. Wertz, 1978].

Quaternions use four parameters with a single constraint, to represent attitude, and are subject to no singularities. This is useful when considering that the attitude of a spacecraft is usually unknown after the release from the launcher. For this reason quaternions are commonly used in space applications and also for this project. Appendix B on page 115 gives a brief description of the quaternions and their algebra.

The modeling of a satellite's rotation is divided into the kinematic equation and the dynamic equation. The kinematic equation describes the change in the attitude parameters of the satellite, regardless of the forces acting on it. The dynamic equation describes the time dependent parameters as functions of outer forces.

Kinematic Equation

Let the attitude of a satellite at time t and $t + \Delta t$ be denoted $\boldsymbol{q}(t)$ and $\boldsymbol{q}(t + \Delta t)$. If the rotation of the satellite in the time period Δt is denoted $\boldsymbol{q}(\Delta t)$, the propagation of the attitude from t to $t + \Delta t$ can be written

$$\boldsymbol{q}(t + \Delta t) = \boldsymbol{q}(t)\,\boldsymbol{q}(\Delta t) \tag{4.30}$$

Writing $\boldsymbol{q}(\Delta t)$ in terms of rotation angle $\Delta\phi$ around the vector $\boldsymbol{u}$ in time Δt, yields

$$\boldsymbol{q}\left(\Delta t\right) = \begin{bmatrix} \cos\left(\frac{\Delta\phi}{2}\right) \\ u_1 \sin\left(\frac{\Delta\phi}{2}\right) \\ u_2 \sin\left(\frac{\Delta\phi}{2}\right) \\ u_3 \sin\left(\frac{\Delta\phi}{2}\right) \end{bmatrix} \tag{4.31}$$

Assuming that $\boldsymbol{u}$ and $\Delta\phi$ are constant over the time Δt, and using the definition of the quaternion product, Equation 4.30 is written

$$\boldsymbol{q}\left(t+\Delta t\right) = \left[\cos\left(\frac{\Delta\phi}{2}\right)\mathbf{1}_{4\times4} + \sin\left(\frac{\Delta\phi}{2}\right)\begin{bmatrix} 0 & -u_1 & -u_2 & -u_3 \\ u_1 & 0 & u_3 & -u_2 \\ u_2 & -u_3 & 0 & u_1 \\ u_3 & u_2 & -u_1 & 0 \end{bmatrix}\right]\boldsymbol{q}\left(t\right) \tag{4.32}$$

where $\mathbf{1}_{4\times4}$ is the 4 by 4 identity matrix. For infinite small time steps, $\Delta\phi$ can be approximated by

$$\Delta\phi = \left|\boldsymbol{\omega}_{\mathrm{s}}\right|\Delta t \tag{4.33}$$

where $\boldsymbol{\omega}_{\mathrm{s}}$ is the instantaneous angular velocity of the satellite. Using small angle approximations of sine and cosine, Equation 4.32 can be expressed as

$$\boldsymbol{q}\left(t+\Delta t\right) = \left[\mathbf{1}_{4\times4} + \frac{\Delta t}{2}\boldsymbol{\Omega}\right]\boldsymbol{q}\left(t\right) \tag{4.34}$$

where

$$\boldsymbol{\Omega} = \left|\boldsymbol{\omega}_{\mathrm{s}}\right|\begin{bmatrix} 0 & -u_1 & -u_2 & -u_3 \\ u_1 & 0 & u_3 & -u_2 \\ u_2 & -u_3 & 0 & u_1 \\ u_3 & u_2 & -u_1 & 0 \end{bmatrix} \tag{4.35}$$

Realizing that $\boldsymbol{u} = \hat{\boldsymbol{\omega}}_{\mathrm{s}}$, Equation 4.35 can be written

$$\boldsymbol{\Omega} = \begin{bmatrix} 0 & -\omega_{\mathrm{s}1} & -\omega_{\mathrm{s}2} & -\omega_{\mathrm{s}3} \\ \omega_{\mathrm{s}1} & 0 & \omega_3 & -\omega_2 \\ \omega_{\mathrm{s}2} & -\omega_{\mathrm{s}3} & 0 & \omega_{\mathrm{s}1} \\ \omega_{\mathrm{s}3} & \omega_{\mathrm{s}2} & -\omega_{\mathrm{s}1} & 0 \end{bmatrix} \tag{4.36}$$

The differential equation of $\boldsymbol{q}(t)$ is defined as

$$\dot{\boldsymbol{q}}(t) = \lim_{\Delta t \to 0} \frac{\boldsymbol{q}(t + \Delta t) - \boldsymbol{q}(t)}{\Delta t} \tag{4.37}$$

Inserting Equation 4.34 yields the sought kinematic differential equation

$$\dot{\boldsymbol{q}}(t) = \frac{1}{2}\boldsymbol{\Omega}\boldsymbol{q}(t) \tag{4.38}$$

Dynamic Equation

The dynamic equation of motion is derived from the change in angular momentum of the spacecraft. An expression for the change in angular velocity, as a function of the applied torques is sought. The angular momentum $\boldsymbol{l}$, is given by

$$\begin{aligned} \boldsymbol{l} &= \sum_{i=1}^{k} \boldsymbol{l}_i \\ &= \sum_{i=1}^{k} \boldsymbol{r}_i \times m_i \boldsymbol{v}_i \end{aligned} \tag{4.39}$$

where $\boldsymbol{r}_i$ is the position of the ith particle with mass m_i and velocity $\boldsymbol{v}_i$. Taking the time derivative of Equation 4.39, yields

$$\dot{\boldsymbol{l}} = \sum_{i=1}^{k} \left[\boldsymbol{v}_i \times m_i \boldsymbol{v}_i + \boldsymbol{r}_i \times m_i \boldsymbol{a}_i\right] \tag{4.40}$$

$\boldsymbol{a}_i$ being the acceleration of the ith particle. The first term under the summation of Equation 4.40 is a cross product of two parallel vectors, which is zero. Realizing that $m_i \boldsymbol{a}_i$ is the force acting on the ith particle, yields

$$\dot{\boldsymbol{l}} = \boldsymbol{n}_{\text{ext}} \tag{4.41}$$

where $\boldsymbol{n}_{\text{ext}}$ is the sum of external torques acting on the spacecraft. Equation 4.41 only holds if the internal torques sum up to zero [James R. Wertz, 1978]. An expression of

the derivative of the angular momentum in terms of the spacecraft's angular velocity is sought, in order to obtain the dynamic equation.

In an inertial frame I, the angular momentum of the spacecraft can be expressed as a function of the angular velocity $\boldsymbol{\omega}_\mathrm{s}$ and the moment of inertia matrix $\boldsymbol{J}$ of the spacecraft, by

$$\boldsymbol{l}^I = \boldsymbol{J}^I \boldsymbol{\omega}_\mathrm{s} \tag{4.42}$$

Since the moment of inertia is more conveniently expressed in the body frame B of the spacecraft, the angular momentum is found in the body frame. The body frame is centered at the spacecraft center of mass, and the axes are aligned with the principal axes of the spacecraft. The attitude matrix $\boldsymbol{A}_I^B$, represents the rotation from the inertial frame to the spacecraft body frame, which is used to represent Equation 4.42 in the body frame, yielding

$$\boldsymbol{l}^B = \boldsymbol{A}_I^B \boldsymbol{l}^I \tag{4.43}$$

The derivative of $\boldsymbol{l}^B$ is given by

$$\begin{aligned} \dot{\boldsymbol{l}}^B &= \frac{\mathrm{d}}{\mathrm{d}t}\left(\boldsymbol{A}_I^B \boldsymbol{l}^I\right) \\ &= \dot{\boldsymbol{A}}_I^B \boldsymbol{l}^I + \boldsymbol{A}_I^B \dot{\boldsymbol{l}}^I \end{aligned} \tag{4.44}$$

In order to obtain an expression for $\dot{\boldsymbol{A}}_I^B$, consider the kinematic equation for rotating systems, which for the angular momentum vector $\boldsymbol{l}$ is

$$\begin{aligned} \left(\dot{\boldsymbol{l}}^I\right)^B &= \dot{\boldsymbol{l}}^B + \boldsymbol{\omega}_\mathrm{s} \times \boldsymbol{l}^B \\ \Updownarrow & \\ \dot{\boldsymbol{l}}^B &= \left(\dot{\boldsymbol{l}}^I\right)^B - \boldsymbol{\omega}_\mathrm{s} \times \boldsymbol{l}^B \end{aligned} \tag{4.45}$$

Since $\left(\dot{\boldsymbol{l}}^I\right)^B = \boldsymbol{A}_I^B \dot{\boldsymbol{l}}^B$, combining Equations 4.44 and 4.45, gives

$$\begin{aligned} \dot{\boldsymbol{A}}_I^B \boldsymbol{l}^I &= -\boldsymbol{\omega}_\mathrm{s} \times \boldsymbol{l}^B \\ &= -\boldsymbol{\omega}_\mathrm{s} \times \left[\boldsymbol{A}_I^B \boldsymbol{l}^I\right] \end{aligned} \tag{4.46}$$

Defining the cross product matrix function as

$$\mathbf{S}\left(\boldsymbol{\omega}\right) \triangleq \begin{bmatrix} 0 & -\omega_3 & \omega_2 \\ \omega_3 & 0 & -\omega_1 \\ -\omega_2 & \omega_1 & 0 \end{bmatrix} \tag{4.47}$$

where $\boldsymbol{\omega}$ is an arbitrary vector, Equation 4.46 is written

$$\dot{\boldsymbol{A}}_I^B \boldsymbol{l}^I = -\mathbf{S}\left(\boldsymbol{\omega}_\mathrm{s}\right) \boldsymbol{A}_I^B \boldsymbol{l}^I \tag{4.48}$$

Since Equation 4.48 holds for all $\boldsymbol{l}^I$, the sought expression for the derivative of the attitude matrix is

$$\dot{\boldsymbol{A}}_I^B = -\mathbf{S}\left(\boldsymbol{\omega}_\mathrm{s}\right) \boldsymbol{A}_I^B \tag{4.49}$$

Inserting Equation 4.49 into Equation 4.44, gives

$$\dot{\boldsymbol{l}}^B = -\mathbf{S}\left(\boldsymbol{\omega}_\mathrm{s}\right) \boldsymbol{A}_I^B \boldsymbol{l}^I + \boldsymbol{A}_I^B \dot{\boldsymbol{l}}^I \tag{4.50}$$

Recalling from Equation 4.41, that the derivative of the angular momentum is the external torques and applying the attitude matrix rotations in Equation 4.50, yields

$$\dot{\boldsymbol{l}}^B = -\mathbf{S}\left(\boldsymbol{\omega}_\mathrm{s}\right) \boldsymbol{l}^B + \boldsymbol{n}_\mathrm{ext}^B \tag{4.51}$$

Finally the angular momentum is expressed in terms of the moment of inertia and the angular velocity, as given in Equation 4.42. Solving with respect to $\dot{\boldsymbol{\omega}}_\mathrm{s}$, gives the sought nonlinear differential equation, written in the form

$$\dot{\boldsymbol{\omega}}_\mathrm{s} = \boldsymbol{J}^{-1}\left[\boldsymbol{n}_\mathrm{ext} - \boldsymbol{\omega}_\mathrm{s} \times \boldsymbol{J}\boldsymbol{\omega}_\mathrm{s}\right] \tag{4.52}$$

where the superscript of frame is left out, since all vectors and matrices are given in the spacecraft's body frame.

4.3 Linearization of Attitude Equations

In this section the attitude dynamic and kinematic equations are linearized around a working point of the states, based on the work in [Dan Bhanderi et al., 2000]. As a consequence the system description will contain the small signals of the states.

The non-linear system matrix $\boldsymbol{F}_{\text{nl}}(\boldsymbol{x}, t)$ describing the satellite's rotation, is found by combining Equations 4.38 on page 54 and 4.52 on the facing page to be

$$\boldsymbol{F}_{\text{nl}}(\boldsymbol{x}, t) = \begin{bmatrix} \frac{1}{2}\Omega\boldsymbol{q} \\ \boldsymbol{J}^{-1}\left(-\boldsymbol{\omega}_{\text{s}} \times \boldsymbol{J}\boldsymbol{\omega}_{\text{s}}\right) \end{bmatrix} \tag{4.53}$$

where

$$\boldsymbol{x} = \begin{bmatrix} \boldsymbol{q} \\ \boldsymbol{\omega}_{\text{s}} \end{bmatrix} \tag{4.54}$$

An expression in the linearized form $\dot{\boldsymbol{x}} = \boldsymbol{F}(t)\,\boldsymbol{x}$ is sought. The kinematic and dynamic equations are linearized separately in the following.

Kinematic Equation

For the linearization of the kinematic equation, the attitude quaternion of the satellite $\boldsymbol{q}$ is written, in terms of a working point $\bar{\boldsymbol{q}}$ and small signal $\tilde{\boldsymbol{q}}$, as

$$\begin{aligned} \boldsymbol{q} &= \bar{\boldsymbol{q}}\tilde{\boldsymbol{q}} \\ &\Updownarrow \\ \tilde{\boldsymbol{q}} &= \bar{\boldsymbol{q}}^{*}\boldsymbol{q} \end{aligned} \tag{4.55}$$

where $\bar{\boldsymbol{q}}^{*}$ is the complex conjugate of $\bar{\boldsymbol{q}}$. Recalling the definition of $\boldsymbol{\Omega}$ in Equation 4.35 on page 53 and the definition of quaternion products, the kinematic equation can be written in terms of a quaternion product, as

$$\dot{\boldsymbol{q}} = \frac{1}{2}\boldsymbol{q}\boldsymbol{q}_{\boldsymbol{\omega}_{\text{s}}} \tag{4.56}$$

where the quaternion $\boldsymbol{q}_{\boldsymbol{\omega}_{\text{s}}}$ is defined by

$$\boldsymbol{q}_{\boldsymbol{\omega}_\mathrm{s}} = \begin{bmatrix} 0 \\ \boldsymbol{\omega}_\mathrm{s} \end{bmatrix} \tag{4.57}$$

Using the chain rule and Equation 4.56, the derivative of the small signal attitude quaternion of Equation 4.55 can be expressed as

$$\begin{aligned} \dot{\tilde{\boldsymbol{q}}} &= \dot{\bar{\boldsymbol{q}}}^* \boldsymbol{q} + \bar{\boldsymbol{q}}^* \dot{\boldsymbol{q}} \\ &= \frac{1}{2} \left[\left(\bar{\boldsymbol{q}} \boldsymbol{q}_{\bar{\boldsymbol{\omega}}_\mathrm{s}} \right)^* \boldsymbol{q} + \bar{\boldsymbol{q}}^* \boldsymbol{q} \boldsymbol{q}_{\boldsymbol{\omega}_\mathrm{s}} \right] \\ &= \frac{1}{2} \left[-\boldsymbol{q}_{\bar{\boldsymbol{\omega}}_\mathrm{s}} \bar{\boldsymbol{q}}^* \boldsymbol{q} + \bar{\boldsymbol{q}}^* \boldsymbol{q} \boldsymbol{q}_{\boldsymbol{\omega}_\mathrm{s}} \right] \\ &= \frac{1}{2} \left[-\boldsymbol{q}_{\bar{\boldsymbol{\omega}}_\mathrm{s}} \tilde{\boldsymbol{q}} + \tilde{\boldsymbol{q}} \boldsymbol{q}_{\boldsymbol{\omega}_\mathrm{s}} \right] \end{aligned} \tag{4.58}$$

where $\boldsymbol{q}_{\bar{\boldsymbol{\omega}}_\mathrm{s}}$ is defined as in Equation 4.57, where the working point of the angular velocity $\bar{\boldsymbol{\omega}}_\mathrm{s}$ is inserted. Note that the complex conjugate of a quaternion represents the opposite rotation. Hence the reverse rotation defined by a sequence of rotations, is the reverse sequence of each rotation complex conjugated. The complex conjugate of $\boldsymbol{q}_{\bar{\boldsymbol{\omega}}_\mathrm{s}}$ is simply $-\boldsymbol{q}_{\bar{\boldsymbol{\omega}}_\mathrm{s}}$, since the scalar part is zero.

The angular velocity is defined, in terms of a working point $\bar{\boldsymbol{\omega}}_\mathrm{s}$ and small signal $\tilde{\boldsymbol{\omega}}_\mathrm{s}$, as

$$\boldsymbol{\omega}_\mathrm{s} = \bar{\boldsymbol{\omega}}_\mathrm{s} + \tilde{\boldsymbol{\omega}}_\mathrm{s} \tag{4.59}$$

hence $\boldsymbol{q}_{\boldsymbol{\omega}_\mathrm{s}}$ can be written

$$\begin{aligned} \boldsymbol{q}_{\boldsymbol{\omega}_\mathrm{s}} &= \begin{bmatrix} 0 \\ \bar{\boldsymbol{\omega}}_\mathrm{s} + \tilde{\boldsymbol{\omega}}_\mathrm{s} \end{bmatrix} \\ &= \boldsymbol{q}_{\bar{\boldsymbol{\omega}}_\mathrm{s}} + \boldsymbol{q}_{\tilde{\boldsymbol{\omega}}_\mathrm{s}} \end{aligned} \tag{4.60}$$

Inserting Equation 4.60 in Equation 4.58, and recognizing that the associative rule applies for quaternions, yields

$$\dot{\tilde{\boldsymbol{q}}} = \frac{1}{2} \left[-\boldsymbol{q}_{\bar{\boldsymbol{\omega}}_\mathrm{s}} \tilde{\boldsymbol{q}} + \tilde{\boldsymbol{q}} \boldsymbol{q}_{\bar{\boldsymbol{\omega}}_\mathrm{s}} \right] + \frac{1}{2} \tilde{\boldsymbol{q}} \boldsymbol{q}_{\tilde{\boldsymbol{\omega}}_\mathrm{s}} \tag{4.61}$$

A quaternion can be expressed, in terms of a scalar part and a vector part, as

$$\boldsymbol{q} = \begin{bmatrix} q_1 \\ \boldsymbol{q}_{2-4} \end{bmatrix} \tag{4.62}$$

where $\boldsymbol{q}_{2-4}$ is a vector containing the 2nd, 3rd and 4th element of $\boldsymbol{q}$. If $\tilde{\boldsymbol{q}}$ is a small rotation, $\tilde{q}_1$ approaches one and $\tilde{\boldsymbol{q}}_{2-4}$ approaches zero. Hence the quaternion product of the last term in Equation 4.61 can be approximated by

$$\begin{aligned} \tilde{\boldsymbol{q}}\boldsymbol{q}_{\tilde{\boldsymbol{\omega}}_\mathrm{s}} &= \begin{bmatrix} 0 & -\tilde{\boldsymbol{\omega}}_\mathrm{s}^\mathrm{T} \\ \tilde{\boldsymbol{\omega}}_\mathrm{s} & -\mathbf{S}\left(\tilde{\boldsymbol{\omega}}_\mathrm{s}\right) \end{bmatrix} \begin{bmatrix} q_1 \\ \tilde{\boldsymbol{q}}_{2-4} \end{bmatrix} \\ &= \begin{bmatrix} -\tilde{\boldsymbol{\omega}}_\mathrm{s}^\mathrm{T}\tilde{\boldsymbol{q}}_{2-4} \\ \tilde{\boldsymbol{\omega}}_\mathrm{s} q_1 - \mathbf{S}\left(\tilde{\boldsymbol{\omega}}_\mathrm{s}\right)\tilde{\boldsymbol{q}}_{2-4} \end{bmatrix} \\ &\approx \boldsymbol{q}_{\tilde{\boldsymbol{\omega}}_\mathrm{s}} \end{aligned} \tag{4.63}$$

where $\mathbf{S}\left(\tilde{\boldsymbol{\omega}}_\mathrm{s}\right)$ is the cross product matrix function, defined in Equation 4.47 on page 56, applied on $\tilde{\boldsymbol{\omega}}_\mathrm{s}$. The terms $\boldsymbol{q}_{\bar{\boldsymbol{\omega}}_\mathrm{s}}\tilde{\boldsymbol{q}}$ and $\tilde{\boldsymbol{q}}\boldsymbol{q}_{\bar{\boldsymbol{\omega}}_\mathrm{s}}$ of Equation 4.61, can be expressed as

$$\begin{aligned} \boldsymbol{q}_{\bar{\boldsymbol{\omega}}_\mathrm{s}}\tilde{\boldsymbol{q}} &= \begin{bmatrix} 0 & -\bar{\boldsymbol{\omega}}_\mathrm{s}^\mathrm{T} \\ \bar{\boldsymbol{\omega}}_\mathrm{s} & -\mathbf{S}\left(\bar{\boldsymbol{\omega}}_\mathrm{s}\right) \end{bmatrix} \begin{bmatrix} q_1 \\ \tilde{\boldsymbol{q}}_{2-4} \end{bmatrix} \\ &= \begin{bmatrix} -\bar{\boldsymbol{\omega}}_\mathrm{s}^\mathrm{T}\tilde{\boldsymbol{q}}_{2-4} \\ \bar{\boldsymbol{\omega}}_\mathrm{s} q_1 - \mathbf{S}\left(\bar{\boldsymbol{\omega}}_\mathrm{s}\right)\tilde{\boldsymbol{q}}_{2-4} \end{bmatrix} \end{aligned} \tag{4.64}$$

and

$$\begin{aligned} \tilde{\boldsymbol{q}}\boldsymbol{q}_{\bar{\boldsymbol{\omega}}_\mathrm{s}} &= \begin{bmatrix} \tilde{q}_1 & -\tilde{\boldsymbol{q}}_{2-4}^\mathrm{T} \\ \tilde{\boldsymbol{q}}_{2-4} & -\mathbf{S}\left(\tilde{\boldsymbol{q}}_{2-4}\right) + \tilde{q}_1\mathbf{1}_{3\times 3} \end{bmatrix} \begin{bmatrix} 0 \\ \bar{\boldsymbol{\omega}}_\mathrm{s} \end{bmatrix} \\ &= \begin{bmatrix} -\tilde{\boldsymbol{q}}_{2-4}^\mathrm{T}\bar{\boldsymbol{\omega}}_\mathrm{s} \\ -\mathbf{S}\left(\tilde{\boldsymbol{q}}_{2-4}\right)\bar{\boldsymbol{\omega}}_\mathrm{s} + \tilde{q}_1\bar{\boldsymbol{\omega}}_\mathrm{s} \end{bmatrix} \end{aligned} \tag{4.65}$$

Inserting the approximation of Equation 4.63 and the results of Equations 4.64 and 4.65 in Equation 4.61, yields

$$\dot{\tilde{\boldsymbol{q}}} = \begin{bmatrix} 0 \\ -\mathbf{S}\left(\bar{\boldsymbol{\omega}}_\mathrm{s}\right) \end{bmatrix} \tilde{\boldsymbol{q}} + \frac{1}{2}\boldsymbol{q}_{\tilde{\boldsymbol{\omega}}_\mathrm{s}} \tag{4.66}$$

which is the sought linearized kinematic equation.

Dynamic Equation

The dynamic equation is linearized using first order Taylor expansion around the working point $\bar{\boldsymbol{\omega}}_\mathrm{s}$. The external torques are disregarded in the linearization, since they are also the control input. They are added as control input in the full state space representation in Section 4.6.

The derivative of the small signal angular velocity describes the linearized dynamics of the system, and can be expressed as

$$\begin{aligned}\dot{\tilde{\boldsymbol{\omega}}}_\mathrm{s} &\approx -\boldsymbol{J}^{-1}\left.\frac{\mathrm{d}\left(\boldsymbol{\omega}_\mathrm{s}\times\boldsymbol{J}\boldsymbol{\omega}_\mathrm{s}\right)}{\mathrm{d}\boldsymbol{\omega}_\mathrm{s}}\right|_{\boldsymbol{\omega}_\mathrm{s}=\bar{\boldsymbol{\omega}}_\mathrm{s}}\tilde{\boldsymbol{\omega}}_\mathrm{s}\\ &= -\boldsymbol{J}^{-1}\left[-\left.\frac{\mathrm{d}}{\mathrm{d}\boldsymbol{\omega}_\mathrm{s}}\mathbf{S}\left(\boldsymbol{J}\boldsymbol{\omega}_\mathrm{s}\right)\boldsymbol{\omega}_\mathrm{s}\right|_{\boldsymbol{\omega}_\mathrm{s}=\bar{\boldsymbol{\omega}}_\mathrm{s}}+\left.\frac{\mathrm{d}}{\mathrm{d}\boldsymbol{\omega}_\mathrm{s}}\mathbf{S}\left(\boldsymbol{\omega}_\mathrm{s}\right)\boldsymbol{J}\boldsymbol{\omega}_\mathrm{s}\right|_{\boldsymbol{\omega}_\mathrm{s}=\bar{\boldsymbol{\omega}}_\mathrm{s}}\right]\tilde{\boldsymbol{\omega}}_\mathrm{s}\\ &= \boldsymbol{J}^{-1}\left[\mathbf{S}\left(\boldsymbol{J}\bar{\boldsymbol{\omega}}\right)-\mathbf{S}\left(\bar{\boldsymbol{\omega}}_\mathrm{s}\right)\boldsymbol{J}\right]\tilde{\boldsymbol{\omega}}_\mathrm{s}\end{aligned} \tag{4.67}$$

Linear Attitude Model

The non-linear system can now be expressed in a linear state space model. However, observing Equation 4.66, it is seen that the scalar element q_1 has zero dynamics. This is expected, since it can be approximated to one for small angles. Hence the state vector is reduced to six states being the small signals of the states in the non-linear model, which is written

$$\boldsymbol{x} = \begin{bmatrix}\tilde{\boldsymbol{q}}_{2-4}\\ \tilde{\boldsymbol{\omega}}_\mathrm{s}\end{bmatrix} \tag{4.68}$$

When obtaining the quaternion from the reduced state vector, the scalar element should be set to one and the result normalized, since this is not ensured by the linearized kinematic equation.

The linearized attitude model can now be expressed as

$$\begin{bmatrix}\dot{\tilde{\boldsymbol{q}}}_{2-4}\\ \dot{\tilde{\boldsymbol{\omega}}}_\mathrm{s}\end{bmatrix} = \begin{bmatrix}-\mathbf{S}\left(\bar{\boldsymbol{\omega}}_\mathrm{s}\right) & \frac{1}{2}\mathbf{1}_{3\times3}\\ \mathbf{0}_{3\times3} & \boldsymbol{J}^{-1}\left[\mathbf{S}\left(\boldsymbol{J}\bar{\boldsymbol{\omega}}_\mathrm{s}\right)-\mathbf{S}\left(\bar{\boldsymbol{\omega}}_\mathrm{s}\right)\boldsymbol{J}\right]\end{bmatrix}\begin{bmatrix}\tilde{\boldsymbol{q}}_{2-4}\\ \tilde{\boldsymbol{\omega}}_\mathrm{s}\end{bmatrix} \tag{4.69}$$

4.4 Solar Pressure

The most significant source of disturbance in the dynamic equations of attitude and relative position, is the solar pressure. Therefor the dynamic equations of the force and torque caused by the Sun are derived.

SMART-2 consists of two fully equipped satellites and the sphere satellite. However when considering solar pressure, the geometry of the fully equipped satellites must also be known. Since the satellites used for DARWIN are telescope flyers, the same geometric composition is assumed for the SMART-2 satellites, except for the sphere satellite.

Solar Force

Figure 4.3 shows a telescope flyer satellite, which is exposed to solar flux, which enters at an angle θ. A sunscreen with radius R_s is mounted on the satellite, to protect the optics from the Sunlight. Integrating over the points of contact, a center of pressure is acquired. The center of mass is in a displacement below the center of pressure. Due to the symmetrical shape of the satellite, both points are on the line spanned by the target star LOS.

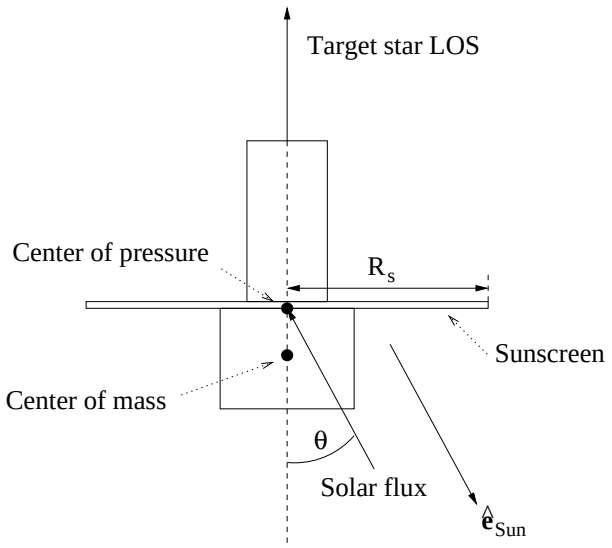

Figure 4.3: *A telescope flyer satellite exposed to the solar flux.*

The force acting on the telescope flyer depends on the angle θ, of the incoming solar flux. The solar flux vector is in the opposite direction of the Sun LOS vector $\hat{e}_{\text{Sun}}$. Since the vector from the center of mass to the center of pressure is parallel to the target star LOS, the resulting force of the solar flux $\boldsymbol{f}_{\text{Sun/tf}}$, is obtained by projecting the solar flux force $\boldsymbol{f}_{\text{flux}}$, acting on the center of pressure, onto the target star LOS, giving

$$\boldsymbol{f}_{\text{Sun/tf}} = \boldsymbol{f}_{\text{flux}} \cos(\theta) \tag{4.70}$$

The force of the flux can be expressed in terms of the the solar momentum and the area of the sunscreen, as [Bonnet, 2000]

$$\boldsymbol{f}_{\text{flux}} = -\frac{2P}{c}\pi R_{\text{s}}^2 \hat{\boldsymbol{e}}_{\text{Sun}} \tag{4.71}$$

where P is the solar flux, c is the vacuum velocity of light, and R_{s} is the radius of the sun screen. The solar momentum is multiplied by a factor two, implying that the surface of the satellite is reflective.

Combining Equations 4.70 and 4.71, yields the equation of the solar force acting on the telescope flyers

$$\boldsymbol{f}_{\text{Sun/tf}} = -\frac{2P}{c}\pi R_{\text{s}}^2 \cos(\theta)\, \hat{\boldsymbol{e}}_{\text{Sun}} \tag{4.72}$$

In a similar manner, the solar force acting on the sphere is derived.

The center of pressure on the sphere satellite is on the surface of the sphere, and the vector from the center of pressure to the center of mass, is always parallel to the incoming flux, as illustrated in Figure 4.4.

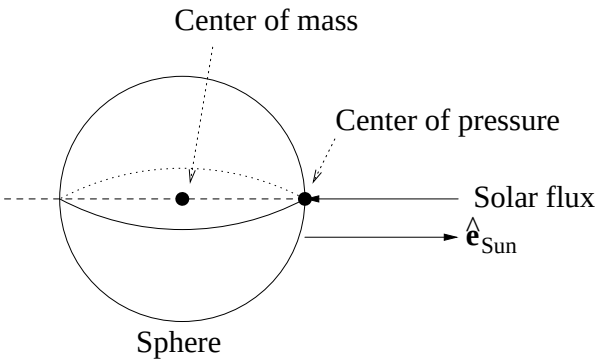

Figure 4.4: *The sphere satellite exposed to solar flux.*

The area of which the solar flux hits the sphere is equal to the surface of half the sphere, and the solar force acting on the sphere can be expressed as

$$\boldsymbol{f}_{\text{Sun/b}} = -\frac{4P}{c}\pi R_{\text{b}}^2 \hat{\boldsymbol{e}}_{\text{Sun}} \tag{4.73}$$

where R_b is the radius of the sphere.

The dynamic equations of relative position, require that the external forces used in the equations are also relative, hence the relative force $\boldsymbol{f}_{\text{Sun/rel}}$ is found to be

$$\begin{aligned}\boldsymbol{f}_{\text{Sun/rel}} =& \boldsymbol{f}_{\text{Sun/tf}} - \boldsymbol{f}_{\text{Sun/b}} \\ &= -\frac{2P}{c}\pi R_\mathrm{s}^2 \cos(\theta)\, \hat{\boldsymbol{e}}_{\text{Sun}} + \frac{4P}{c}\pi R_\mathrm{b}^2 \hat{\boldsymbol{e}}_{\text{Sun}} \\ &= \frac{2P}{c}\pi \left[2R_\mathrm{b}^2 - R_\mathrm{s}^2 \cos(\theta)\right] \hat{\boldsymbol{e}}_{\text{Sun}}\end{aligned} \tag{4.74}$$

Dividing the forces by the masses of the telescope flyer and the sphere satellite, respectively, the relative acceleration is given by

$$\boldsymbol{a}_{\text{Sun/rel}} = \frac{2P}{c}\pi \left[2\frac{R_\mathrm{b}^2}{m_\mathrm{b}} - \frac{R_\mathrm{s}^2}{m_\mathrm{s}} \cos(\theta)\right] \hat{\boldsymbol{e}}_{\text{Sun}} \tag{4.75}$$

The fictive force, to be inserted in the relative position dynamics of Equation 4.29 on page 51, is found by using Newton's second law of motion

$$\boldsymbol{f}_{\text{Sun}} = m_\mathrm{s} \boldsymbol{a}_{\text{Sun/rel}} \tag{4.76}$$

When the solar force is inserted in Equation 4.29 on page 51, the relative acceleration is added to the derivative of the velocity state. The fact that inputs to the dynamics is divided by m_s to obtain the acceleration of the chaser relative to the sphere, is the reason why a relative force must be inserted. For control inputs, the thruster force is always relative, since they only accelerate the satellite on which they are mounted.

It should be noted that the modeling of the solar pressure assumes that the solar flux is constant. Since the solar flux in fact varies around a working point, it is simulated as a biased white noise.

Solar Torque

The torque resulting from the solar flux can be found as the cross product of the force and the vector pointing from the center of mass to the center of pressure. For the sphere satellite this torque is always zero, since the two vectors are parallel at all times. For the telescope flyer satellite, the solar torque $\boldsymbol{n}_{\text{Sun}}$ is

$$\boldsymbol{n}_{\text{Sun}} = \boldsymbol{r}_{\text{COP}} \times \boldsymbol{f}_{\text{Sun/tf}} \tag{4.77}$$

where $\boldsymbol{r}_{\text{COP}}$ is the vector from the center of mass to the center of pressure. Inserting $\boldsymbol{f}_{\text{Sun/tf}}$ as given in Equation 4.72, yields

$$\boldsymbol{n}_{\text{Sun}} = -\frac{2P}{c}\pi R_{\text{s}}^2 \left[\hat{\boldsymbol{r}}_{\text{COP}} \times \boldsymbol{e}_{\text{Sun}}\right] \tag{4.78}$$

4.5 Modeling Sensors and Actuators

This section derives the models used for the sensor and actuator hardware. The sensor system consists of gyroscopes, star trackers and the laser metrology system. The actuators are Field Emitting Electric Propulsion (FEEP) thrusters with μN quantization.

The modeling of the hardware is not investigated in detail, hence the derived models are simplified, compared to model in other documents. The models are assumed adequate for simulation purposes.

The quantization of the digital components are not included in the mathematical models, but are included in the simulation model.

Gyroscopes

Gyroscopes are used to measure the angular velocity of a satellite with respect to an inertial frame. The output of a gyroscope is a voltage that is proportional to the angular velocity about an input axis, defined by the gyroscope's orientation. The angular velocity of the satellite $\boldsymbol{\omega}_{\text{s}}$ is given by [James R. Wertz, 1978]

$$\boldsymbol{\omega}_{\text{s}} = C u_{\text{Gyro}} \hat{\boldsymbol{e}}_{\text{Gyro}} \tag{4.79}$$

where u_{Gyro} is the voltage output of the gyroscope and $\hat{e}_{\text{Gyro}}$ is the input axis. The proportional factor C, known as the scale factor, is not known precisely, hence there is a biased error in the measurement. Misalignment in the input axis also causes a bias. Due to an internal drift in the gyroscopes hardware, there is a drift in the output, which diverges at a certain rate over time. Hence the measured angular velocity $\boldsymbol{\omega}_{\text{Gyro}}$ can be expressed as [James R. Wertz, 1978]

$$\boldsymbol{\omega}_{\text{Gyro}} = \left(1 + \epsilon_{\text{sf}}\right) \hat{\boldsymbol{e}}_{\text{Gyro}} \cdot \boldsymbol{\omega}_{\text{s}} + \boldsymbol{\epsilon}_{\text{align}} + \boldsymbol{\epsilon}_{\text{drift}} + \boldsymbol{w} \tag{4.80}$$

where ϵ_{sf} is the scale factor error, $\boldsymbol{\epsilon}_{\text{align}}$ is the alignment error of the gyroscope's input axis, $\boldsymbol{\epsilon}_{\text{drift}}$ is the internal drift and $\boldsymbol{w}$ is zero mean white noise.

Usually the configuration of the gyroscopes enables the measurement of the angular velocity even if one gyroscope falls out. However for the simulation used for this project, three gyroscopes will be configured with the spacecraft body axes as input axes. Hence the obtained angular velocity from Equation 4.80 for each of the three gyroscope, will be the estimated element of the satellites angular velocity, corresponding to the input axis. The estimate of the satellite's angular velocity $\hat{\boldsymbol{\omega}}_{\mathrm{s}}$ can be written

$$\hat{\boldsymbol{\omega}}_{\mathrm{s}} = \boldsymbol{\omega}_{\mathrm{Gyro1}} + \boldsymbol{\omega}_{\mathrm{Gyro2}} + \boldsymbol{\omega}_{\mathrm{Gyro3}} \tag{4.81}$$

where $\boldsymbol{\omega}_{\mathrm{Gyro}i}$ is the measurement of the gyroscope which has the ith body axis as input axis.

Star Trackers

In order to determine the attitude of a satellite, star trackers make use of the pattern of the stars. The measurement of the attitude is biased by an alignment error of the star tracker. In addition there is a white noise, which is commonly expressed as a dispersion in the Euler angles. In quaternion notation, the attitude $\boldsymbol{q}_{\mathrm{st}}$ measured by the star tracker is given by

$$\boldsymbol{q}_{\mathrm{st}} = \boldsymbol{q}_{\mathrm{st}} \boldsymbol{q}_{w} \boldsymbol{q}_{\mathrm{align}} \tag{4.82}$$

where $\boldsymbol{q}_{\mathrm{sat}}$ is the true attitude of the star tracker, $\boldsymbol{q}_{w}$ is the attitude resulting from zero mean white noise in the Euler angles and $\boldsymbol{q}_{\mathrm{align}}$ is the attitude bias caused by the error in orientation of the star tracker. The noise attitude $\boldsymbol{q}_{w}$ is obtained by an Euler 1-2-3 rotation sequence of the roll, pitch and yaw errors.

Due to the CCD in a star tracker, the measured attitude of Equation 4.82 is subject to quantization, which is included in the simulation model.

Laser Metrology System

The laser metrology system is used to measure the relative position between two satellites. The system consists of a laser source and a CCD. The laser beam exiting the satellite must be pointed in a known direction, and the CCD mounted with a certain orientation. Both are biased due to alignment errors. In addition the CCD causes quantization on the measurement vector $\boldsymbol{m}$, which depends on the resolution of the CCD. This is included in the simulation model.

FEEP Thrusters

FEEP thrusters apply the necessary force and torque to stabilize the satellite. The direction of the applied force is biased, caused by misalignment of the thruster. The resulting force $\boldsymbol{f}_{\text{FEEP}}$ of the input force magnitude f_{ctrl} from the controller, can be modeled by

$$\boldsymbol{f}_{\text{FEEP}} = w\left(1+\epsilon_{\text{sf}}\right) f_{\text{ctrl}} \left[\tilde{\boldsymbol{d}} + \boldsymbol{d}_{\epsilon}\right] \quad , \quad \left|\tilde{\boldsymbol{d}} + \boldsymbol{d}_{\epsilon}\right| = 1 \tag{4.83}$$

where w is white noise with mean value of one, ϵ_{sf} is a scale factor bias, $\hat{\boldsymbol{d}}$ is the estimated direction of the thrust which is an error of $\boldsymbol{d}_{\epsilon}$ from the true direction. The scale factor ϵ_{sf} is only a true bias under the assumption that the thrust is proportional to the input of the hardware, which is assumed.

The FEEP thrusters are subject to quantizations in the magnitude of the thrust and in the minimum impulse time, included in the simulation model.

4.6 Full State Space Model

From the previous sections of this chapter, a state space model is sought containing all states. The system model of the satellite is written in the form

$$\dot{\boldsymbol{x}} = \boldsymbol{F}\boldsymbol{x} + \boldsymbol{G}\boldsymbol{u} \tag{4.84}$$

$$\boldsymbol{y} = \boldsymbol{H}\boldsymbol{x} \tag{4.85}$$

The working point of the satellite's angular velocity, is for SMART-2 zero, since satellites are sought three axis stabilized. If the spacecrafts are spinning the laser metrology system is inapplicable. This is inserted in the attitude model.

Combining the relative position model in Equation 4.29 on page 51 and the linearized attitude model in Equation 4.69 on page 60, yields

$$
\begin{bmatrix} \dot{\tilde{\boldsymbol{q}}}_{2-4} \\ \dot{\tilde{\boldsymbol{\omega}}}_{\mathrm{s}} \\ \dot{\boldsymbol{r}}_{\mathrm{s}} \\ \ddot{\boldsymbol{r}}_{\mathrm{s}} \end{bmatrix} =
$$

$$
\begin{bmatrix} \mathbf{0}_{3\times3} & \frac{1}{2}\mathbf{1}_{3\times3} & & & \mathbf{0}_{6\times6} & & \\ \mathbf{0}_{3\times3} & \mathbf{0}_{3\times3} & & & & & \\ & & & \mathbf{0}_{3\times3} & & \mathbf{1}_{3\times3} & \\ & \mathbf{0}_{6\times6} & 0 & 0 & 0 & 0 & 0 & 2\omega_{\mathrm{o}} \\ & & 0 & -\omega_{\mathrm{o}}^2 & 0 & 0 & 0 & 0 \\ & & 0 & 0 & 3\omega_{\mathrm{o}}^2 & -2\omega_{\mathrm{o}} & 0 & 0 \end{bmatrix} \begin{bmatrix} \tilde{\boldsymbol{q}}_{2-4} \\ \tilde{\boldsymbol{\omega}}_{\mathrm{s}} \\ \boldsymbol{r}_{\mathrm{s}} \\ \dot{\boldsymbol{r}}_{\mathrm{s}} \end{bmatrix}
$$

$$
+ \begin{bmatrix} \mathbf{0}_{3\times6} \\ \boldsymbol{J}^{-1} \quad \mathbf{0}_{3\times3} \\ \mathbf{0}_{3\times6} \\ \mathbf{0}_{3\times3} \quad \frac{1}{m_s}\mathbf{1}_{3\times3} \end{bmatrix} \begin{bmatrix} \boldsymbol{n}_{\mathrm{ctrl}} \\ \boldsymbol{f}_{\mathrm{ctrl}} \end{bmatrix} \tag{4.86}
$$

where the input vector $\boldsymbol{u}$ is the control torque and force generated by the FEEP thrusters, denoted $\boldsymbol{n}_{\mathrm{ctrl}}$ and $\boldsymbol{f}_{\mathrm{ctrl}}$, respectively.

The output equation stated in Equation 4.85, depends on the measurable quantities of the state vector. Using star trackers, gyroscopes and the laser metrology system, nine of the twelve states can be measured. Hence the output equation becomes

$$
\begin{bmatrix} \tilde{\boldsymbol{q}}_{2-4} \\ \tilde{\boldsymbol{\omega}}_{\mathrm{s}} \\ \boldsymbol{r}_{\mathrm{s}} \end{bmatrix} = \begin{bmatrix} \mathbf{1}_{9\times9} & \mathbf{0}_{9\times3} \end{bmatrix} \begin{bmatrix} \tilde{\boldsymbol{q}}_{2-4} \\ \tilde{\boldsymbol{\omega}}_{\mathrm{s}} \\ \boldsymbol{r}_{\mathrm{s}} \\ \dot{\boldsymbol{r}}_{\mathrm{s}} \end{bmatrix} \tag{4.87}
$$

The system matrices of Equations 4.84 and 4.85 are identified as

$$
\boldsymbol{F} = \begin{bmatrix} \mathbf{0}_{3\times3} & \frac{1}{2}\mathbf{1}_{3\times3} & & & \mathbf{0}_{6\times6} & & \\ \mathbf{0}_{3\times3} & \mathbf{0}_{3\times3} & & & & & \\ & & & \mathbf{0}_{3\times3} & & \mathbf{1}_{3\times3} & \\ & \mathbf{0}_{6\times6} & 0 & 0 & 0 & 0 & 0 & 2\omega_{\mathrm{o}} \\ & & 0 & -\omega_{\mathrm{o}}^2 & 0 & 0 & 0 & 0 \\ & & 0 & 0 & 3\omega_{\mathrm{o}}^2 & -2\omega_{\mathrm{o}} & 0 & 0 \end{bmatrix} \tag{4.88}
$$

$$
\boldsymbol{G} = \begin{bmatrix} \mathbf{0}_{3\times6} \\ \boldsymbol{J}^{-1} \quad \mathbf{0}_{3\times3} \\ \mathbf{0}_{3\times6} \\ \mathbf{0}_{3\times3} \quad \frac{1}{m_s}\mathbf{1}_{3\times3} \end{bmatrix} \tag{4.89}
$$

$$
\boldsymbol{H} = \begin{bmatrix} \mathbf{1}_{9\times9} & \mathbf{0}_{9\times3} \end{bmatrix} \tag{4.90}
$$

System Poles

The system poles are given by the eigenvalues of the system matrix $\boldsymbol{F}$ [Gene F. Franklin et al., 1994]. The system has six poles in zero, and four poles on the imaginary axis, as plotted in Figure 4.5. Note that the four complex poles are equal in pairs of two, and close to zero. Considering the magnitude of the angular velocity of an Earth trailing, helio centric orbit, this result is expected.

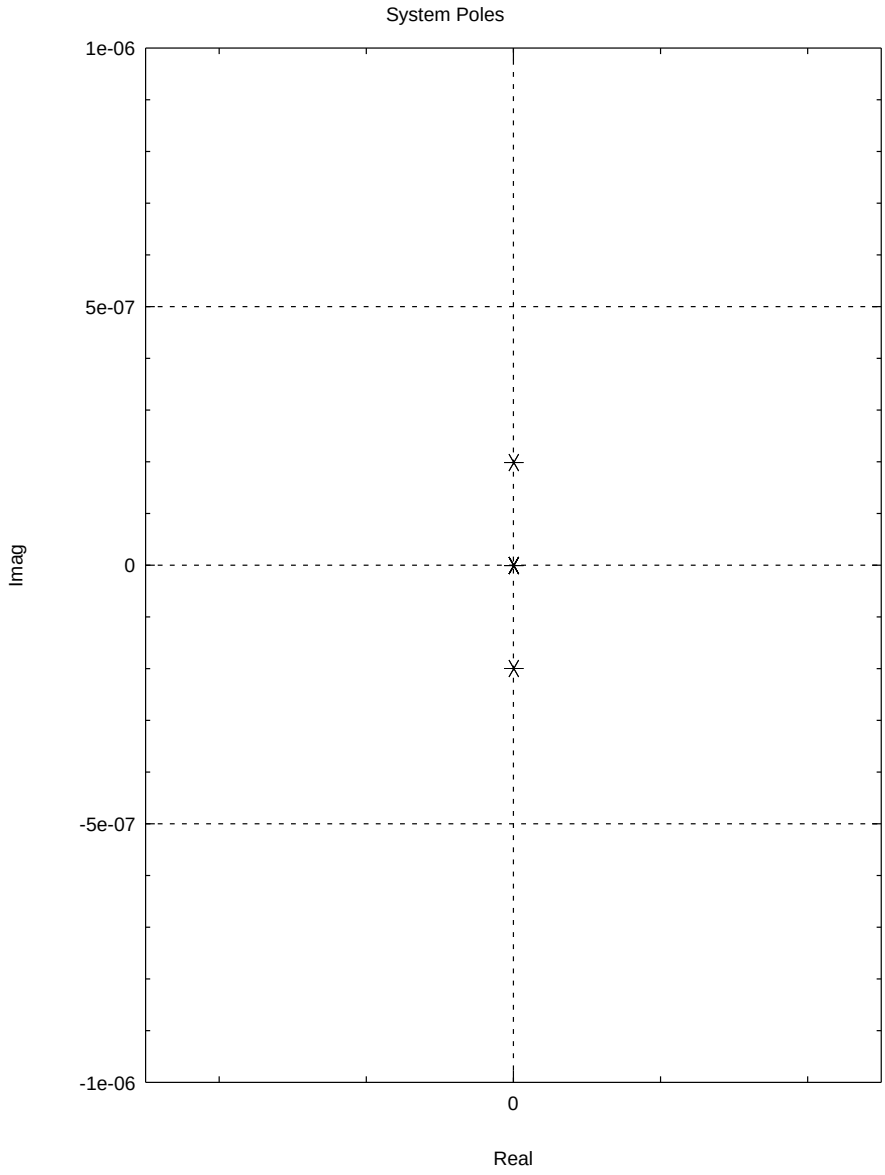

Figure 4.5: *Plot of the system poles, equivalent to the eigenvalues of* $\boldsymbol{F}$*, in the complex plane.*

Chapter 5

Laser Metrology Configuration

Before the design of controllers can commence, a configuration of the laser metrology system is investigated. The system operates on baselines spanning from 25m to 250m, when measured from the sphere to the satellite. It must be guaranteed that the reflected laser beam will hit the CCD of the satellite, for all baselines in this interval.

The configuration is done by selecting the following parameters appropriately (see Figure 3.11 on page 32):

- $\boldsymbol{r}_{\text{l-s}}$. The placement of the laser source, or more accurately, the point where the laser beam will exit the plane spanned by the CCD surface.
- γ. The pitch angle of the exiting laser beam, measured from the CCD plane normal.
- α. A rotation of the laser frame, defining the direction of the pitch angle γ.
- R_b. The radius of the sphere.

The position of the reflected laser beam on the CCD plane, is given by the measurement vector $\boldsymbol{m}$. It is the length of this vector which is sought limited, such that the reflected laser beam will hit the CCD, which is limited in size. Due to the symmetry of the sphere, α is chosen to zero for this analysis, since α only influences the direction of $\boldsymbol{m}$. Given the dimensions of the satellite surface, on which the CCD is to be placed, α can be chosen appropriately. Due to the same circumstances, the placement of the laser $\boldsymbol{r}_{\text{l-s}}$ is only varied in one direction on the satellite surface, since it is only the length of $\boldsymbol{r}_{\text{l-s}}$ which varies the length of $\boldsymbol{m}$.

Given the above considerations, the configuration can be analyzed in the $\boldsymbol{xz}$ plane of the laser frame, when choosing a reference of the satellite position in the same plane,

and assuming that the satellite reference attitude aligns the axes of the sphere frame and the laser frame at this reference position. The setup is illustrated in Figure 5.1.

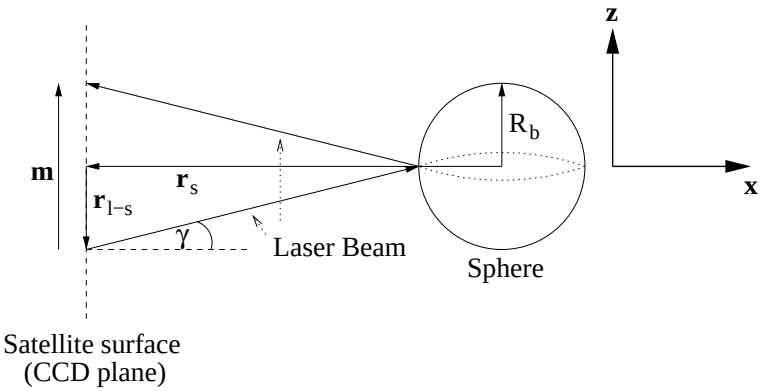

Figure 5.1: *Setup used for analyzing possible configurations of the laser metrology system.*

Working only in the $\boldsymbol{xz}$ plane simplifies the limits of $\boldsymbol{m}$ to a limit on the third element m_3. The placement of the laser reduces to varying $r_{\text{l-s3}}$ and the baseline length is given by r_{s1}.

Selecting a sphere radius of $R_b = 0.5$m, the length of the measurement vector m_3, can be plotted as a function of the laser placement and pitch angle. Figure 5.2 shows this plot for a baseline length of 25m.

Figure 5.2 shows the lengths of the measurement vector, forming the reflection surface, as a function of moving the laser in the negative direction of $\boldsymbol{z}$, and pitching it a negative angle. Choosing negative placement and negative pitch angle results in the configuration of Figure 5.1, where the laser source is under the horizontal of $z = 0$ and the reflection is above. In addition to m_3, two planes are plotted in Figure 5.2, i.e. the laser position plane and the CCD limit surfaces, described in the following.

The laser position plane is the position of the laser on the satellite surface. The plane is given by $m_3 = r_{\text{l-s3}}$. The intersection of the laser position plane and the reflection surface is a line, where the configuration will result in a laser beam reflected back to the source, e.g. when $r_{\text{l-s3}}$ and γ are zero, as shown in Figure 3.8 on page 30. The configuration must be chosen such that the reflected laser beam is either above or under the laser source for all distances, otherwise m_3 will be unobservable at some baseline length.

The CCD limit surfaces, illustrates the height of a CCD placed adjacent to the laser source, assumed to be approximately 2cm, given a resolution of 2048×2048 and a pixel separation of 9μm. The configuration should be chosen such that the reflection surface is between the laser position plane and either the positive or negative CCD limit plane, for all baselines.

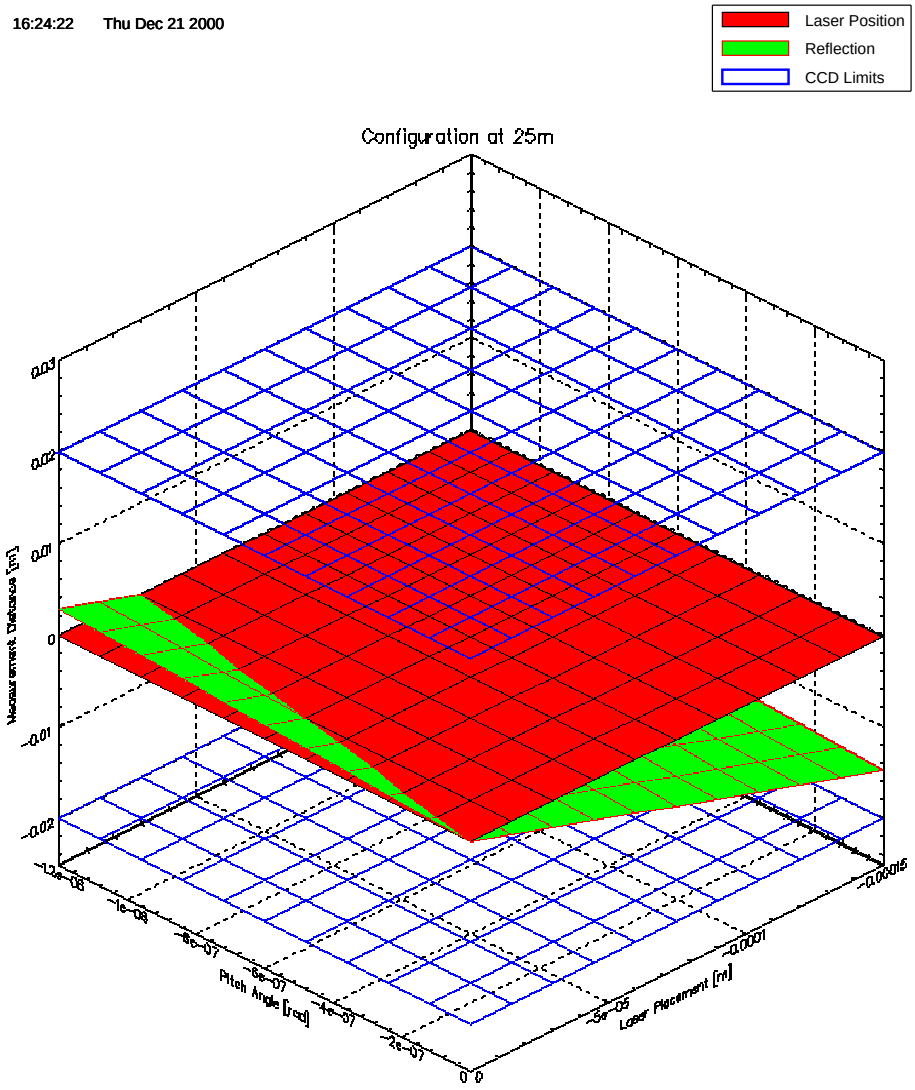

Figure 5.2: *Plot of the distance to the point where the reflected laser beam hits the satellite surface, as a function of the laser placement* $r_{l\text{-}s3}$ *and pitch* γ*, for a baseline length of* $25m$*.*

For the values of $r_{\text{l-s3}}$ and γ in Figure 5.2, the surface of the reflection is within these limits, but this is not the case at maximum baseline length of 250m, as shown in Figure 5.3.

From Figure 5.3 it is seen that m_3 is very sensitive to configuration adjustments, illustrated by the large slope of the surface. In both plots it is seen that when altering $r_{\text{l-s3}}$ and γ simultaneously at a rate given by the intersection of the reflection surface and any horizontal plane, m_3 can be held constant. This means that the placement of the laser can be arbitrary large if the pitch angle is adjusted accordingly. However the difference in direction of these intersections in the two plots, shows that the parameters $r_{\text{l-s3}}$ and γ must be held close to zero. In addition it seen from the large slope of the reflection surface for a baseline length of 250m, that a small error in the pitch angle, will result in a large increment of m_3. These two important conditions can be emphasized by additional plots.

Figure 5.4 illustrates a plot of m_3 at multiple baseline lengths, spanning from 25m to 250m. As an example choose $r_{\text{l-s3}}$ to be -0.1mm. With a baseline length of 250m, it can be derived from Figure 5.4 that a pitch angle of 4.4×10^{-7}rad will result in a measurement length of approximately 2cm. However this configuration will result in a negative m_3 for a baseline length of 25m. This means that somewhere in between these two baseline lengths, m_3 is on the laser surface. Hence this configuration will result in an unobservable working point of the laser. That is, the laser will be reflected back to the laser source, where a CCD would block the optical path.

The only configuration which will result in m_3 being within the limits of 2cm and above the laser surface, for all baselines, are the combinations near the origin, i.e. a placement and pitch angle close to zero. Choosing $r_{\text{l-s3}} = 0$, the pitch angle is limited only by the requirements of the longest baseline. From Figure 5.3 a maximum numerical pitch angle of -0.8×10^{-7}rad is found when $r_{\text{l-s3}} = 0$. Given this configuration m_3 can be plotted as a function of the baseline length, to illustrate the working area of m_3 for all baselines. This plot is shown in Figure 5.5.

From Figure 5.5 it is seen that the reflected laser beam is limited within the requirements of the CCD. For baseline lengths close to 25m and 250m the working point of the laser is at the edge of the CCD. However, as mentioned above, m_3 is very sensitive to parameter adjustments, which means that the laser must be mounted accurately, in a magnitude that is practically impossible.

It can be shown that if the laser is pointed at the center of the CCD, the working area is still too small. If the working point is chosen to be at the center of the CCD, the pitch angle can be found from Figure 5.3 to be -40×10^{-9}rad for a baseline length of 250m. The limit of m_3 is at pitch angle -80×10^{-9}rad, requiring the error in the pitch angle to be less than 40×10^{-9}rad or -8.3×10^{-3}mas. Note that even if the laser is mounted at an exact angle, the attitude control system will have to meet the same requirements.

Realizing that the laser metrology system is unfeasible at large baselines, the require-

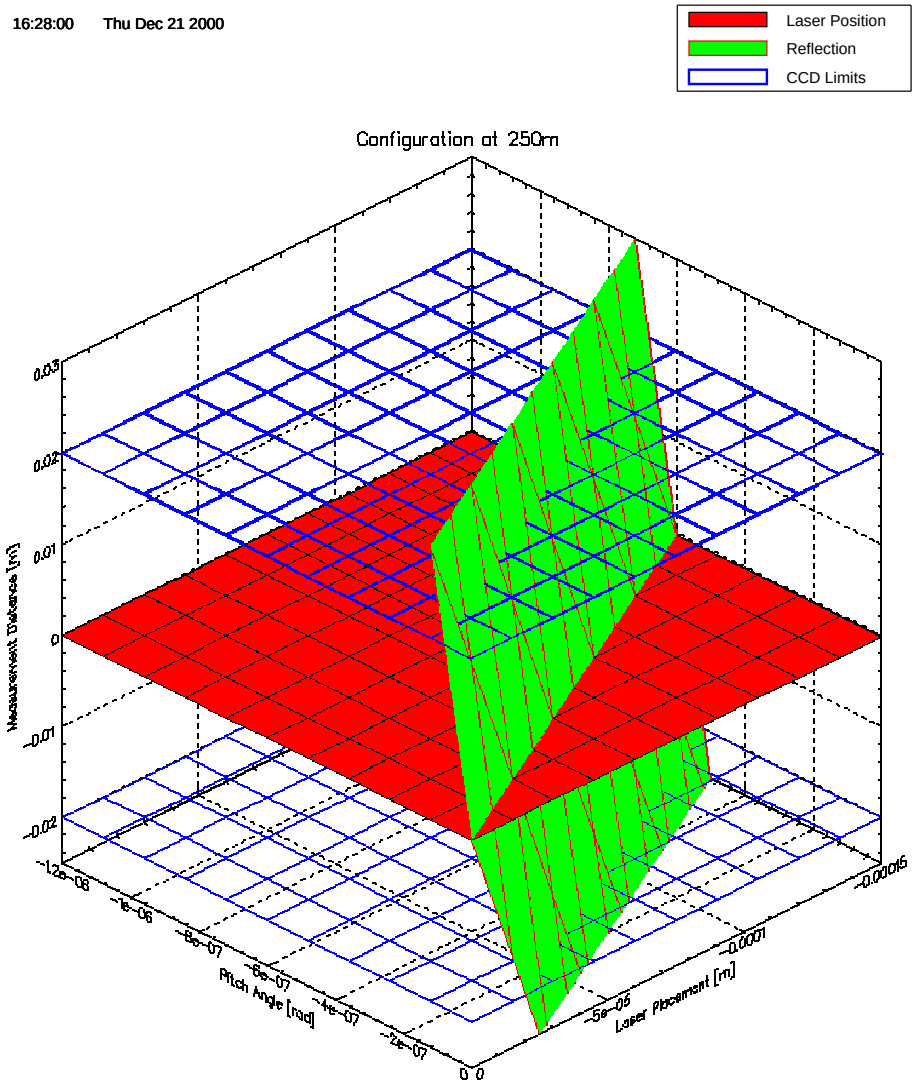

Figure 5.3: *Plot of the distance to the point where the reflected laser beam hits the satellite surface, as a function of the laser placement* $r_{l\text{-}s3}$ *and pitch* γ*, for a baseline length of* $250m$*.*

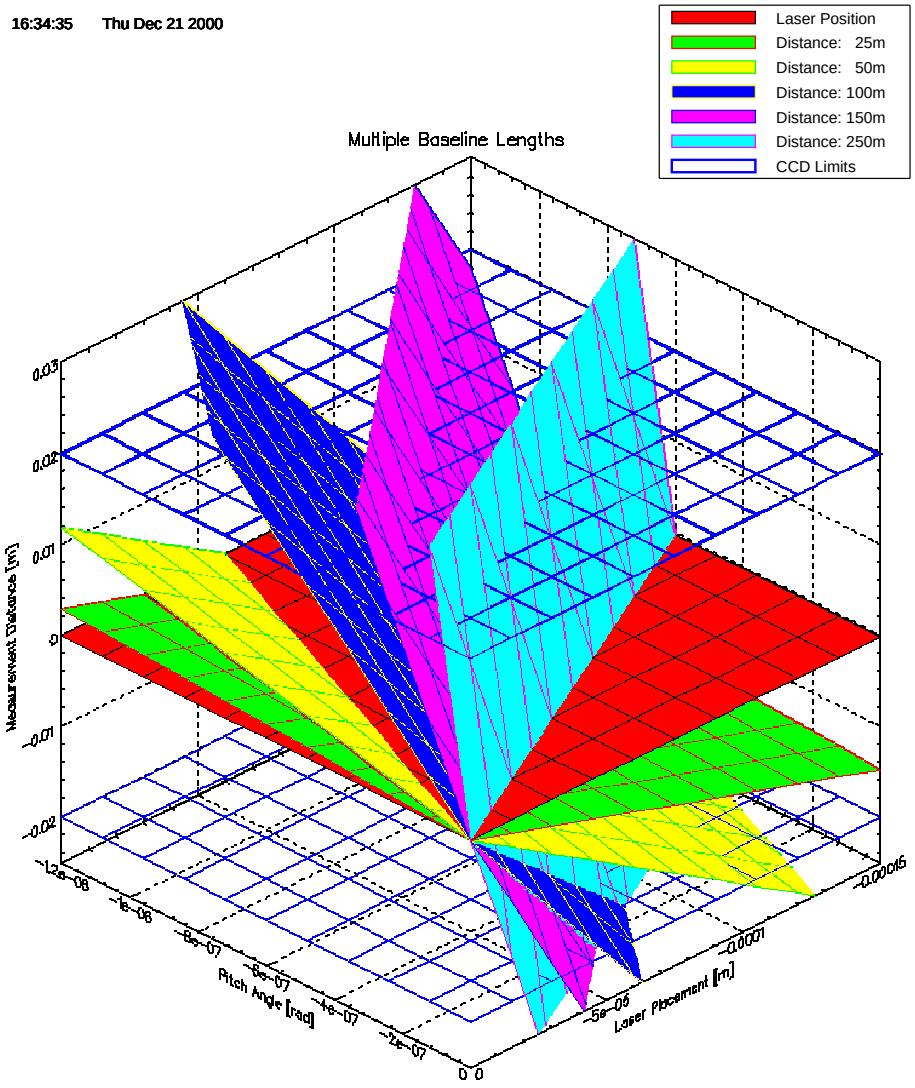

Figure 5.4: *Plot of the distance to the point where the reflected laser beam hits the satellite surface, as a function of the laser placement* $r_{l\text{-}s3}$ *and pitch* γ*, for baseline lengths of* $25m$*,* $50m$*,* $100m$*,* $150m$ *and* $250m$*.*

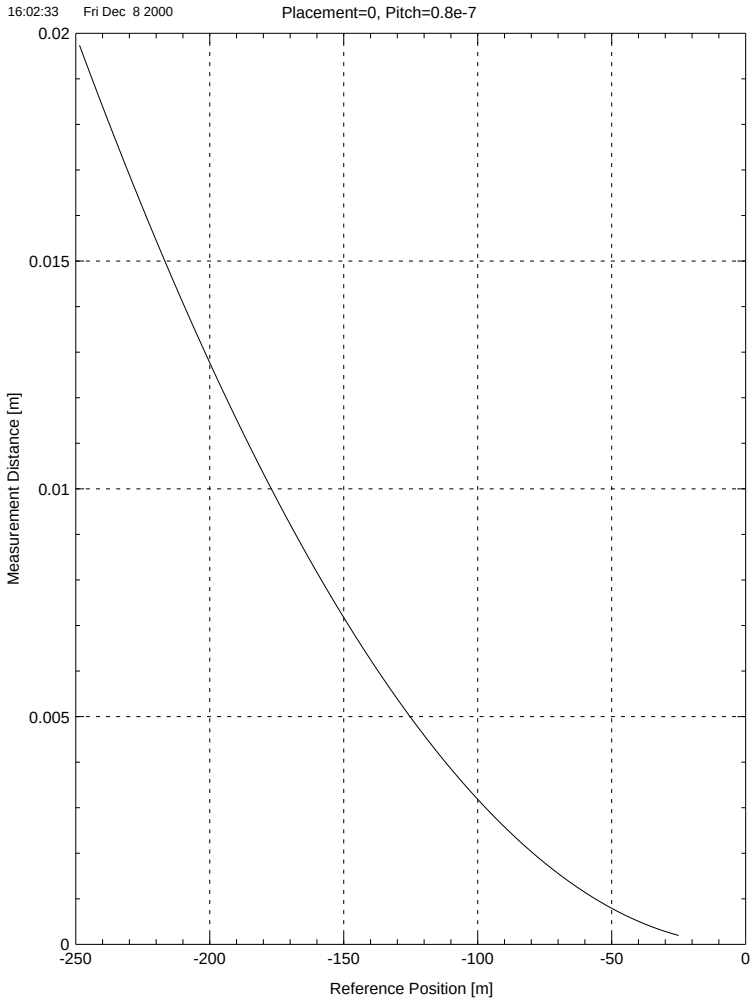

Figure 5.5: *Plot of the distance to the point where the reflected laser beam hits the satellite surface, as a function of the satellite reference position* r_{s1}*, with parameters* $r_{l\text{-}s3} = 0m$ *and* $\gamma = -0.8 \times 10^{-7} rad$.

ments at minimum baseline length are investigated.

Figure 5.6 shows the configuration parameters at a baseline length of 25m. The figure is the same as Figure 5.2 except that γ is scaled to show the angle where m_3 will exceed the limits of the CCD.

In order to allow largest possible errors on the mounting of the laser and the attitude control system, the working point of the laser is again chosen to be at the center of the CCD. From the data plotted in Figure 5.6 it can be derived that choosing $r_{\text{l-s3}}$ to be zero and a pitch angle of -4.0×10^{-6}rad will give the sought working point on the center of the CCD. It is also derived that a pitch angle of -8.1×10^{-6}rad is the pitch angle where m_3 leaves the CCD. This means that for a baseline of 25m, the error of the pitch angle must be smaller than 4.1×10^{-6}rad or approximately 0.85mas. Recall that this error is the sum of the mounting error of the laser source and the attitude control precision. It can know be concluded that the lase metrology system is unfeasible for all desired baseline lengths.

The only parameter which has not been investigated to this point is the radius of the sphere. All the above values are based on a sphere radius of 0.5m. To illustrate the effect of varying the radius of the sphere, the length of the measurement vector m_3 is plotted as a function of the baseline length for a number of sphere radii R_b. The plot is given in Figure 5.7. The parameters $r_{\text{l-s3}}$ and γ are set to 0 and $-0.8 \times$ rad, respectively. Recall that these values were found to limit m_3 within the requirements of the CCD for all baselines.

It is seen from Figure 5.7 that the working area of m_3 is halved, when increasing the radius of the sphere by a factor two. Since there is a similar linearity between the working area of m_3 and the pitch angle, which can be derived from Figure 5.4, the requirements of the pitch angle error can be halved if the radius of the sphere is doubled. The same linearity also means that the requirements of the pitch angle can be halved if the surface of the CCD is increased by a factor two.

However since a feasible estimate of the control precision of the satellite is in the neighborhood of 10as, the requirements of the pitch angle should be lowered by a factor in the magnitude of 10^4 for the smallest baseline length. This would require a CCD of 12×12cm^2 or a sphere radius of 2.7m, not considering mounting errors.

From the above estimations, it can be concluded that it is impossible to configure the laser metrology system, for all or even a single baseline configuration, when using a reflecting sphere. The reason is the high requirement of the pitch angle, to which m_3 is highly sensitive. In order to verify the results, the source of the vast gain of the pitch angle to the length of the measurement vector is identified.

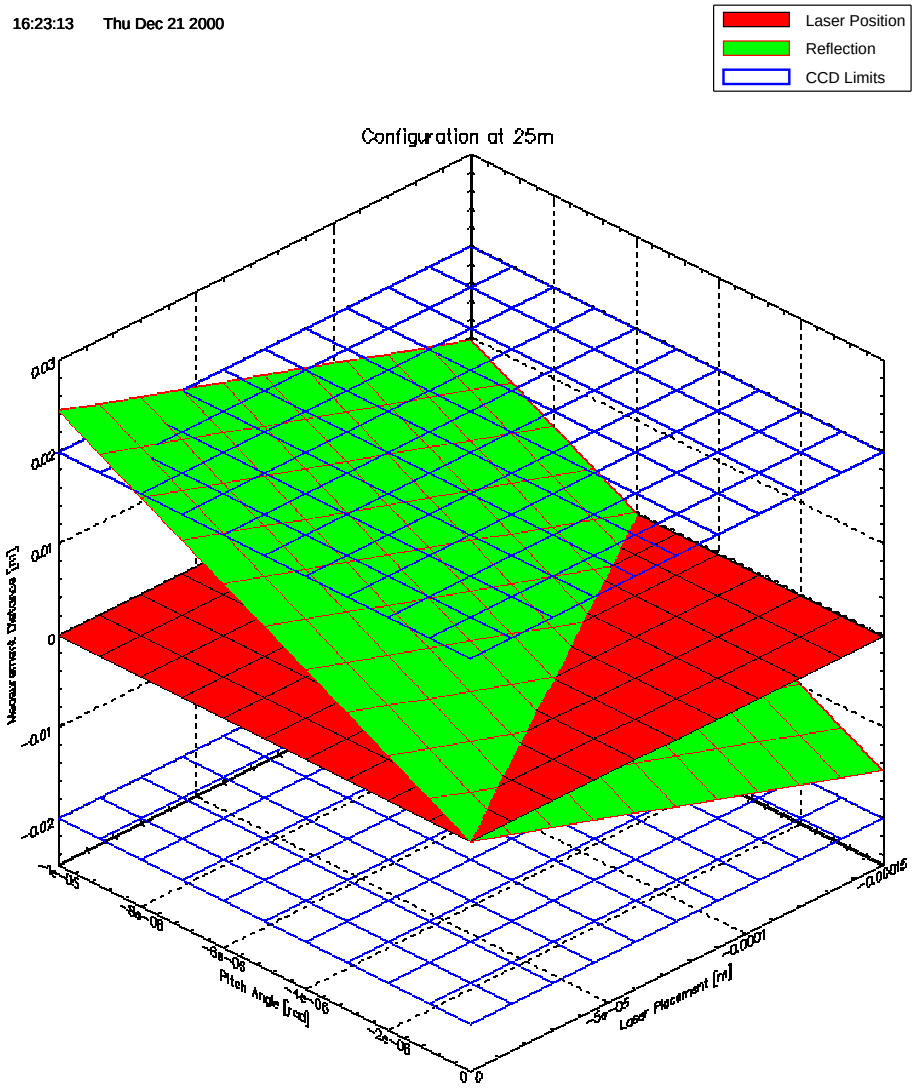

Figure 5.6: *Plot of the distance to the point where the reflected laser beam hits the satellite surface, as a function of the laser placement* $r_{l\text{-}s3}$ *and pitch* γ*, for a baseline length of* $25m$*.*

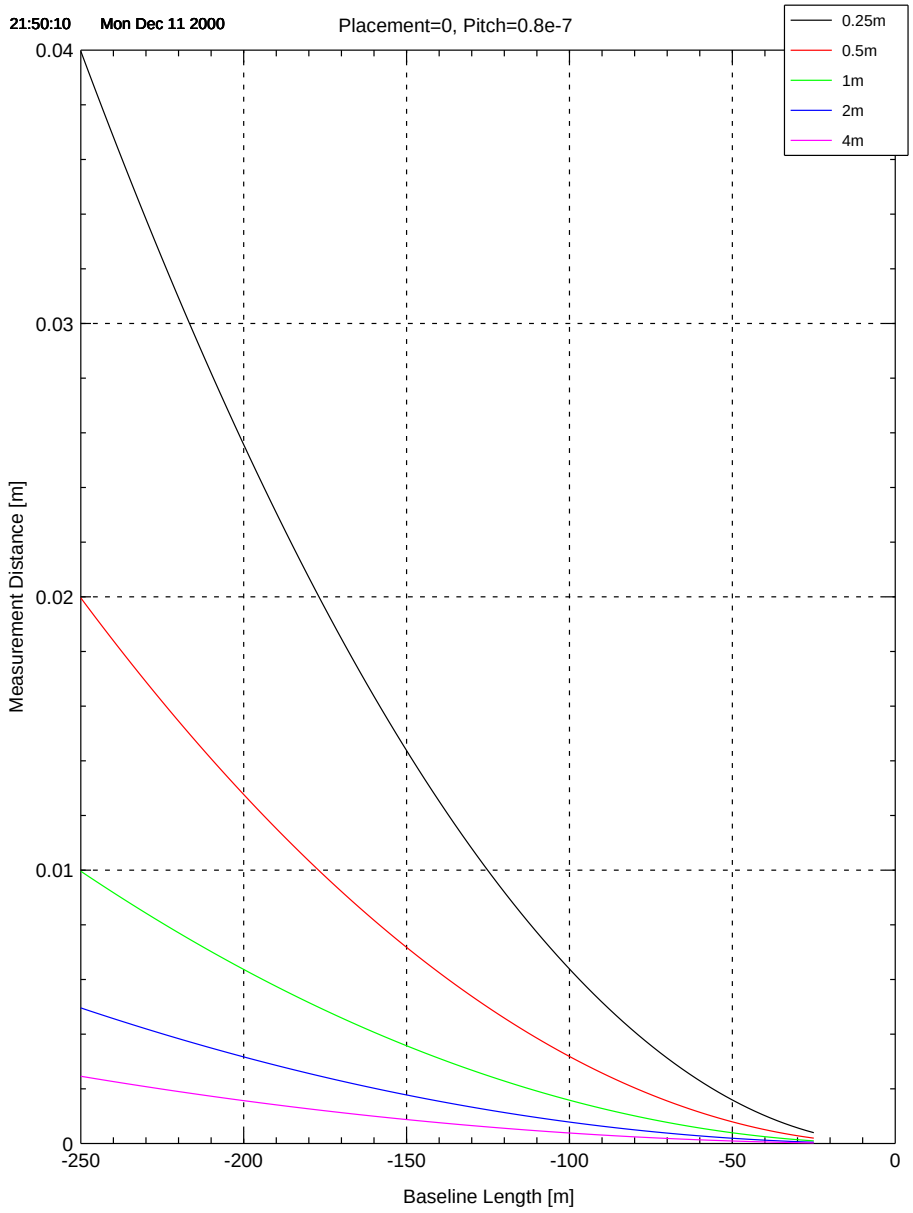

Figure 5.7: *Plot of the distance to the point where the reflected laser beam hits the satellite surface, as a function of the satellite reference position* r_{s1}*, for sphere radii of* $0.25m$*,* $0.5m$*,* $1m$*,* $2m$*,* $4m$*.*

5.1 Spherical Gain

When considering reflections, the reflection angle is of importance. For a reflection on a plane surface, the reflection angle is known to be equal to the angle of entrance. For the spherical case this does not apply. The reflection on the sphere is given by the tangential plane on the surface of the reflection point. The orientation of this plane changes, as the reflection point changes.

Consider the setup in Figure 5.8. The entrance angle is the pitch angle γ. The reflection angle θ of the laser beam, is a function of the vertical angle of the tangential plane ψ and the entrance angle γ. The angle ψ is also a function of the entrance angle γ. The laser crosses the horizontal, at a distance l from the center of the sphere.

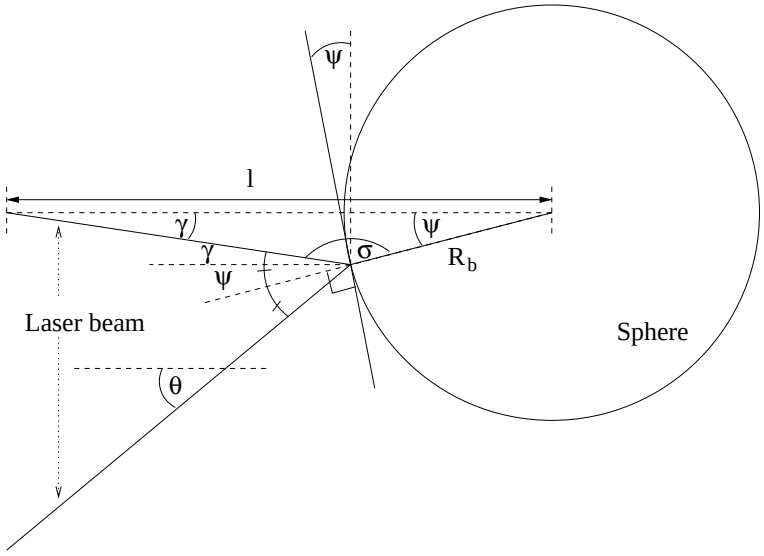

Figure 5.8: *Setup for investigating the gain of the reflection angle θ as a function of the entrance angle γ.*

Using this setup, the gain of the spherical reflection can be calculated for different distances, i.e. baseline lengths. In order to calculate the exit angle θ, the angle σ is found. Using sine relations of the triangle containing the angles γ, ψ and θ, yields

$$\frac{\sin(\sigma)}{l} = \frac{\sin(\gamma)}{R_b}$$

$$\Updownarrow$$

$$\sigma = \pi - \sin^{-1}\left(\frac{l}{R_b}\sin(\gamma)\right) \tag{5.1}$$

where R_b is the radius of the sphere. Note that the obtuse angle is found, because the angle σ is always larger than $\pi/2$, but the solution of the inverse sine function is the acute angle.

The angle ψ of the triangle can now be expressed as a function of γ, by

$$\begin{aligned}\psi &= \pi - \sigma - \gamma \\ &= \sin^{-1}\left(\frac{l}{R_b}\sin(\gamma)\right) - \gamma \end{aligned} \tag{5.2}$$

From Figure 5.8 it is seen that the angle θ can be expressed as

$$\theta = 2\psi + \gamma \tag{5.3}$$

Inserting Equation 5.2, yields

$$\theta = 2\sin^{-1}\left(\frac{l}{R_b}\sin(\gamma)\right) - \gamma \tag{5.4}$$

which is the sought function, expressing the reflection angle as a function of the entrance angle. If γ is assumed to be small, small angle approximations can be applied, which gives

$$\begin{aligned}\theta &= \left[2\frac{l}{R_b} - 1\right]\gamma \\ &\approx 2\frac{l}{R_b}\gamma \quad , \qquad \frac{l}{R_b} \gg 1\end{aligned} \tag{5.5}$$

From Equation 5.5 it is clear that the gain of the pitch angle is proportional to the baseline length and inversely proportional to the radius of the sphere.

Figure 5.9 illustrates the gain of the entrance angle at different baseline lengths, for a spherical radius of 0.5m. It also contains the line $\theta = \gamma$, which is the reflection angle for a plane mirror reflection. This line is approximately horizontal, due to the large gains of the spherical mirror.

The gains of the reflections in Figure 5.9 are also stated in Table 5.1, calculated using Equation 5.5.

The gain factors of Table 5.1 can be verified by observing Figure 5.9. The calculated gains reflect the problem of the previous section, where it is concluded that the length

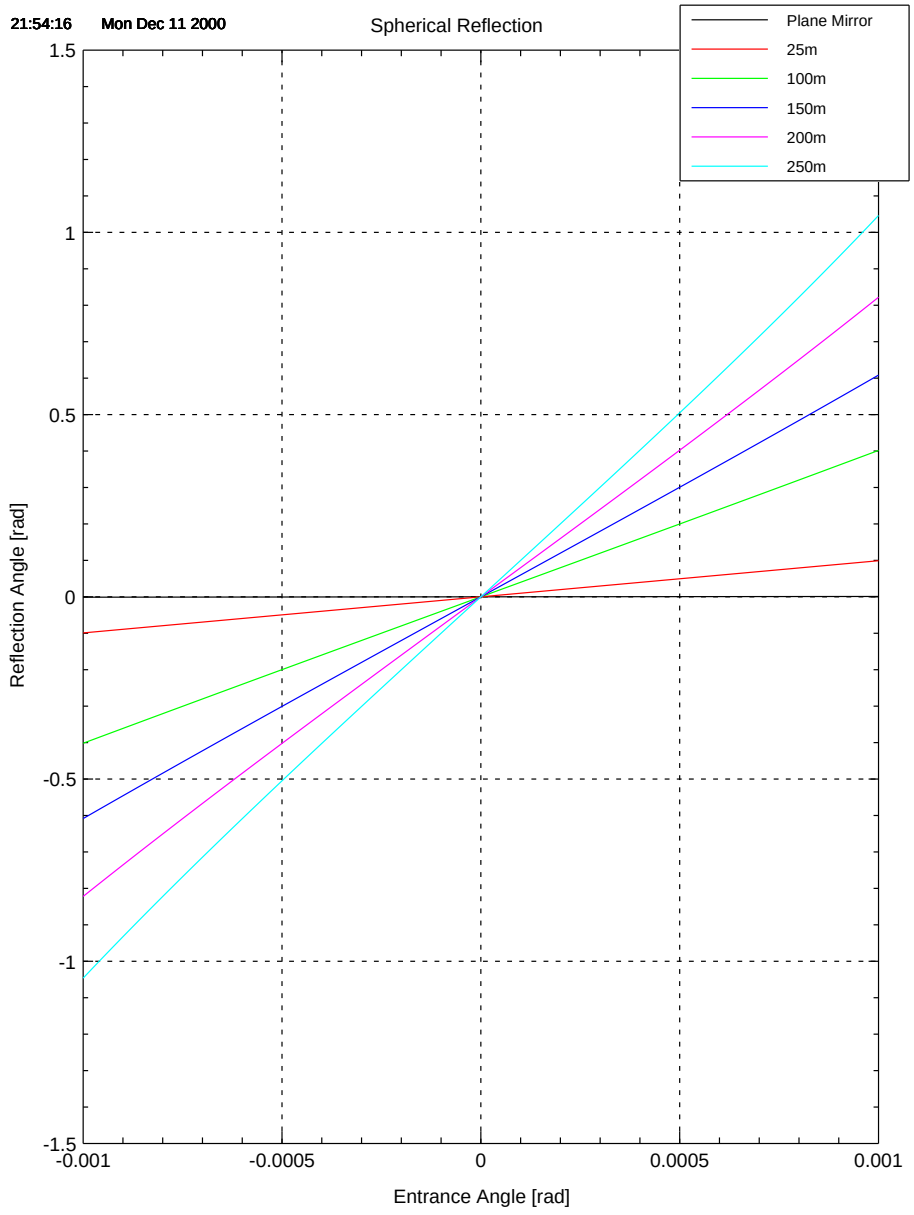

Figure 5.9: *Plot of the reflection angle θ as a function of the entrance angle γ, for a plane mirror reflection and the reflections of a sphere with radius $0.5m$, for baseline lengths of $25m$, $100m$, $150m$, $200m$ and $250m$.*

Baseline Length [m]	**Gain Factor**
25	100
50	200
100	400
150	600
200	800
250	1000

Table 5.1: *Gain factors of a spherical reflection at different baseline lengths, given a sphere radius of* $0.5m$.

of the measurement vector is too sensitive to pitch angle errors. The problem can be isolated to the reflection angle, given by the approximation of Equation 5.5. Based on this observation, it can be concluded, that the laser metrology system is unfeasible with a spherical reference satellite.

Chapter 6

Kalman Filter

In order to estimate the state vector $\boldsymbol{x}$ from the noise inflicted measurements, a Kalman filter is designed. It is chosen to design a continuous-discrete Kalman filter, which reflects the true behavior of the system. A continuous-discrete filter is used for a continuous system with discrete measurements, since it is based on a continuous differential equation and a discrete output equation.

The Kalman filter propagates a previous estimation of the states, using the state space equations, and corrects the propagation using measured states. In the following sections, the Kalman filter is described in general, followed by the derivation of a steady-state Kalman gain. Finally the system state space equations used for the filter, are expanded in order to estimate disturbances.

6.1 General Description

This section is based on the work in [Mohinder S. Grewal and Angus P. Andrews, 1993]. The Kalman filter is based on a general state space description. For a continuous-discrete filter, the model differential equation is continuous and the output equation is discrete. The model differential equation is written

$$\dot{\boldsymbol{x}}(t) = \boldsymbol{F}(t)\,\boldsymbol{x}(t) + \boldsymbol{G}(t)\,\boldsymbol{u}(t) + \boldsymbol{w}(t) \tag{6.1}$$

where $\boldsymbol{w}(t)$ is a vector of random variables, representing the process noise, which is assumed to be Gaussian white noise. The statistics of $\boldsymbol{w}(t)$ are

$$\mathrm{E}\left(\boldsymbol{w}\left(t\right)\right) = \mathbf{0} \tag{6.2}$$

$$\mathrm{E}\left(\boldsymbol{w}\left(t\right)\boldsymbol{w}^{\mathrm{T}}\left(t+\tau\right)\right) = \boldsymbol{Q}\left(t\right)\delta\left(\tau\right) \tag{6.3}$$

where $\mathrm{E}\left(\boldsymbol{w}\left(t\right)\right)$ is the expected value function, and $\delta\left(t\right)$ is Dirac's delta function. The discrete output equation is written

$$\boldsymbol{z}_k = \boldsymbol{H}_k\boldsymbol{x}_k + \boldsymbol{v}_k \tag{6.4}$$

where $\boldsymbol{v}_k$ is a vector of random variables, representing measurement noise, assumed to be Gaussian white noise with statistics

$$\mathrm{E}\left(\boldsymbol{v}_k\right) = \mathbf{0} \tag{6.5}$$

$$\mathrm{E}\left(\boldsymbol{v}_k\boldsymbol{v}_{k+n}\right) = \boldsymbol{R}_k\Delta\left(n\right) \tag{6.6}$$

where $\Delta\left(n\right)$ is the Kronecker delta function. Note the shorthand

$$\boldsymbol{x}_k \equiv \boldsymbol{x}\left(kT\right) \tag{6.7}$$

where T is the time period between samples.

Starting with an estimate at time (kT), denoted $\hat{\boldsymbol{x}}_k$, the predictor of the filter calculates an a priori estimate using Equation 6.1. The propagated estimate, denoted $\hat{\boldsymbol{x}}_{k+1}^{-}$, is an estimate of the state at time $(kT+T)$, based only on the dynamics described by the differential equation of the system. Given the measurements at time $(kT+T)$ $\boldsymbol{z}_{k+1}$, the a priori estimate can be corrected into the a posteriori estimate at time $(kT+T)$, denoted $\hat{\boldsymbol{x}}_{k+1}$.

The covariance matrices of the a priori and a posteriori estimation errors at time kT, are defined as

$$\hat{\boldsymbol{P}}_k^{-} = \mathrm{E}\left(\left[\boldsymbol{x}_k - \hat{\boldsymbol{x}}_k^{-}\right]\left[\boldsymbol{x}_k - \hat{\boldsymbol{x}}_k^{-}\right]^{\mathrm{T}}\right) \tag{6.8}$$

$$\hat{\boldsymbol{P}}_k = \mathrm{E}\left(\left[\boldsymbol{x}_k - \hat{\boldsymbol{x}}_k\right]\left[\boldsymbol{x}_k - \hat{\boldsymbol{x}}_k\right]^{\mathrm{T}}\right) \tag{6.9}$$

The a priori estimate of $\boldsymbol{P}$ is propagated using the differential equation

$$\dot{\boldsymbol{P}}(t) = \boldsymbol{F}(t)\boldsymbol{P}(t) + \boldsymbol{P}(t)\boldsymbol{F}^{\mathrm{T}}(t) + \boldsymbol{Q}(t) \tag{6.10}$$

derived in [Mohinder S. Grewal and Angus P. Andrews, 1993]. As with the state estimate, the a posteriori covariance matrix $\hat{\boldsymbol{P}}_{k+1}$ is obtained by correcting the a priori covariance matrix $\hat{\boldsymbol{P}}_{k+1}^{-}$. An illustration of the Kalman filter is given in Figure 6.1. Note that the closed loop of the Kalman filter requires initial values of the state estimate and covariance of the estimation error, denoted $\hat{\boldsymbol{x}}_0$ and $\hat{\boldsymbol{P}}_0$ respectively.

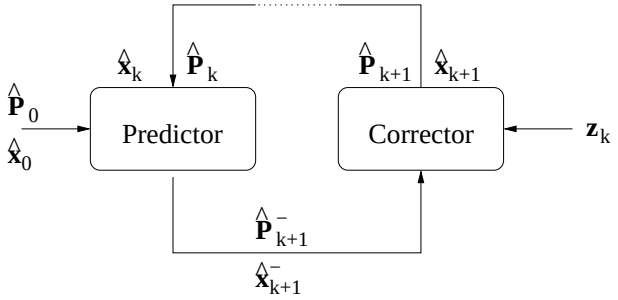

Figure 6.1: *Illustration of the Kalman filter.*

The corrector of the filter updates the predicted estimates using the output equation of Equation 6.4 and the measurement vector $\boldsymbol{z}_k$. The update of the state estimate is given by

$$\hat{\boldsymbol{x}}_k = \hat{\boldsymbol{x}}_k^{-} + \boldsymbol{K}_k\left[\boldsymbol{z}_k - \boldsymbol{H}_k\hat{\boldsymbol{x}}_k^{-}\right] \tag{6.11}$$

where $\boldsymbol{K}_k$ is the Kalman gain. The Kalman gain is calculated using

$$\boldsymbol{K}_k = \hat{\boldsymbol{P}}_k^{-}\boldsymbol{H}_k^{\mathrm{T}}\left[\boldsymbol{H}_k\hat{\boldsymbol{P}}_k^{-}\boldsymbol{H}_k^{\mathrm{T}} + \boldsymbol{R}_k\right]^{-1} \tag{6.12}$$

It is important to note from Equation 6.11, that the Kalman gain is a weight factor, which weighs the update of the prediction. From Equation 6.12 it is seen that if $\boldsymbol{R}_k$ approaches zero, the Kalman gain will increase. This results in a large update of the prediction, which means that the measurement is weighed higher than the prediction. If $\hat{\boldsymbol{P}}$ approaches zero, the Kalman gain will decrease, and the prediction is weighed higher. When $\boldsymbol{R}_k$ and $\hat{\boldsymbol{P}}$ increase, they will have the opposite effects on the Kalman gain.

The corrector equation for the covariance matrix is

$$\hat{\boldsymbol{P}}_k = \hat{\boldsymbol{P}}_k^- - \boldsymbol{K}_k \boldsymbol{H}_k \hat{\boldsymbol{P}}_k^- \tag{6.13}$$

where $\boldsymbol{K}_k$ is the Kalman gain of Equation 6.12.

6.2 Steady-State Kalman Gain

The Kalman filter requires the computation of a Kalman gain between each sample. For time invariant systems, this gain will converge to a constant, named the steady-state Kalman gain, which can be found prior to use. In the following, the steady-state Kalman gain is derived.

From Equation 6.12, it is seen that $\boldsymbol{K}_k$ varies with the covariance matrix prediction. For time invariant systems, $\boldsymbol{H}_k$ and $\boldsymbol{R}_k$ are constant, hence if a steady-state solution of the covariance matrix can be found, this solution can be used to calculate the steady-state Kalman gain.

In order to find the steady-state covariance matrix, denoted $\hat{\boldsymbol{P}}_\infty$, the equations of the predictor and corrector must be combined. Since the predictor is given in continuous time and the corrector in discrete time, the equations of the corrector are transformed to continuous time. The transformation of the corrector equation, is based on the calculation of the Kalman-Bucy filter in [Mohinder S. Grewal and Angus P. Andrews, 1993].

The propagation of the covariance matrix is accomplished using the differential equation of Equation 6.10. However it is only propagated in a time interval of kT, using the corrected value as initial state. The corrector equation is a correction of the propagation, which can be inserted directly Equation 6.10, as

$$\dot{\boldsymbol{P}}(t) = \boldsymbol{F}(t)\boldsymbol{P}(t) + \boldsymbol{P}(t)\boldsymbol{F}^{\mathrm{T}}(t) + \boldsymbol{Q}(t) - \boldsymbol{K}(t)\boldsymbol{H}(t)\boldsymbol{P}(t) \tag{6.14}$$

which requires that the Kalman gain can be expressed in continuous time. Finding the limit of the Kalman gain of Equation 6.12, when the sampling period T approaches zero, is accomplished using

$$\lim_{T\to 0}\left(\frac{\boldsymbol{K}_k}{T}\right) = \lim_{T\to 0}\left(\frac{1}{T}\hat{\boldsymbol{P}}_k^- \boldsymbol{H}_k^{\mathrm{T}}\left[\boldsymbol{H}_k \hat{\boldsymbol{P}}_k^- \boldsymbol{H}_k^{\mathrm{T}} + \boldsymbol{R}_k\right]^{-1}\right) \tag{6.15}$$

The discrete measurement noise can be written in terms of the continuous noise matrix, as

$$\boldsymbol{R}_k = \frac{\boldsymbol{R}(kT)}{T} \tag{6.16}$$

assuming that the variance of the noise is constant over the time interval T. Inserted in Equation 6.15, gives

$$\lim_{T\to 0}\left(\frac{\boldsymbol{K}_k}{T}\right) = \lim_{T\to 0}\left(\hat{\boldsymbol{P}}_k^- \boldsymbol{H}_k^{\mathrm{T}}\left[\boldsymbol{H}_k \hat{\boldsymbol{P}}_k^- \boldsymbol{H}_k^{\mathrm{T}} T + \boldsymbol{R}(t)\right]^{-1}\right)$$

$$\Updownarrow$$

$$\boldsymbol{K}(t) = \hat{\boldsymbol{P}}(t)\boldsymbol{H}^{\mathrm{T}}(t)\boldsymbol{R}^{-1}(t) \tag{6.17}$$

The steady-state of $\hat{\boldsymbol{P}}$ will result in zero dynamics, which means that the differential equation of $\boldsymbol{P}$ in Equation 6.14 can be set to zero, and is written, using Equation 6.17, as

$$\boldsymbol{F}(t)\boldsymbol{P}(t) + \boldsymbol{P}(t)\boldsymbol{F}^{\mathrm{T}}(t) + \boldsymbol{Q}(t) - \hat{\boldsymbol{P}}(t)\boldsymbol{H}^{\mathrm{T}}(t)\boldsymbol{R}^{-1}(t)\boldsymbol{H}(t)\boldsymbol{P}(t) = 0 \tag{6.18}$$

Equation 6.18 takes the form of an Algebraic Riccati Equation. The solution to this Riccati Equation is the steady-state covariance matrix $\hat{\boldsymbol{P}}_\infty$. The matrix is obtained using Xmath, hence the analytic solution will not be discussed in this project.

Given $\hat{\boldsymbol{P}}_\infty$ the steady-state Kalman gain $\boldsymbol{K}_\infty$ can be calculated using Equation 6.12, giving

$$\boldsymbol{K}_\infty = \hat{\boldsymbol{P}}_\infty \boldsymbol{H}_k^{\mathrm{T}}\left[\boldsymbol{H}_k \hat{\boldsymbol{P}}_\infty \boldsymbol{H}_k^{\mathrm{T}} + \boldsymbol{R}_k\right]^{-1} \tag{6.19}$$

Recall that $\boldsymbol{H}_k$ and $\boldsymbol{R}_k$ are time invariant, hence $\boldsymbol{K}_\infty$ can be calculated once, and used in the corrector as a constant. The Kalman filter is then simplified to two equations. The prediction of the state, using the system differential equation, and the corrector:

$$\dot{\boldsymbol{x}}(t) = \boldsymbol{F}(t)\boldsymbol{x}(t) + \boldsymbol{G}(t)\boldsymbol{u}(t) \tag{6.20}$$

$$\hat{\boldsymbol{x}}_k = \hat{\boldsymbol{x}}_k^- + \boldsymbol{K}_\infty\left[\boldsymbol{z}_k - \boldsymbol{H}_k \hat{\boldsymbol{x}}_k^-\right] \tag{6.21}$$

where $\boldsymbol{K}_\infty$ is calculated using Equation 6.19.

6.3 State Expansion

This section redefines the state space equations used for the observer, in order to estimate the disturbances.

In Chapter 4 on page 45 several sources of disturbances are described. These disturbances include solar pressure and hardware biases and white noise. Of these, the most significant is the solar pressure. The remaining disturbances are assumed to be negligible. This is a result of a trade of between model complexity and model precision.

The state vector $\boldsymbol{x}$ is expanded to be

$$\boldsymbol{x} = \begin{bmatrix} \tilde{\boldsymbol{q}}_{2-4} \\ \tilde{\boldsymbol{\omega}}_{\mathrm{s}} \\ \boldsymbol{r}_{\mathrm{s}} \\ \dot{\boldsymbol{r}}_{\mathrm{s}} \\ \boldsymbol{f}_{\mathrm{Sun}} \end{bmatrix} \tag{6.22}$$

The solar force is modeled with zero dynamics, since the model already is linearized around a working point. This can also be seen from Equation 4.76 on page 63, which is constant when using small angle approximations. The solar torque of Equation 4.77 on page 63 can be written as

$$\boldsymbol{n}_{\mathrm{Sun}} = \mathbf{S}\left(\boldsymbol{r}_{\mathrm{COP}}\right) \boldsymbol{f}_{\mathrm{Sun}} \tag{6.23}$$

where $\mathbf{S}\left(\boldsymbol{r}_{\mathrm{COP}}\right)$ is the cross product matrix function defined in Equation 4.47 on page 56.

Combining the above with the system differential equation of the model in Equation 4.84 on page 66, the state space differential equation of the observer can be written

$$
\begin{bmatrix} \dot{\tilde{\boldsymbol{q}}}_{2-4} \\ \dot{\tilde{\boldsymbol{\omega}}}_{\mathrm{s}} \\ \dot{\boldsymbol{r}}_{\mathrm{s}} \\ \ddot{\boldsymbol{r}}_{\mathrm{s}} \\ \dot{\boldsymbol{f}}_{\mathrm{Sun}} \end{bmatrix} =
$$

$$
\begin{bmatrix}
\mathbf{0}_{3\times3} & \frac{1}{2}\mathbf{1}_{3\times3} & & & & & & \mathbf{0}_{3\times3} \\
\mathbf{0}_{3\times3} & \mathbf{0}_{3\times3} & & & \mathbf{0}_{6\times6} & & & \mathbf{S}\left(\boldsymbol{r}_{\mathrm{COP}}\right) \\
& & & \mathbf{0}_{3\times3} & & & \mathbf{1}_{3\times3} & \\
& & 0 & 0 & 0 & 0 & 0 & 2\omega_{\mathrm{o}} \\
& \mathbf{0}_{6\times6} & 0 & -\omega_{\mathrm{o}}^2 & 0 & 0 & 0 & 0 \\
& & 0 & 0 & 3\omega_{\mathrm{o}}^2 & -2\omega_{\mathrm{o}} & 0 & 0 \\
& & & & & & & \\
\mathbf{0}_{3\times6} & & & & \mathbf{0}_{3\times6} & & & \mathbf{0}_{3\times3}
\end{bmatrix}
\begin{bmatrix} \tilde{\boldsymbol{q}}_{2-4} \\ \tilde{\boldsymbol{\omega}}_{\mathrm{s}} \\ \boldsymbol{r}_{\mathrm{s}} \\ \dot{\boldsymbol{r}}_{\mathrm{s}} \\ \boldsymbol{f}_{\mathrm{Sun}} \end{bmatrix}
$$

$$
+ \begin{bmatrix} \mathbf{0}_{3\times6} \\ \boldsymbol{J}^{-1} \quad \mathbf{0}_{3\times3} \\ \mathbf{0}_{3\times6} \\ \mathbf{0}_{3\times3} \quad \frac{1}{m_{\mathrm{s}}}\mathbf{1}_{3\times3} \\ \mathbf{0}_{3\times6} \end{bmatrix}
\begin{bmatrix} \boldsymbol{n}_{\mathrm{ext}} \\ \boldsymbol{f}_{\mathrm{rel}} \end{bmatrix} \tag{6.24}
$$

The output equation is written

$$
\begin{bmatrix} \tilde{\boldsymbol{q}}_{2-4} \\ \tilde{\boldsymbol{\omega}}_{\mathrm{s}} \\ \boldsymbol{r}_{\mathrm{s}} \end{bmatrix} = \begin{bmatrix} \mathbf{1}_{9\times9} & \mathbf{0}_{9\times6} \end{bmatrix}
\begin{bmatrix} \tilde{\boldsymbol{q}}_{2-4} \\ \tilde{\boldsymbol{\omega}}_{\mathrm{s}} \\ \boldsymbol{r}_{\mathrm{s}} \\ \dot{\boldsymbol{r}}_{\mathrm{s}} \\ \boldsymbol{f}_{\mathrm{Sun}} \end{bmatrix} \tag{6.25}
$$

Chapter 7

Controller

This chapter describes the controller used for the system. A controller is needed to bring the satellites to reference position and counteract the disturbances of the system, mainly solar pressure. It is assumed that the initial conditions of the system are close reference. Hence collision avoidance is ignored.

The requirements of the controller are derived from the intended requirements of the DARWIN mission. These requirements are discussed in the following section. Subsequent the design of the controller is described.

7.1 Requirements

The SMART-2 mission is to show the feasibility of the DARWIN mission, hence the requirements of the controller is derived from the DARWIN mission specifications. However the specifications of the DARWIN mission is conditioned by the development of high precision star trackers and fringe trackers. Hence the requirements of the SMART-2 mission should be based on the hardware capabilities.

The requirements of the DARWIN mission are derived in Appendix A on page 111. Since it is assumed that the wide field cameras, which are high precision star trackers, are unavailable for SMART-2, the requirements of the SMART-2 control system will be those of the baseline control mode (BCM). This means that the attitude is to be controlled within 10as and the baseline within 1cm, as stated in Table A.1 on page 114.

7.2 Design

This section describes the design of a controller for the system. It is based on the linear quadratic design method described in [Ian Hesselberg Rasmussen, 1998] and [Dan Bhanderi et al., 1999].

The controller of the system is designed to minimize a performance index, by selecting a feedback gain $\boldsymbol{L}$, which moves the system poles to an optimal place. The performance index is a quadratic function of the states and input signals, given by

$$\boldsymbol{I} = \int_0^\infty \left(\boldsymbol{x}^{\mathrm{T}} \boldsymbol{W} \boldsymbol{x} + \boldsymbol{u}^{\mathrm{T}} \boldsymbol{V} \boldsymbol{u} \right) \mathrm{d}t \tag{7.1}$$

where $\boldsymbol{W}$ is a n by n quadratic matrix weighing the n states of the system, and $\boldsymbol{V}$ is a m by m quadratic matrix weighing the m control signals. The choice of the weight matrices is to some extend done by trial and error. A good initial value of $\boldsymbol{W}$ and $\boldsymbol{V}$ is the inverse of the squared maximum values of the states and control signals in the diagonal [Ian Hesselberg Rasmussen, 1998].

Using the Xmath function *lqgltr*, the gain matrix L has been found. The control signal $\boldsymbol{u}$ is then given by the control law

$$\boldsymbol{u} = -\boldsymbol{L} \boldsymbol{x} \tag{7.2}$$

The controller has been implemented in a simulation program, and the obtained results are discussed in the following chapter.

Chapter 8

Simulation

This chapter discusses the simulation implementation and results of the model, estimator and controller, derived in the previous chapters. The system is simulated in Xmath, which is comparable to the well known program Matlab. Like Matlab's Simulink, Xmath has a graphical implementation environment named System Build, where the equations can be implemented by connecting signals between blocks. The integration algorithm used in System Build is Kutta-Merson if none other is specified.

The purpose of the simulator is mainly to verify the functionality of the Kalman Filter and LQG controller, used with the laser metrology system. However, since the laser metrology system has been found to be inapplicable, due to the circumstances discussed in Chapter 5 on page 71, the model of the laser system is removed, and it is assumed that the relative position can be measured by other means.

In addition to verifying the filter and controller, their performance is investigated, in order to evaluate hardware requirements.

8.1 Implementation

The implementation of the system is done in System Build. Figure 8.1 is a screen shot of the System Build implementation of the system. To the right is the Kalman block which estimates the states from the model block, in the middle of the figure. The states of the model are biased and added with white noise, simulating sensor noise. When the states have been estimated, the control signals are calculated by the two gain blocks to the left, and the signals are quantized and limited in magnitude, simulating the FEEP thrusters.

Due to the limited time frame of the project, certain elements previously intended for

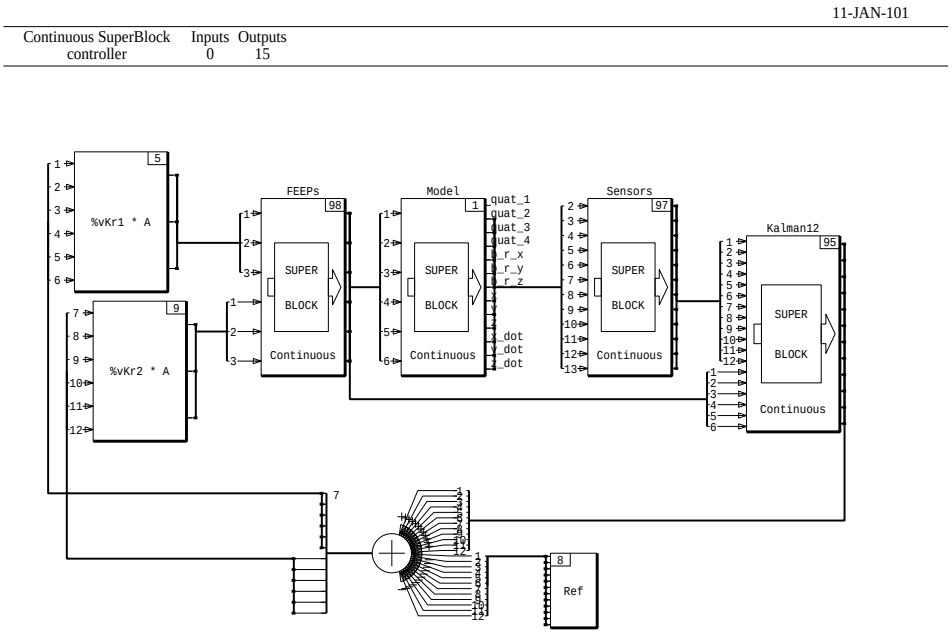

Figure 8.1: *Overview of the implementation in System Build.*

implementation are left out:

- Time quantization of FEEP thrusters, simulating a minimum thrust time. It is expected that the minimum period of thrust is small for FEEPs.
- Estimation of the solar pressure. The Kalman filter is only implemented with twelve states, leaving out $\boldsymbol{f}_{\text{Sun}}$.
- Gyroscope drift. Only the bias and white noise is added to the angular velocity state to simulate gyroscope noise.

The Kalman filter has been implemented as a continuous-continuous filter, which means that the corrector part in Equation 6.21 on page 89, is derived as a continuous equation. Since the Kalman gain is constant, only the measurement vector is discrete, and has to be made continuous. Simulating on a computer, the only difference is that the time step of the corrector is given by the time propagation of the simulation, since a computer can't simulate in continuous time.

In order for the Kalman filter to converge, it has been necessary to assume that all twelve states are measurable. Hence the matrix $\boldsymbol{H}$ in the measurement equation of Equation 4.85 on page 66 becomes the 12 by 12 identity matrix.

The laser system is implemented as two blocks. One block calculates the measurement vector on the CCD, and the distance of the optical path. The other calculates the state from the measurement vector, distance and the satellite attitude. It is left out of the main implementation, but used for the analysis of the laser configuration described in Chapter 5 on page 71.

The system has only been simulated with a single satellite and the sphere, since the simulation of a second satellite is done in the same way.

8.2 Model

The model of the attitude and relative position of the satellite is implemented as non-linear differential equations. In addition the solar pressure has been added as disturbance to the system. Leaving the system in an initial state, the solar pressure will make the system diverge, implying the need of a control system. Figures 8.2 and 8.3 show the uncontrolled attitude and relative position as functions of time.

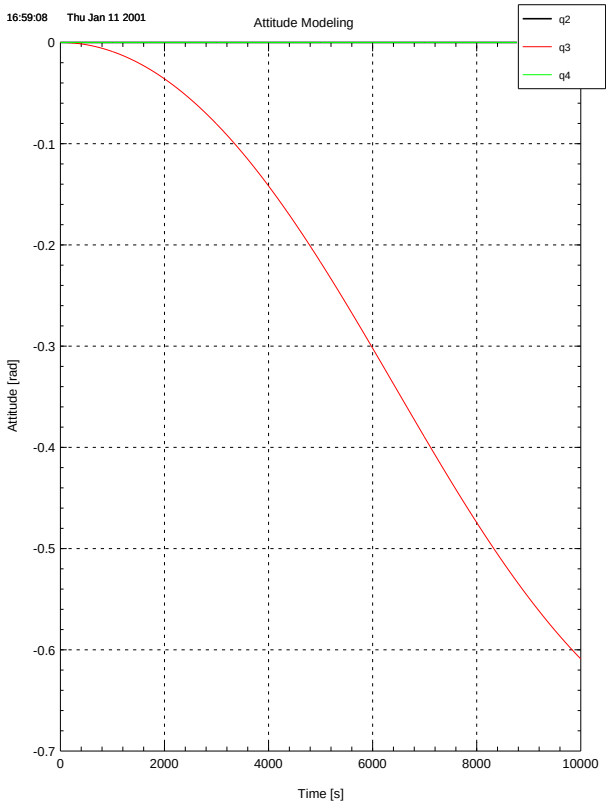

Figure 8.2: *Plot of the uncontrolled attitude parameters as function of time.*

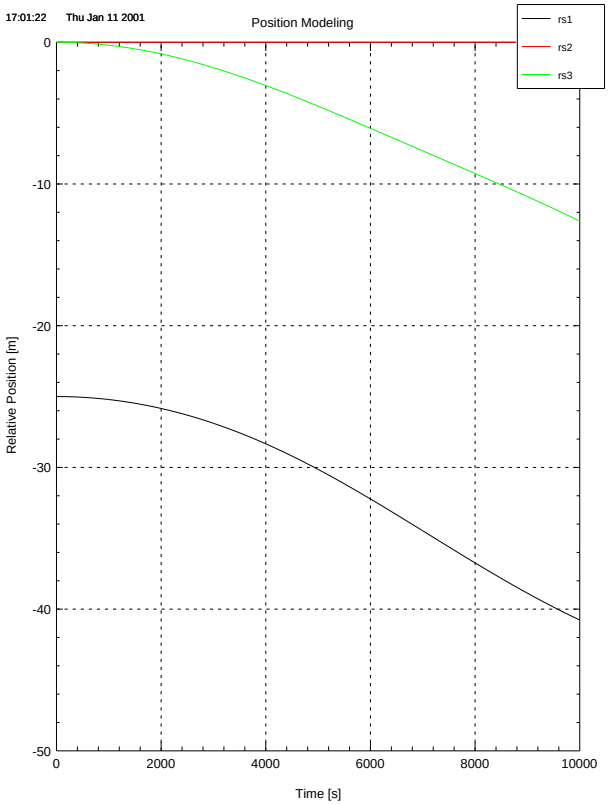

Figure 8.3: *Plot of the uncontrolled relative position vector as function of time.*

8.3 Estimator

The measurements of the sensor hardware is simulated with bias and white noise. In order to achieve an improved estimate of the true position and attitude, a Kalman filter is implemented. Figures 8.4 and 8.5 shows the error between the true state vector, and the estimated position and attitude, respectively.

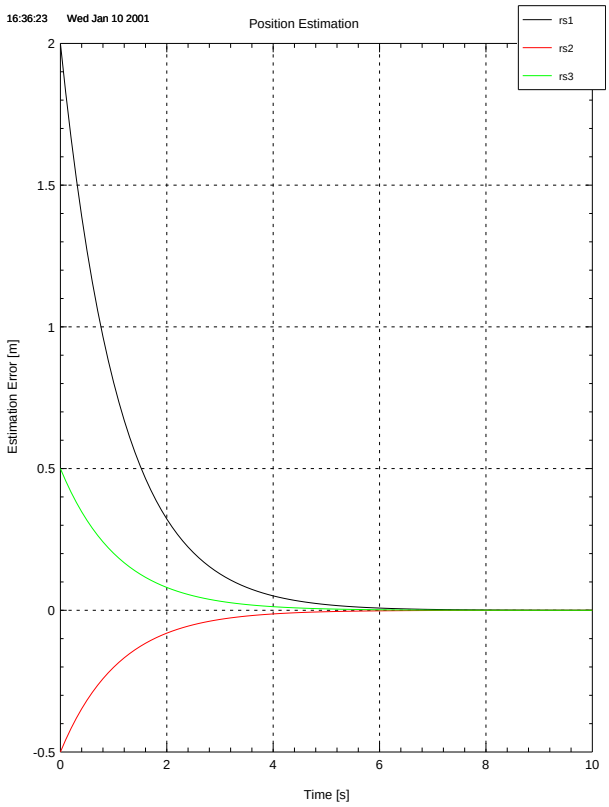

Figure 8.4: *Error of the relative position estimate.*

It is seen that the filter converges to the the true states within ten seconds. That the estimated state is better than the measured values, can be verified by calculating the root mean squared (RMS) values of the errors in estimates and measurements. Figure 8.6 is a plot of the measured, estimated and true value of the second element in the attitude quaternion of the satellite.

The RMS values are shown in Table 8.1. The measurements are done by star trackers, with a precision of 10as, and white noise is added according to this. White noise of the same magnitude is added to the angular velocity.

It is seen that the estimate improves the obtained state by approximately 33%. The RMS values of the position measurements and estimates have also been evaluated and

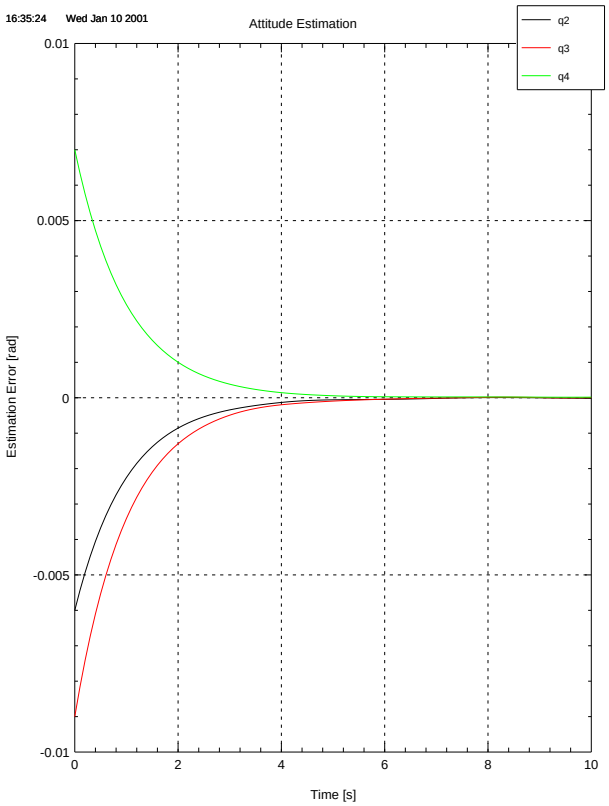

Figure 8.5: *Error of the attitude estimate.*

	RMS
Measurement	$[24.7 \times 10^{-6}]^{\circ}$
Estimate	$[16.6 \times 10^{-6}]^{\circ}$

Table 8.1: *RMS values associated with the second element of the satellite attitude quaternion.*

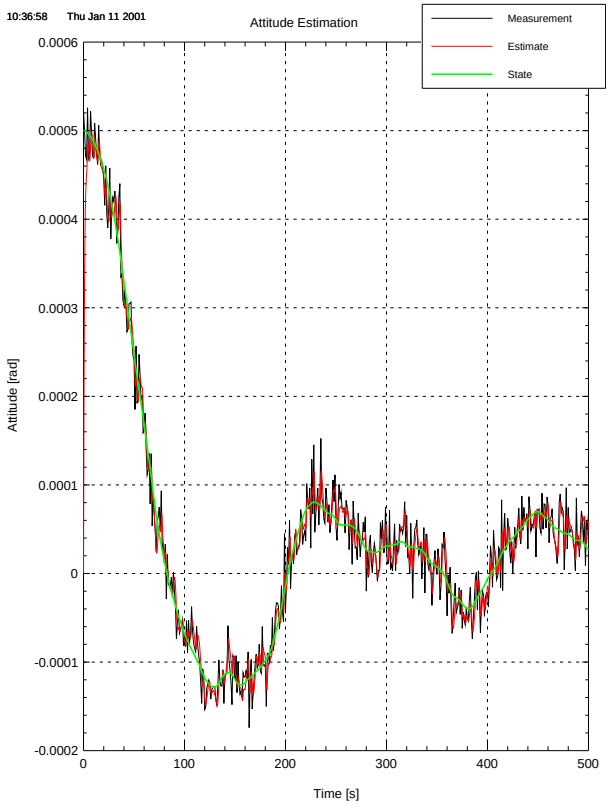

Figure 8.6: *The measured, estimated and true value of the satellite quaternion's second element* $\tilde{q}_2$.

are shown in Table 8.2. It is assumed that the relative position can be measured with a precision of 0.1mm and the relative velocity with a precision of 0.1mm/s.

	RMS
Measurement	0.111×10^{-3}m
Estimate	69.9×10^{-6}m

Table 8.2: *RMS values associated with the first element of the relative position vector.*

In this case the estimate is approximately 37% better than the measurement.

From the above, it can be concluded that the Kalman filter works as intended, and improves the obtained state vector with approximately 33%, when compared with the measured state vector.

8.4 Controller

The attitude and relative position of the satellite is sought controlled, to counteract the solar pressure. The controller is actually two independent controllers. Figure 8.7 shows the controlled attitude parameters. It is seen that the parameters approaches the reference value of zero. However it takes approximately 700s, due to the limits in thrust, which is approximately 0.4mN per thruster [Bonnet, 2000]. In addition, there is an overshoot which can be avoided by using a different controller. This is important for the fuel/energy budget of the satellite. This has not been investigated further in this project.

Figure 8.8 shows the controlled velocity vector. As with the attitude parameters, there is an overshoot, which suggests a controller redesign, if the fuel/energy budget is to be optimized.

The first element of $\boldsymbol{r}_{\mathrm{s}}$, which has reference different from zero, takes longer to converge than the other two elements. If the reference is changed to zero, it converges in the same time as the others. This suggests that the reference is introduced in a non-optimal place in the system. In Figure 8.1 on page 96 it can be seen that the reference is subtracted from the estimated state. The reference can be moved to a different place in the loop, to optimize system performance [Gene F. Franklin et al., 1994]. This has not been investigated further.

The controlled attitude parameters have RMS values of 21as, when the reference values have been reached. This is based on measurements with a white noise of 10as. Due to the requirement of attitude control within 10as, as mentioned in Section 7.1, the controller should be redesigned. Since the controller is a simple proportional controller, a redesign could improve the precision noticeable. However, with the current controller, a measurement precision of 5as will result in a RMS value of 10.5as, which means that better hardware will make the current system meet the requirements.

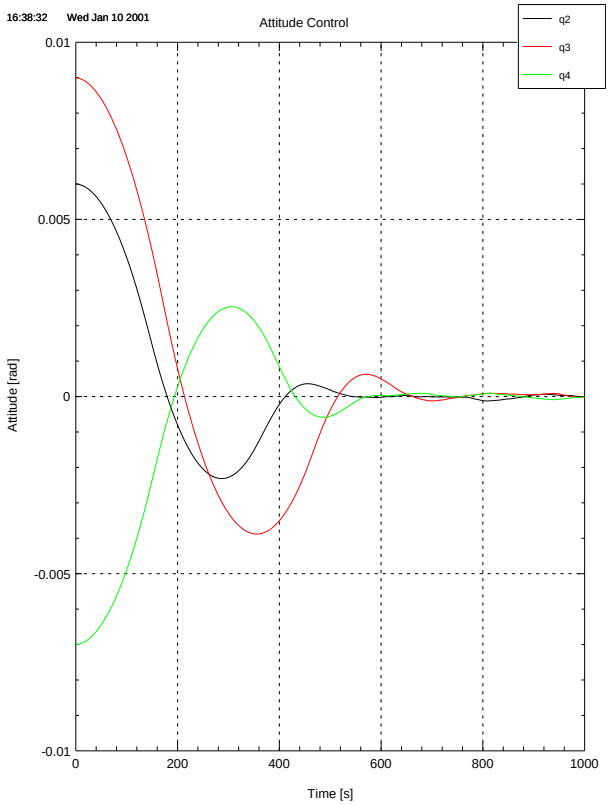

Figure 8.7: *Plot of the controlled attitude parameters of the satellite.*

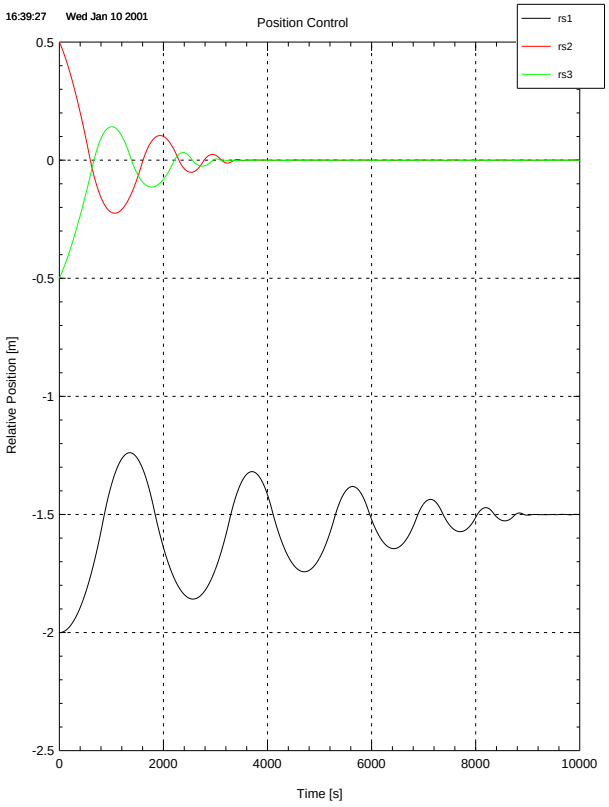

Figure 8.8: *Plot of the controlled relative position vector of the satellite. The reference position of the satellite has been made smaller for better illustration.*

The controlled position elements have RMS values of 0.2mm. This is vastly more precise than the requirement of 10mm. However the sensors are assumed to be precise within 0.1mm, which may be optimistic. With the current system, a precision within 1mm will result in RMS values of 3mm, which is still well within the requirements. In addition, with a better controller, the hardware precision could be even less.

Chapter 9

Conclusion

The main purpose of this project was to investigate the feasibility of using a spherical mirror together with two other satellites for SMART-2, in order to form a formation, that could demonstrate formation flying, preceding the DARWIN mission. The use of a spherical mirror was intended to minimize the costs of the SMART-2 mission. A mirror was suggested in order to apply a laser metrology system proposed for the DARWIN mission.

A mathematical analysis of the laser metrology system in conjunction with a spherical mirror was done. Equations for obtaining the relative position of the satellites, with respect to the spherical mirror, given the measurement of attitude by star trackers, have been derived.

In addition a RF metrology system is proposed. This system is suggested in order to enable the laser metrology system from random conditions. No in-depth investigation was performed, and collision avoidance was ignored.

Based on the mathematical description of the laser metrology system, a suitable configuration of the system was analyzed. This study proved that that the mounting of the laser was limited due to the vast gain of the reflection angle of the laser beam. This gain resulted in the need of unfeasible requirements to mounting precision of the laser, or unrealistic requirements to CCD or sphere sizes.

Based on these results the use of a spherical mirror was found to be inapplicable. Due to this conclusion, an investigation of the following areas was set aside:

- Requirements to geometrical precision of the spherical mirror.
- Precision of center of mass.

If the center of mass is not at the center of the sphere, the rotation of the sphere would

influence the reflection of the laser beam. Distortion of the reflection may also occur as a consequence of using a non-perfect sphere. An investigation in these areas could also conclude the in-feasibility of using a spherical mirror for SMART-2. It may also lead to the conclusion that the requirements of the spherical mirror would make production costs exceed the prize of using three fully equipped satellites. This investigation has been ignored in this project, since the spherical mirror is already found to be inapplicable.

For the educational purpose of the project, it was assumed that the position of the satellites could be obtained by other means, and mathematical models of attitude and position of the satellites were derived. In addition a Kalman filter and a controller were designed. The system was implemented in Xmath, and successfully simulated in the graphical simulation environment System Build.

The simulation showed that the system would diverge due to the solar pressure, which was expected. The controller was able to keep the position well within the required margin of 1cm. In order to meet the requirements of the attitude, the performance of the star trackers had to be changed from a precision margin of 10as to 5as. However due to the limited time frame of the project, a single proportional controller was designed. A controller redesign could confirm the the requirement of 10as.

The Kalman filter was proved to increase the estimate of the measurements by approximately 33%. The Kalman filter was not expanded to 15 states in order to estimate the solar pressure, since a steady state Kalman gain could not be found before the deadline of the project.

The main goal of the project was to study the feasibility of using a spherical mirror in a laser metrology system. This goal has been successfully achieved.

Bibliography

(2000). *Study for the ESA SMART-2 Mission, Final Presentation*.

Ankersen, F. (2000). Derivation of relative motion equations for rvd.

Bonnet, H. (2000). Irsi - darwin, draft technical note on the baseline pointing and opd control system. Technical report, Alcatel Space.

Dan Bhanderi, Thomas Bai Andersen, Rasmus Andersen, Kristian Poulsen, and Claus Schroeder (1999). Balancerende pind. Technical report, Aalborg University.

Dan Bhanderi, Thomas Bai Andersen, Soeren Gottlieb Michelsen, Martin Jansen Schmidt, Claus Schroeder, and Anders Tietze (2000). High precision attitude determination using gps. Technical report, Aalborg University.

ESA (2000). Official homepage of esa. www.esa.int.

Gene F. Franklin, J. David Powell, and Abbas Emami-Naeini (1994). *Feedback Control of Dynamic Systems*. Adison-Wesley Publishing Company.

Ian Hesselberg Rasmussen (1998). Optimal and robust attitude control of the champ satellite. Technical report, Aalborg University.

James R. Wertz, editor (1978). *Spacecraft Attitude Determination and Control*. Kluwer Academic Publishers.

Lund, G. (2000). Irsi - darwin, executive summary. Technical report, Alcatel Space.

Mohinder S. Grewal and Angus P. Andrews (1993). *Kalman Filtering Theory and Practice*. Prentice Hall.

Appendix A

Introduction to DARWIN

This section is an introduction to the concept of the DARWIN project, which is currently being developed at the European Space Agency (ESA). The main goal of the DARWIN project is to identify Earth-like planets (considering temperature and atmosphere) orbiting distant stars. This is only possible using an interferometer, because of the contrast between the star and the planet, which makes a planet undetectable using conventional telescopes.

Figure A.1 shows the formation intended for the DARWIN satellites. At the bottom is the satellite used for communication with the ground station. Through this satellite all the satellites can be controlled. Above the communication satellite are six satellites which span a plane. In the middle is the hub satellite, which collects the reflected light from the surrounding telescope flyers. The number of telescope flyers is not given even though the illustration shows five.

The line between two telescope flyers is called a baseline. If interferometry is used on the light from two telescope flyers, destructive interference will filter the light from the star out of the signal, and in addition it will gain the light from the planet at angle θ, using constructive interference (see Figure A.2). The angle of which the interferometry will gain the light signal, is conditioned by the position of telescope flyers relative to each other.

The interferometry equipment is placed in the hub satellite. Since the optical path of the light signal must be precise within approximately 8nm, an internal delay line is implemented. Without the internal delay line, the distance between each of the telescope flyers and the hub would have to be set and kept within the 8nm threshold which is practically impossible. The internal delay lines consist of mirrors, which can shorten or lengthen the optical path in order to meet the requirements. The difference in path lengths between light signals from two telescope flyers is the optical path difference.

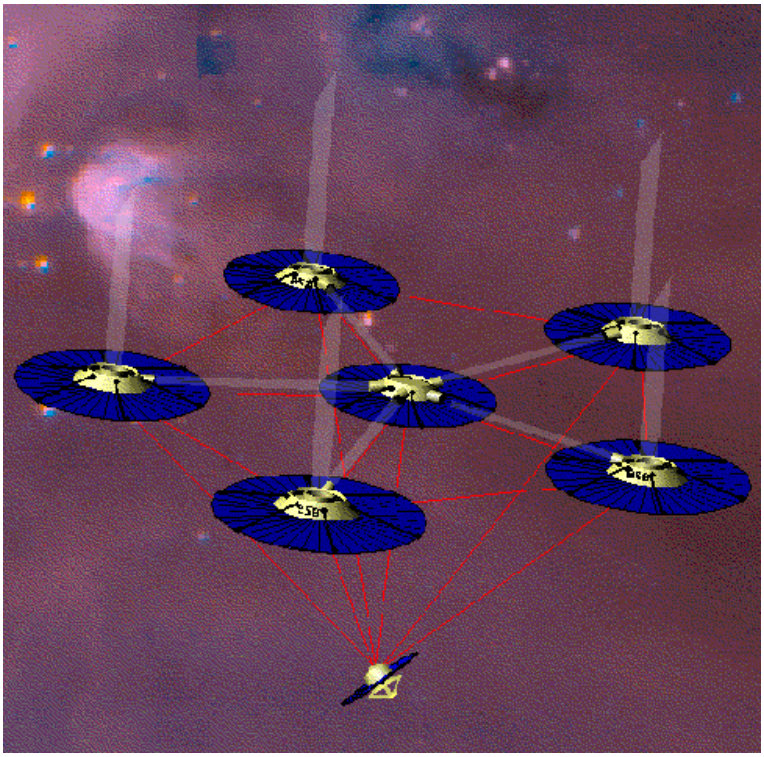

Figure A.1: *Illustration of the satellites in the DARWIN project. The hub in middle surrounded by the telescope flyers. At the bottom is the satellite used to communicate with Earth [ESA, 2000].*

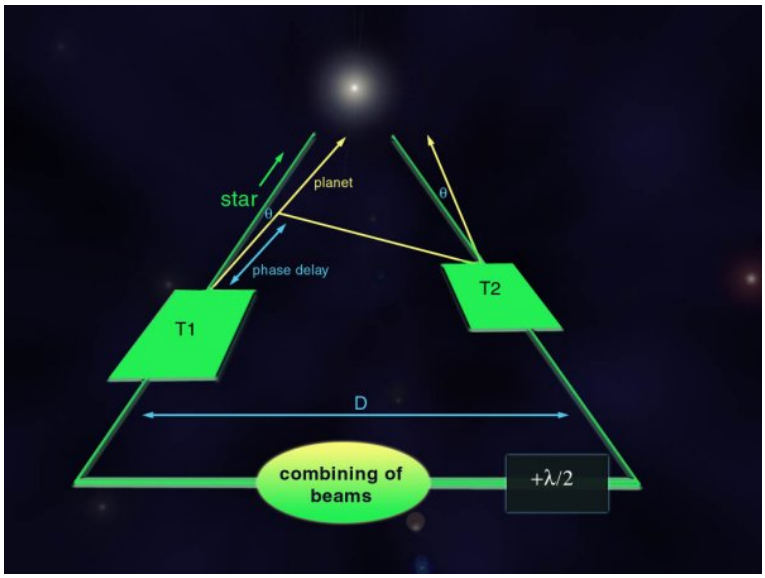

Figure A.2: *The interferometry principle. The two telescope flyers T1 and T2 reflect the light signal to the hub, which uses interferometry to filter the signal [ESA, 2000].*

A.1 Control Requirements

The DARWIN mission control modes have been divided into three phases:

- Baseline Control Mode (BCM)
- Fringe Acquisition Mode (FAM)
- Normal Operation Mode (NOM)

The performance and requirements of the system which is summarized in the following, is stated in [Bonnet, 2000].

The BCM mode uses an RF ranging in order to configure the array, from an initial distribution of the satellites within a sphere of 15km, to the requirements of the FAM in order to establish an optical link between the satellites. FAM uses laser metrology to acquire the fringe measurable on the fringe trackers. Once a fringe has been acquired, the NOM will use the fringe trackers to control the OPD.

In BCM the random attitude and position of the satellites requires an omni-directional ranging system. For this purpose the RF ranging is used. Attitude measurements are acquired by star trackers. As control actuators mN field emitting electric propulsion (FEEP) thrusters are used, as opposed to μN FEEP thrusters, in order to minimize the

time used to configure the formation. Note that BCM is also used when slewing the array LOS towards a new target star. When the baselines of the array are controlled within 1cm, and the attitude of the flyers within 10as at sampling frequency of 10Hz, optical links for the laser metrology are established, hence FAM is entered.

Based on the laser metrology and Wide Field Cameras, FAM uses μN FEEP thrusters to meet the initial requirements of the NOM. The attitude of the satellites must have an overall attitude accuracy below 5mas, and the drift of the optical path must be below 0.5μm$/$s. The out-of-plane drift, caused by rigid rotations of the formation must be controlled within 25μm at a sampling rate of 10Hz. These requirements must be met until a fringe is acquired on the fringe trackers.

Upon entering NOM the main control requirement is to keep the optical path difference between the light from two Telescope Flyers below 20nm. This is accomplished using the fringe trackers placed in the hub satellite.

The requirements of the three modes are summarized in Table A.1.

BCM	
Attitude control	10as@10Hz
Baseline control	1cm
FAM	
Attitude control (overall accuracy)	5mas
Rigid rotation control	25μm@10Hz
OPD drift	0.5μm$/$s
NOM	
OPD	20nm

Table A.1: *Summary of the control requirements in each operation mode.*

Appendix B

Quaternions

This chapter is a brief description of the quaternions and their algebra. It is based on [James R. Wertz, 1978] but modified to the notation used in this project.

Quaternions is one of many ways to represent attitude. The quaternion has the advantage of being without singularities for all attitudes.

A quaternion $\boldsymbol{q}$ is defined by its four vector elements q_1, q_2, q_3 and q_4, as

$$\boldsymbol{q} = q_1 + iq_2 + jq_3 + kq_4 = \begin{bmatrix} q_1 \\ q_2 \\ q_3 \\ q_4 \end{bmatrix} \tag{B.1}$$

where i, j and k are hyper imaginary numbers satisfying

$$i^2 = j^2 = k^2 = -1 \tag{B.2}$$
$$ij = -ji = k \tag{B.3}$$
$$jk = -kj = i \tag{B.4}$$
$$ki = -ik = j \tag{B.5}$$

The four parameters of a quaternion are subject to the constraint that

$$q_1^2 + q_2^2 + q_3^2 + q_4^2 = 1 \tag{B.6}$$

which means that the quaternion has three degrees of freedom, corresponding to the minimum set of parameters needed for attitude representation [James R. Wertz, 1978].

The first element q_1 of the quaternion $\boldsymbol{q}$ is named the scalar element, and the 2nd, 3rd and 4th the complex elements. The complex part of the quaternion is written $\boldsymbol{q}_{2-4}$, hence a quaternion may be written

$$\boldsymbol{q} = \begin{bmatrix} q_1 \\ \boldsymbol{q}_{2-4} \end{bmatrix} \tag{B.7}$$

A rotation $\Delta\phi$ around a unit vector $\boldsymbol{u}$, is represented by the quaternion

$$\boldsymbol{q} = \begin{bmatrix} \cos\left(\frac{\Delta\phi}{2}\right) \\ \boldsymbol{u}\sin\left(\frac{\Delta\phi}{2}\right) \end{bmatrix} \tag{B.8}$$

The complex conjugate of the quaternion is defined as

$$\boldsymbol{q}^* = q_1 - iq_2 - jq_3 - kq_4 = \begin{bmatrix} q_1 \\ -\boldsymbol{q}_{2-4} \end{bmatrix} \tag{B.9}$$

Note that

$$\boldsymbol{q}\boldsymbol{q}^* = \begin{bmatrix} 1 \\ 0 \\ 0 \\ 0 \end{bmatrix} \tag{B.10}$$

which is the unit quaternion representing the zero rotation, i.e. no rotation.

The product of two quaternions q and q' is defined in matrix form as

$$q'' = qq' = \begin{bmatrix} q'_1 & -q'_2 & -q'_3 & -q'_4 \\ q'_2 & q'_1 & q'_4 & -q'_3 \\ q'_3 & -q'_4 & q'_1 & q'_2 \\ q'_4 & q'_3 & -q'_2 & q'_1 \end{bmatrix} \begin{bmatrix} q_1 \\ q_2 \\ q_3 \\ q_4 \end{bmatrix} \tag{B.11}$$

Note that the multiplication of quaternions is not commutative, which is also the case for attitude matrices.

Representing the attitude of $\boldsymbol{q}$ by the attitude matrix $\boldsymbol{A}(q)$, the rotation sequence of Equation B.11, can be written in terms of the associated attitude matrices, as

$$\boldsymbol{A}(q'') = \boldsymbol{A}(q')\,\boldsymbol{A}(q) \tag{B.12}$$

Note the reverse order of multiplication.